ornl

OAK RIDGE
NATIONAL
LABORATORY

LOCKHEED MARTIN

Report No. ORNL/TM-13642

FISSILE DEPOSIT CHARACTERIZATION AT THE FORMER OAK RIDGE K-25 GASEOUS DIFFUSION PLANT BY ^{252}CF-SOURCE-DRIVEN MEASUREMENTS

Taner Uckan
Mark S. Wyatt
John T. Mihalczo
Timothy E. Valentine
James A. Mullens
Terry F. Hannon

May 1998

Prepared by the
Oak Ridge National Laboratory
Oak Ridge, Tennessee 37831-6285
managed by
Lockheed Martin Energy Research Corporation.
for
U.S. DEPARTMENT OF ENERGY
under contract DE-AC05-96OR22464

DISCLAIMER

Portions of this document may be illegible in electronic image products. Images are produced from the best available original document.

ORNL/TM-13642

FISSILE DEPOSIT CHARACTERIZATION AT THE FORMER OAK RIDGE K-25 GASEOUS DIFFUSION PLANT BY ^{252}CF-SOURCE-DRIVEN MEASUREMENTS

Taner Uckan, Mark S. Wyatt[1], John T. Mihalczo,
Timothy E. Valentine, and James A. Mullens

Oak Ridge National Laboratory[2]
P.O. Box 2008
Oak Ridge, Tennessee 37830-6004
(423) 574-0973

Terry F. Hannon

Bechtel Jacobs Company LLC[3]
P.O. Box 4699
Building K-1024, MS-7328
Oak Ridge, TN 37831
(423) 574-8985

May 1998

[1] University of Tennessee, Department of Nuclear Engineering, Knoxville, TN 37996-2300.
[2] Managed by Lockheed Martin Energy Research Corporation for the U. S. Department of Energy under contract DE-AC05-96OR22464.
[3] Managed by Bechtel Jacobs Company LLC for the United States Department of Energy under Contract Number DE-AC05-98OR22700.

This page intentionally left blank.

TABLE OF CONTENTS

LIST OF FIGURES

LIST OF TABLES

ACRONYMS AND ABBREVIATIONS

CFD	constant fraction discriminator
CFSDT	^{252}Cf-source-driven transmission (measurement)
DOE	U. S. Department of Energy
ETTP	East Tennessee Technology Park
H/U	ratio of hydrogen to uranium
HV	high voltage
LMES	Lockheed Martin Energy Systems, Inc.
LV	low voltage
NDA	nondestructive assay
NIM	nuclear instrument module
NP	not physical
NWIS	Nuclear Weapons Identification System
ORGDP	Oak Ridge Gaseous Diffusion Plant
ORNL	Oak Ridge National Laboratory
TOF	time-of-flight
UF_6	Uranium hexafluoride
UO_2F_2	Uranyl fluoride

This page intentionally left blank.

EXECUTIVE SUMMARY

The Deposit Removal Project was undertaken with the support of the U. S. Department of Energy at the East Tennessee Technology Park (ETTP) formerly the Oak Ridge K-25 Site. The project team performed the safe removal of the hydrated uranyl fluoride (UO_2F_2) deposits from the K-29 Building of the former Oak Ridge Gaseous Diffusion Plant. The deposits had developed as a result of air leakage into UF_6 gas process pipes; UO_2F_2 became hydrated by moisture from the air and deposited inside the pipes. The mass, its distribution, and the hydrogen content [that is, the ratio of H to U (H/U)], were the key parameters that controlled the nuclear criticality safety of the deposits. Earlier gamma-ray spectrometry measurements in K-29 had identified the largest deposits in the building. The first and third largest deposits in the building were measured in this program. The first deposit, found in the Unit 2, Cell 7, B-Line Outlet process pipe (called the "Hockey Stick") was about 1,300 kg (± 50% uncertainty) at 3.34 wt % ^{235}U enrichment (± 50% uncertainty) and according to the gamma-ray spectroscopy was uniformly distributed. The second deposit (the third-largest deposit in the building), found in the Unit 2, Cell 6, A-Line Outlet process pipe (called the "Tee-Pipe"), had a uranium deposit estimated to be about 240 kg (± 50% uncertainty) at 3.4 wt % ^{235}U enrichment (± 20% uncertainty).

Before deposit removal activities began, the Deposit Removal Project team needed to survey the inside of the pipes intrusively to assess the nuclear criticality safety of the deposits. Therefore, the spatial distribution of the deposits, the total uranium deposit mass, and the moderation level resulting from hydration of the deposits, all of which affect nuclear criticality safety were required. To perform the task safely and effectively, the Deposit Removal Project team requested that Oak Ridge National Laboratory (ORNL) characterize the two largest deposits with the ^{252}Cf-source-driven transmission (CFSDT) technique, an active neutron interrogation method developed for use at the Oak Ridge Y-12 Plant to identify nuclear weapons components in containers. The active CFSDT measurement technique uses CFSDT time-of-flight measurements of prompt neutrons and gamma rays from an externally introduced ^{252}Cf source.

CFSDT deposit characterization measurements were successfully performed on two of the three largest deposits in K-29. The measurement results indicated that the deposits were annular and that most of the deposit material in the lower part of the Hockey Stick was on top

of the process pipe, located around an elbow. The average measured H/U was 3.5 ± 0.19. A total uranium mass of 542 ± 92 kg was obtained from the deposit distribution measured along the process pipe. The average values were obtained from two different adjacent detectors, which yielded H/U of 3.4 ± 0.25 and 3.6 ± 0.24 and uranium masses of 552 and 532 kg (± 17% uncertainty), respectively. The adjacent detectors showed that the deposit thickness was very irregular, varying in some cases by more than a factor of 2 in. a distance of 4.5 in. along the pipe. The Tee-Pipe deposit measurements showed a very thin deposit of material distributed on the wall of the process pipe. The total uranium mass of 93 kg was estimated for the Tee-Pipe as an upper bound from the measurements.

The measurement results were used to select the locations on the process pipes for the visual observations of the deposits. Some time after completion of the measurements, a fiber-optic camera was inserted through a number of holes drilled into both process pipes. At the same time, a special tool was inserted for measuring the deposit thickness. The fiber-optic camera observations and thickness measurements were performed at a number different locations along the process pipes. In general, the intrusive camera observations at various locations were consistent with the results of the CFSDT deposit profile measurements for both the Hockey Stick and the Tee-Pipe. The dominant orange and yellow-green colors observed with the fiber-optic camera indicated an H/U ~ 3–4, which was consistent with the CFSDT measurements.

The Hockey Stick and the Tee-Pipe deposits were successfully removed, weighted, and the estimated total uranium masses were 479 kg and 98.5 kg (± 50 uncertainty), respectively, which are consistent with the CFSDT measurement findings.

The use of CFSDT for characterization of the K-29 deposits successfully demonstrated that it is a reliable active method for deposit characterization measurements. The CFSDT system was developed by ORNL (managed by Lockheed Martin Energy Research Corp.) at the Oak Ridge Y-12 Plant [managed by Lockheed Martin Energy Systems, Inc. (LMES)] for a defense program for identifying uranium weapons components in storage containers. Its application at ETTP is an example of how a technology developed for defense program needs was used in an environmental restoration project at another Lockheed Martin Energy Systems facility. This technique is also useful for measuring deposits in process pipes at other facilities that handle UF_6 and that carry out other processes with nuclear material.

1. INTRODUCTION

The U. S. Department of Energy (DOE) initiated the Deposit Removal Project in the East Tennessee Technology Park (ETTP) to address the issue of safe removal of the hydrated uranyl fluoride deposits from process pipes and equipment in the Oak Ridge K-29 Building of the former Oak Ridge Gaseous Diffusion Plant (ORGDP). The deposits developed inside the pipes, during operation or after shutdown, from moist air leakage into the uranium hexafluoride (UF_6) gas, where uranyl fluoride (UO_2F_2) became hydrated from the moisture in the air. In general, the UO_2F_2 deposits can be described as a $UO_2F_2 \cdot nH_2O$ mixture, where n depends on the level of hydration. Because hydrogen moderates neutrons, the hydrogen content [i.e., the ratio of H to U (H/U)] is one of the key parameters that controls the nuclear criticality safety of the deposit. Earlier nondestructive assay (NDA) measurements by gamma-ray spectroscopy at K-29 identified two deposits as the first and third largest deposits in the K-29 Building [Ref. 1]. The first deposit was found in the Unit 2, Cell 7, B-Line Outlet process pipe (Fig. 1.1), called the "Hockey Stick," a 17-ft-long, 24-in.-OD pipe in which the deposit was estimated by gamma-ray spectroscopy to have a uniformly distributed uranium mass of 1,300 kg (± 50% uncertainty) at 3.34% ^{235}U enrichment (± 50% uncertainty). The second deposit was found in the Unit 2, Cell 6, A-Line Outlet (Fig. 1.2), called the "Tee-Pipe," which is a 30-in.-OD process pipe with a 10-ft-long horizontal section combined with a 24-in.-OD riser section that is about 12 ft long. The estimated uranium mass in the Tee-Pipe process pipe identified by gamma-ray spectrometry was approximately 240 kg (± 50% uncertainty) at 3.4% ^{235}U enrichment (± 20% uncertainty).

The main concern for nuclear criticality safety was that both process pipes may have had enough ^{235}U to result in a nuclear criticality accident [Ref. 2], if the H/U is high enough (for example, for a stable deposit compound, H/U = 4), and if the deposit distribution achieves a favorable geometry. The earlier measurements made use of passive neutron and gamma-ray interrogation techniques for determining the deposit profiles and their distribution along the process pipes. The gamma-ray technique is susceptible to surrounding background radiation and self-shielding of the gamma rays by the deposits; therefore, the measurements could only determine that the deposits were uniform, but they could not yield an estimate of the correct thicknesses of the deposits nor their distribution.

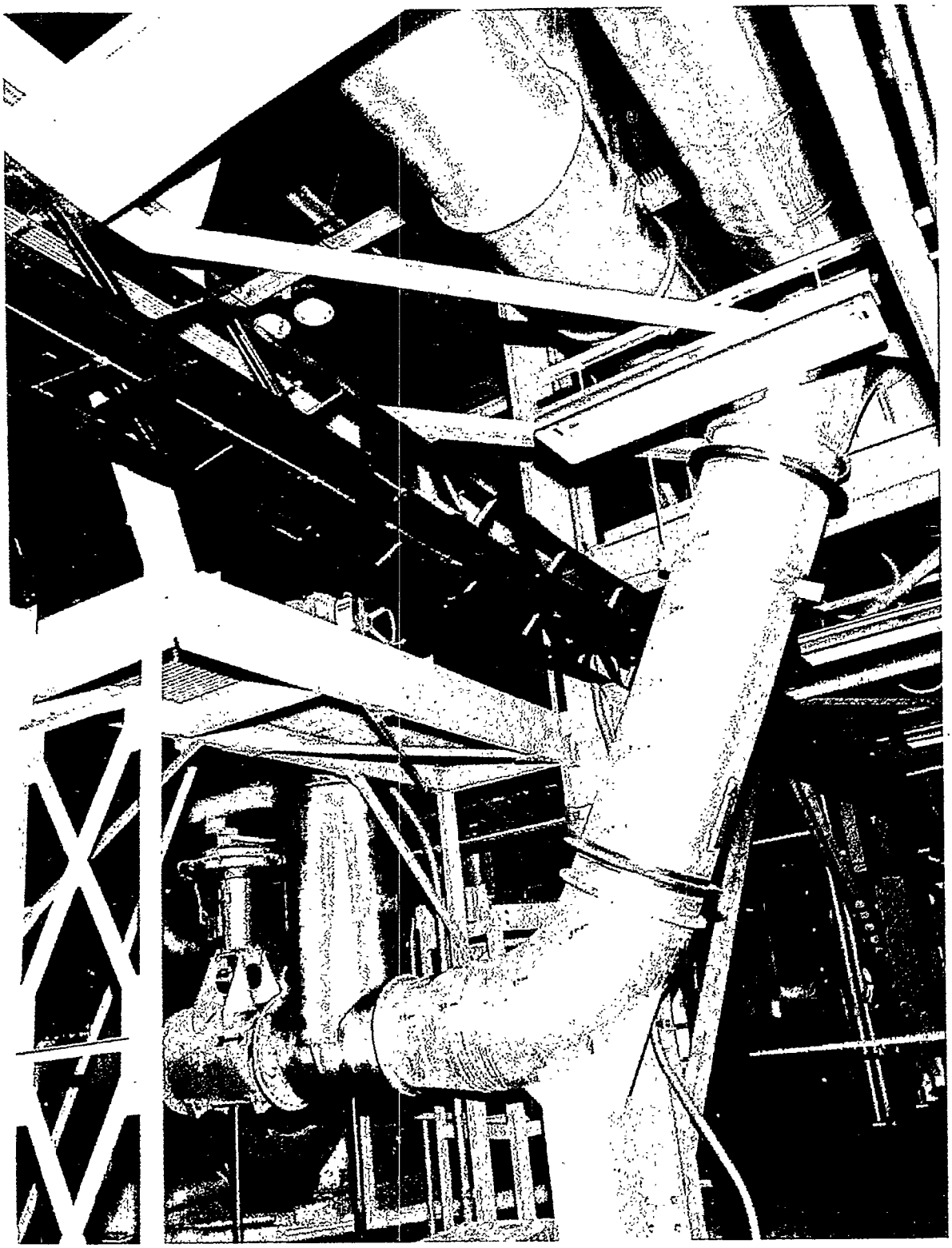

Fig. 1.1. Unit 2, cell 7, B-line outlet process pipe, called the Hockey Stick.

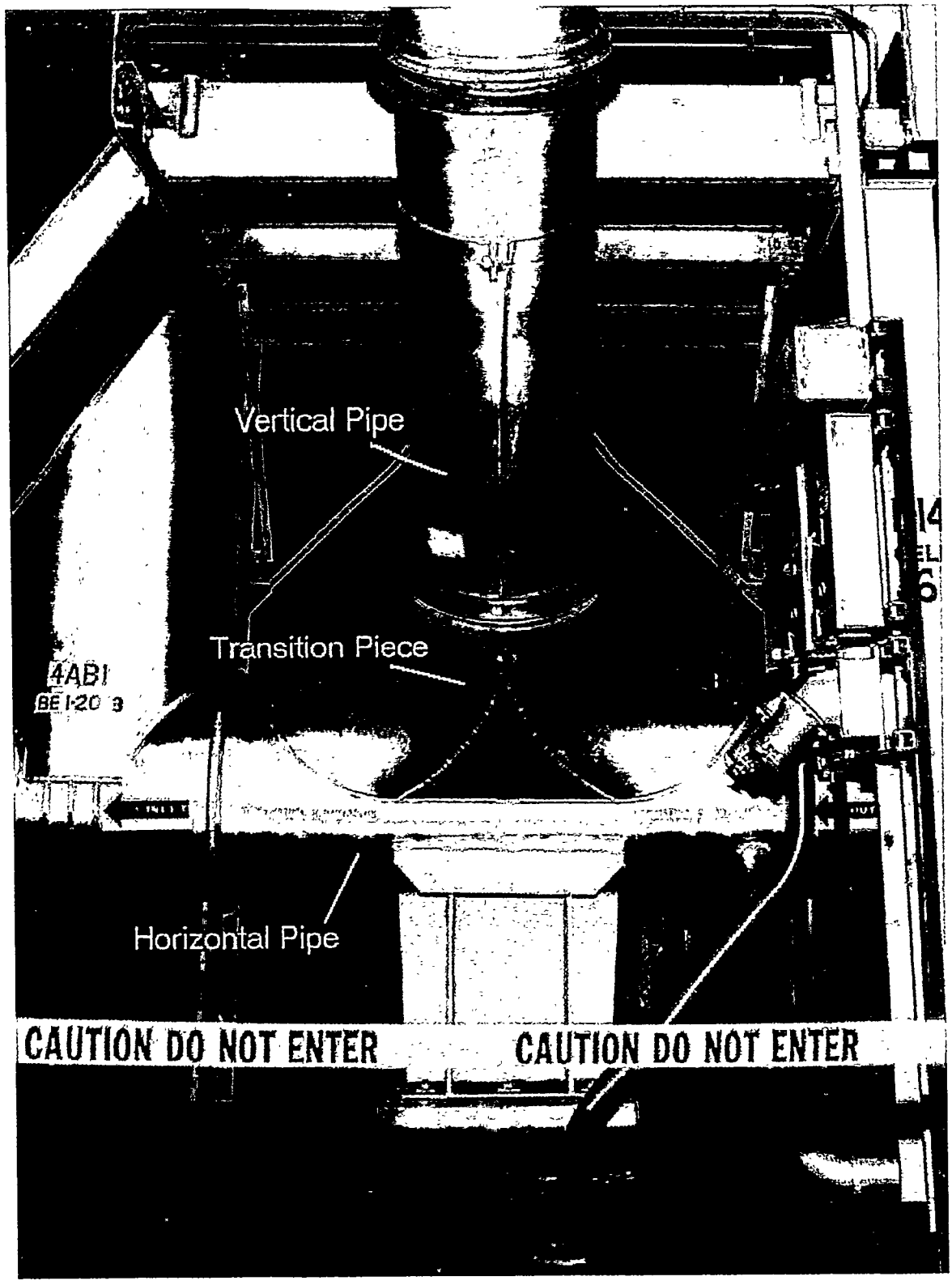

Fig. 1.2. Unit 2, Cell 6, A-line outlet process pipe, called the Tee-Pipe.

Measurements of the spatial distribution of the deposits, the moderation level resulting from hydration of the deposits, and the total uranium mass of the deposits were needed. Furthermore, to address their nuclear criticality safety concerns, the Deposit Removal Project team also planned to survey the inside of the deposit pipes intrusively with a fiber-optic camera introduced into the deposit pipes through holes drilled before the deposit removal process began. To perform this task safely and effectively, the Deposit Removal Project team requested that Oak Ridge National Laboratory (ORNL) characterize these two largest deposits by an active neutron and gamma-ray interrogation method. The ^{252}Cf-source-driven transmission (CFSDT) time-of-flight [Ref. 3] measurements of neutrons and gamma rays from an external californium source were implemented and were used successfully to perform these deposit characterization measurements. This active interrogation method with its hardware was developed by ORNL (managed by Lockheed Martin Energy Research Corp.) as a Nuclear Weapons Identification System (NWIS) for the Oak Ridge Y-12 Plant [managed by Lockheed Martin Energy Systems, Inc. (LMES)] for identification of nuclear weapons components in containers. Its application at ETTP is an example of how a technology developed for defense program needs was used at another DOE facility operated by LMES. CFSDT characterization of the K-29 deposits and any future deployment of this measurement technology benefit both DOE and LMES as additional returns from the original capital investment.

In this report the measurement technique and the results obtained from the deposit characterization measurements are discussed. The report is organized as follows. In Sect. 2 the measurement methodology and analysis techniques are presented for obtaining the deposit profile, the H/U, and the total uranium mass of the deposit. The results of the deposit measurements on the Hockey Stick and Tee-Pipe are given in Sects. 3 and 4, respectively. In Sect. 5 the visual deposit observations and the general discussions are presented; the conclusion follows in Sect. 6.

2. MEASUREMENT METHOD AND ANALYSIS

The main objectives of the hydrated UO_2F_2 deposit characterization measurements in the process pipes were to (1) image the deposit profile, (2) determine the moderation [i.e., the hydration level (or H/U)] of the deposits, and (3) determine the total uranium mass of the deposits, all of which are required for nuclear criticality safety evaluation. The measurements discussed in this section are based on an active technique in which an external fission neutron and gamma-ray source is placed outside the process pipe and the transmitted neutrons and gamma rays are measured on the opposite side of the pipe. As discussed later in detail, while the attenuation of neutrons and gamma rays strongly depends on the deposit thickness, the interaction probabilities of neutrons and gamma rays with the deposits are distinct from each other. The neutron interaction probability for the high-energy (>6-MeV) neutrons is not very sensitive to the deposit hydration (or H/U) whereas gamma-ray interaction strongly depends on the density or the level of hydration. The ability to differentiate between neutrons and gamma rays transmitted through the deposit material by timing provides a neutron and gamma-ray radiograph of the deposit for measuring the deposit thickness and the hydration (or density).

The californium-252 (^{252}Cf) isotope was used as an external interrogation fission source because spontaneous fission of ^{252}Cf provides both neutrons and gamma rays from a relatively low-strength source (537 μCi/μg). Typically, a ^{252}Cf source emits an average number of 2.32×10^6 prompt neutrons/s/μg with an average neutron energy of 2.13 MeV, and 4.78×10^6 prompt gamma rays/s/μg with an average gamma-ray energy of 0.88 MeV. (See Table 2.1 for the general characteristics and Fig. 2.1 for the energy spectra of neutrons [Ref. 4] and gamma rays of the ^{252}Cf source [Ref. 5]).

The neutrons and the gamma rays transmitted through the process pipe were measured within a time resolution of <2 ns with an organic plastic scintillator for neutrons that undergo elastic scattering with protons (proton-recoil scintillation), and gamma rays that undergo the usual process of interactions with electrons as the dominant energy-loss mechanism.

Table 2.1. Nuclear characteristics of ^{252}Cf source[a]

Parameter	Value
Half-life	2.65 years
Specific activity	537 μCi/μg
Spontaneous fission rate	6.14×10^5 fissions/s/μg
Average number of neutrons from fission	3.771
Average neutron energy	2.13 MeV (see Fig. 2.1 for energy spectrum)
Rate of neutron emission	2.32×10^6 neutrons/s/μg
Rate of gamma-ray emission	4.78×10^6 gamma rays/s/μg
Average number of gamma rays from fission	7.79
Average gamma-ray energy	0. 88 MeV (see Fig. 2.1 for energy spectrum)

[a] A. Prince, "Nuclear and Physical Properties of ^{252}Cf," *in Proc. of Symposium on Californium -252, CONF-681032* (ANS, New York, 1968), page 23.

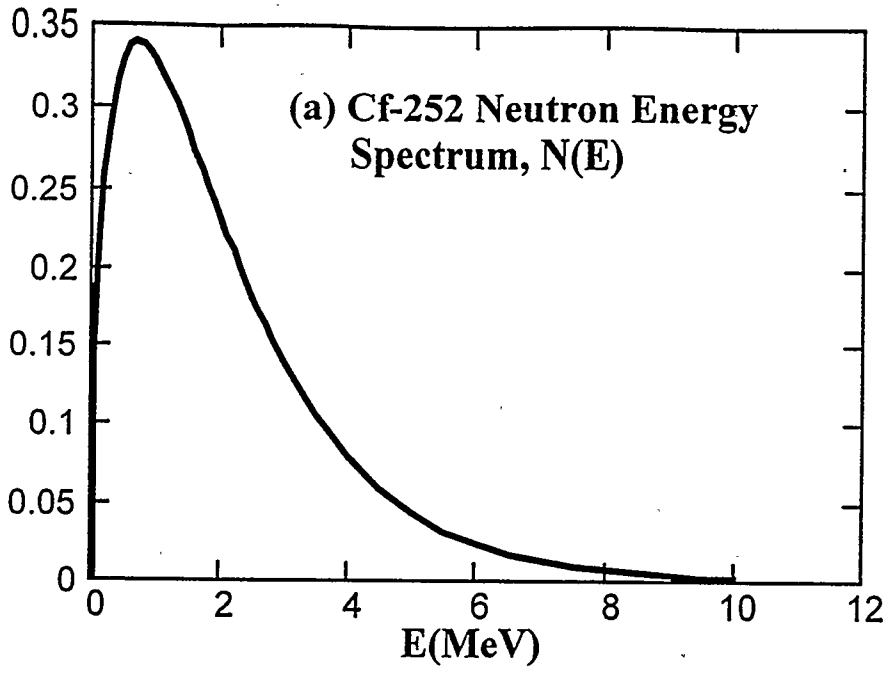

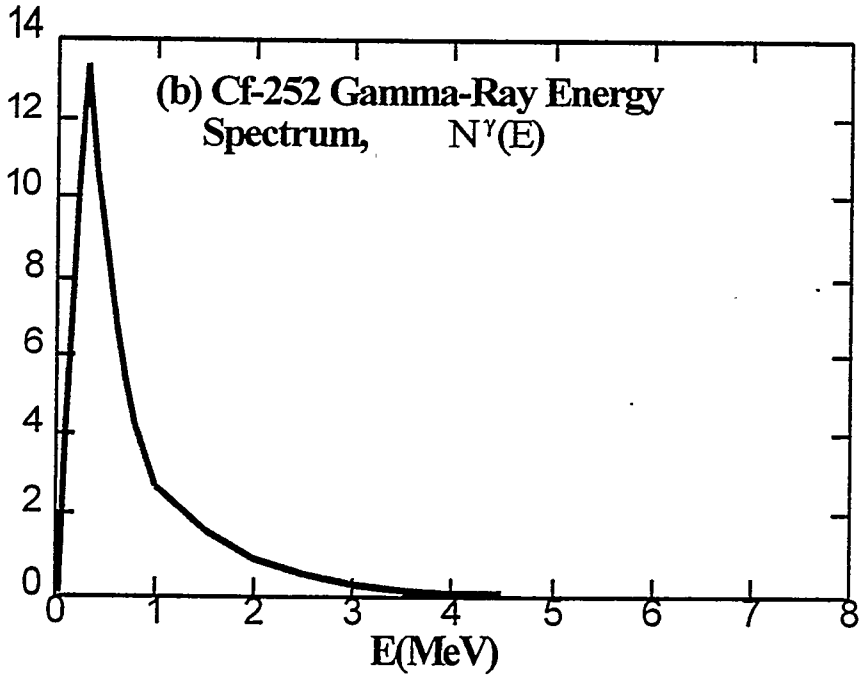

Fig. 2.1. Energy spectra of neutrons and gamma rays of the ^{252}Cf source.

By measuring the time-of-flight (TOF) of the neutrons across the process pipe, the neutron energy distribution can be obtained. The TOF measurement is accomplished by using the ^{252}Cf source in a parallel-plate ionization chamber for obtaining a timed source of prompt neutrons and gamma rays resulting from the spontaneous fission of ^{252}Cf. The timed signal for the start of the fission is known, and the TOFs of the prompt fission neutrons and the prompt gamma rays are measured. The transmitted neutrons (or gamma rays) arrive at the detector located across the process pipe as shown in Fig. 2.2. This time-correlated measurement signature, or the time domain signature (shown in Fig. 2.3), is equivalent to the right half of the cross-correlation function between the ^{252}Cf source (the ionization chamber as detector #1) and the detector (as detector #2) cross correlation function between detector #2 and the Cf source. This is also equivalent to a randomly pulsed neutron measurement [Ref. 3]. Therefore, this time-correlated active technique is called a ^{252}Cf-source-driven transmission (CFSDT) measurement. A typical cross correlation function between detector #2 and the Cf source as a function of time is shown in Fig. 2.3. The cross correlation function between detector #2 and the ^{252}Cf source counts are normalized to the number of ^{252}Cf fissions, and the TOF is measured from the start of the ^{252}Cf fission, which is at time zero in Fig. 2.3. The first peak is for transmitted gamma rays and the second peak is mainly for neutrons. The time spread of the gamma-ray peak is caused by the finite time resolution of the measuring system.

The Nuclear Weapons Identification System (NWIS) processor, which is being developed at the Oak Ridge Y-12 Plant [Refs. 6, 7] for identification of nuclear weapons components in containers, is used to sample and record the input detection pulses from the detector and the source. The cross correlation function between detector #2 and the ^{252}Cf source is then obtained [Ref. 8] from the source and detector #2 measurements.

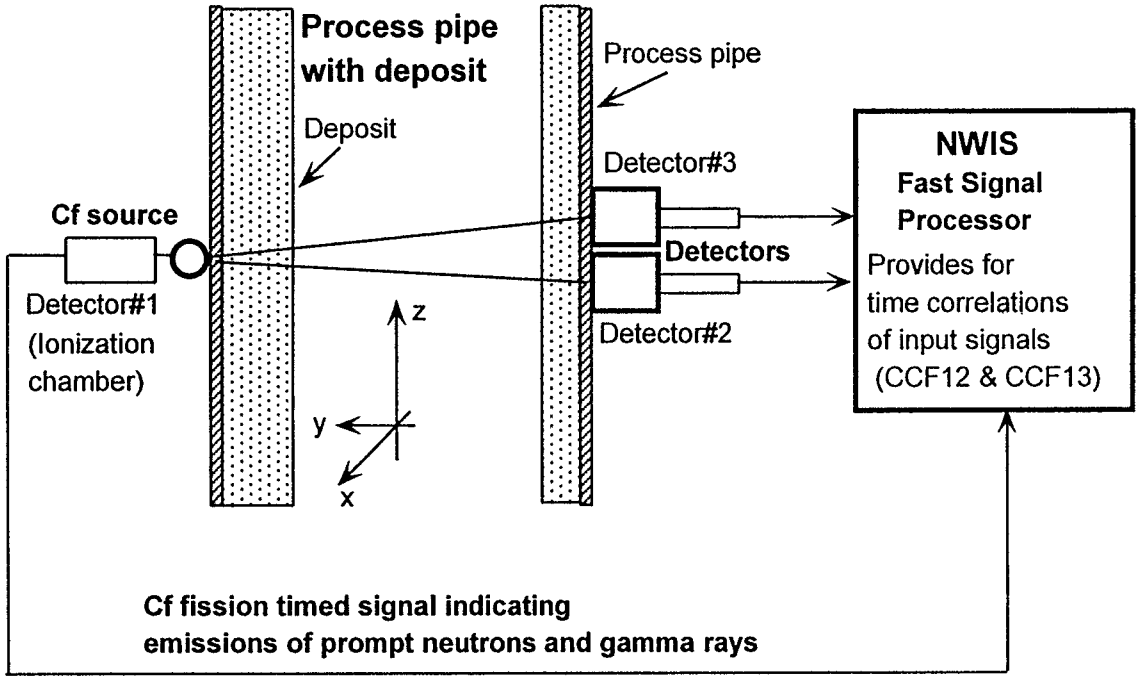

Source: Neutrons and gamma rays from spontanous Cf-252 fission penetrate deposit material.
Detectors: Transmitted particles are detected by organic (plastic) proton-recoil scintillators.

Fig. 2.2. Schematic of measurement configuration placed on a process pipe shown together with the fast signal processor NWIS in use.

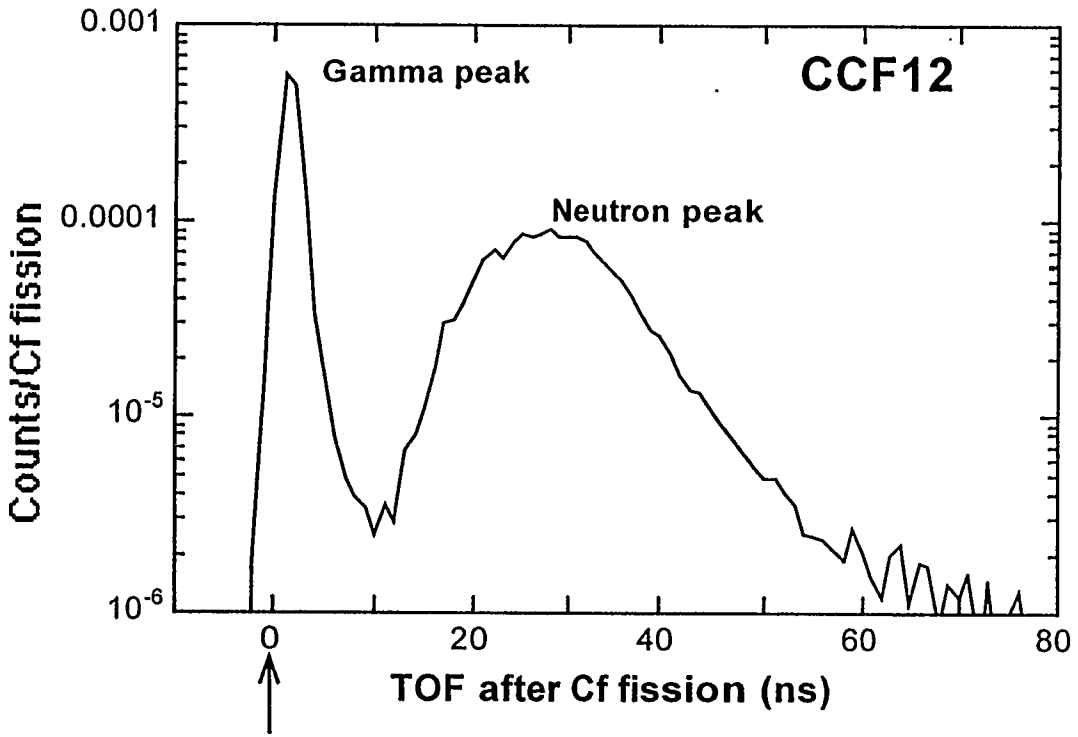

Fig. 2.3. The time-correlated measurement signature, or the time domain signature, shown for a typical CFSDT TOF data. This is equivalent to the right half of the cross-correlation function (CCF12) between the ^{252}Cf source (as detector #1) and the detector (as detector #2).

2.1. NWIS Measurement Hardware

The NWIS measurement hardware [Ref. 9] is comprised of a ^{252}Cf source contained in an ionization chamber, a pair of detectors for measuring neutrons and gamma rays, detector electronics, data-processing boards, and a computer for data acquisition and display. Fig. 2.4 is a photograph of the NWIS processor displayed for a measurement with a weapons component in a container at the Oak Ridge Y-12 Plant; a block diagram of the NWIS configuration is given in Fig. 2.5. The source and two detector signals are input to electronic modules for processing, and then the signals are input to the data-processing components for data acquisition. Electronic pulses from the source and detectors are sampled by the NWIS in time with a fast data acquisition processor, which samples at 1-GHz rates the input detection pulses from up to five detectors producing time-dependent source and detector responses. In these measurements, the time-dependent responses are for 512 time intervals of 1-ns width. Several statistical signatures are obtained from these time-dependent signals [Ref. 8].

The ^{252}Cf source, as shown in Fig. 2.6, is part of a parallel-plate ionization chamber, 1 in. OD and 1.25 in. long, with approximately 0.6 μg of ^{252}Cf electroplated onto one plate [Ref. 10]. The ^{252}Cf-source ionization chamber, which requires a 200-VDC power supply, produces a timed electrical pulse each time the source emits neutrons and gamma rays produced by the spontaneous fission. A high-gain fast amplifier increases the amplitude of the pulse from the source ionization chamber. The high-gain fast amplifier requires 15-VDC to power the amplifier and produces an electrical pulse as output. The output of the source high-gain fast amplifier is input to an ORTEC-935 constant fraction discriminator [Ref. 11]. The constant fraction discriminator eliminates unwanted pulses above selected thresholds and produces an output timing pulse. The timing pulse is independent of the incoming signal height, which has constant amplitude and adjustable width. The output of the constant fraction discriminator is input to an ORTEC-425 delay module [Ref. 11], which is used to delay the arrival time of pulses from the source to the data processor. The discriminator and the delay module are contained within a commercially available nuclear instrument module (NIM) bin, which supplies power to the components.

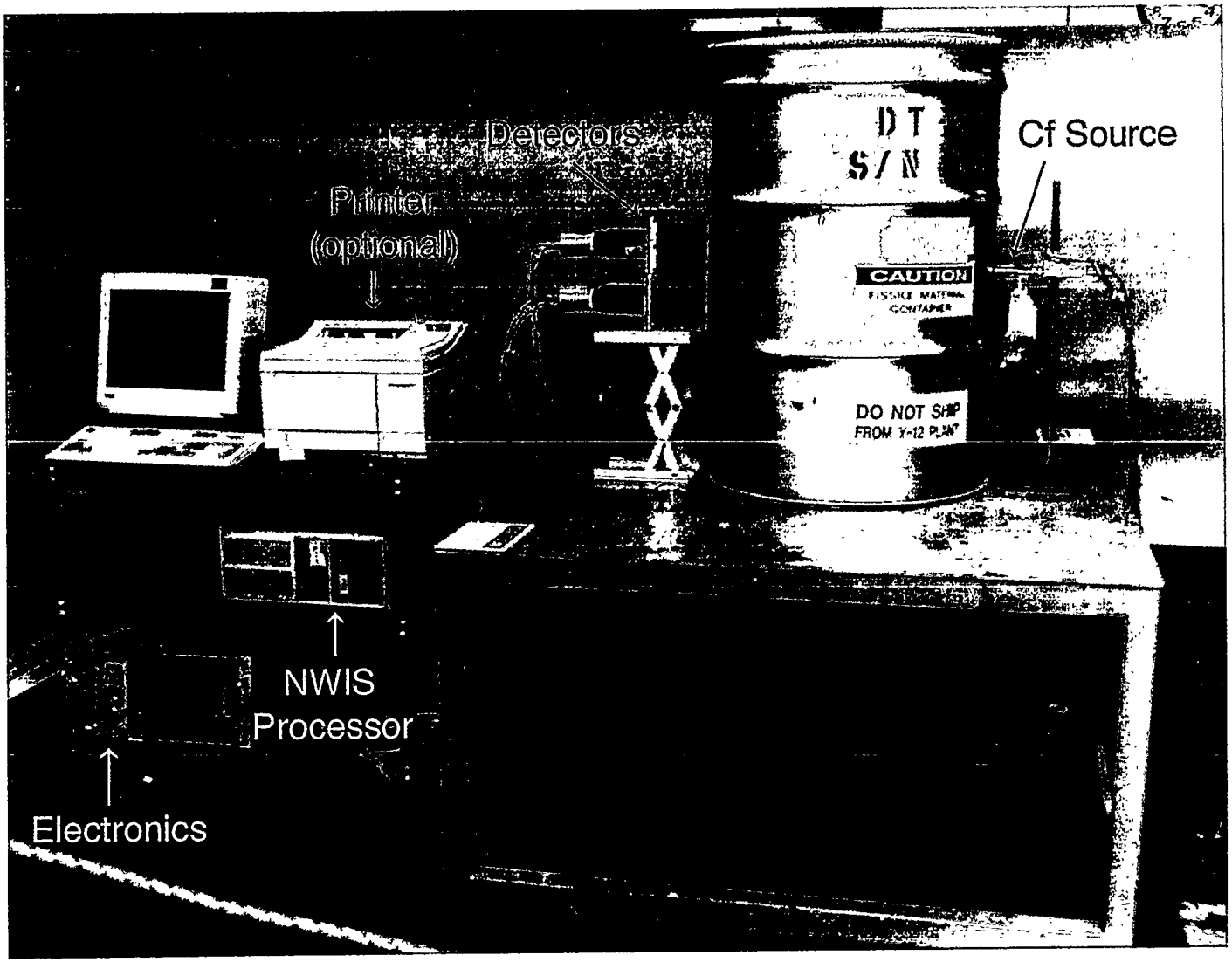

Fig. 2.4. Photograph of NWIS processor and typical measurement configuration.

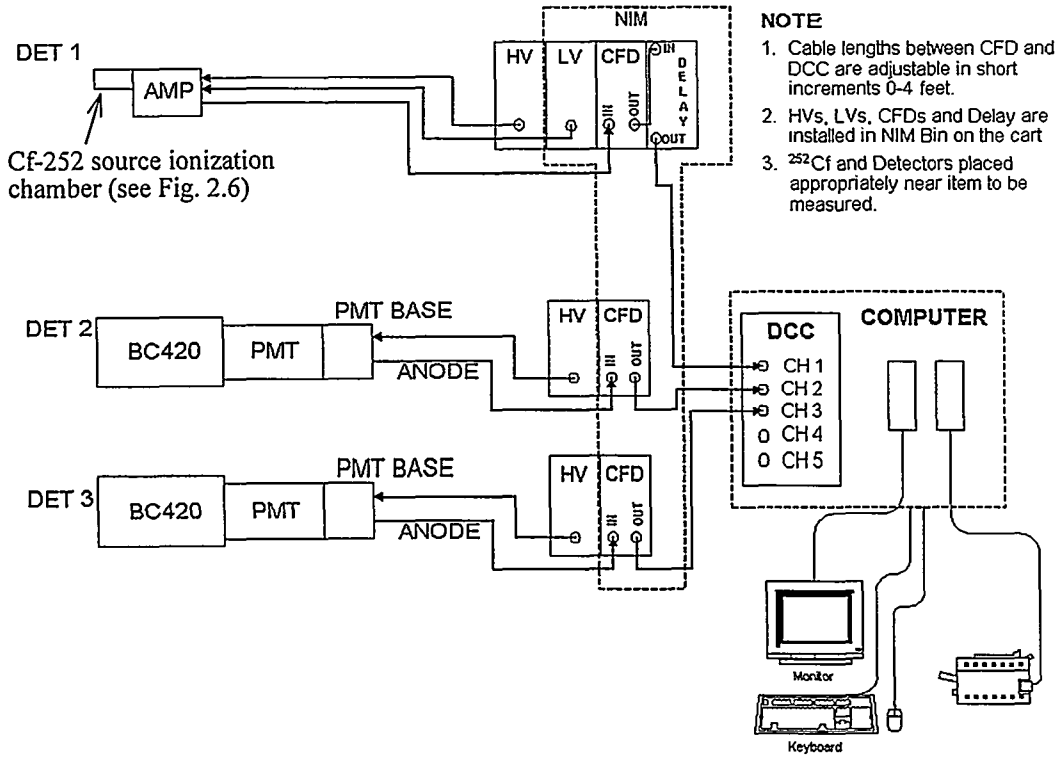

Fig. 2.5. Schematic of NWIS measurement configuration.
(Here HV and LV donate the high and the low voltage power supplies, respectively.)

The two detectors are commercially available organic plastic scintillators that measure fast neutrons and gamma rays. The detectors are 4-in.-thick BC-420 plastic scintillators (manufactured by BICRON [Ref. 12]) mounted on a photomultiplier tube. The scintillators are 3.75 × 3.75 in. square and are enclosed in a 0.125 in. thick and 4 × 4 in. square aluminum can that has a 0.25-in.-thick lead shield on the sides. As shown in Fig. 2.2, two NWIS detectors are placed side-by-side along the process pipe such that the distance between the centers of the detectors is 4.5 in. A photograph of the detector used for the measurements is shown in Fig. 2.7. Neutrons and gamma rays interact within the detector and produce light from the scintillation process. The light is converted into an electrical pulse by means of a photomultiplier tube and a photomultiplier tube base that provides power to the photomultiplier tube. An ORTEC-556 power supply [Ref. 11] is used to power the photomultiplier tube. The output of the photomultiplier tube anode signal is input to a constant fraction discriminator (CFD); the output of the constant fraction discriminator is input to the data processor, as shown in Fig. 2.5. The constant fraction discriminator eliminates unwanted pulses below an adjustable threshold level and produces an output pulse that has constant amplitude and fixed width.

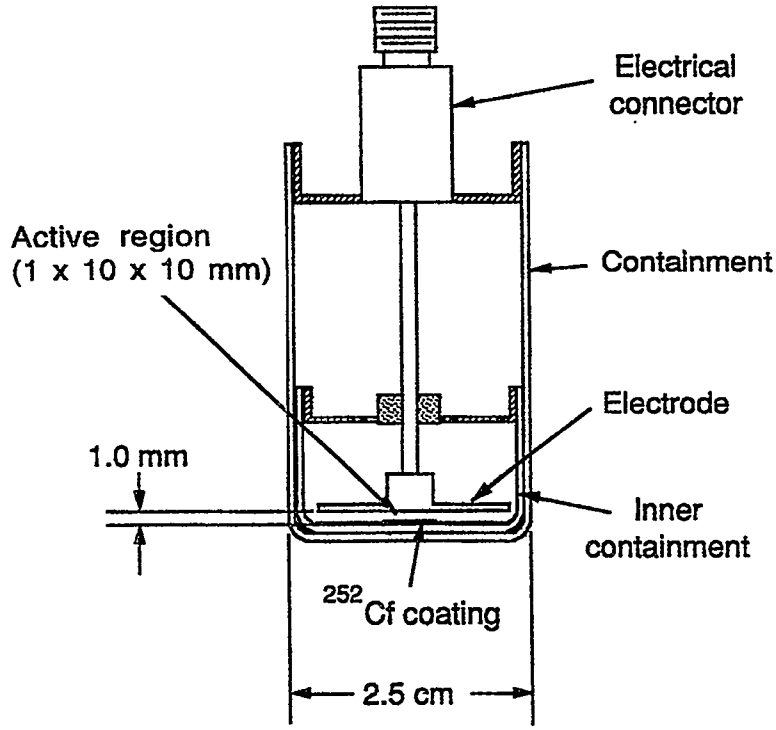

(a)

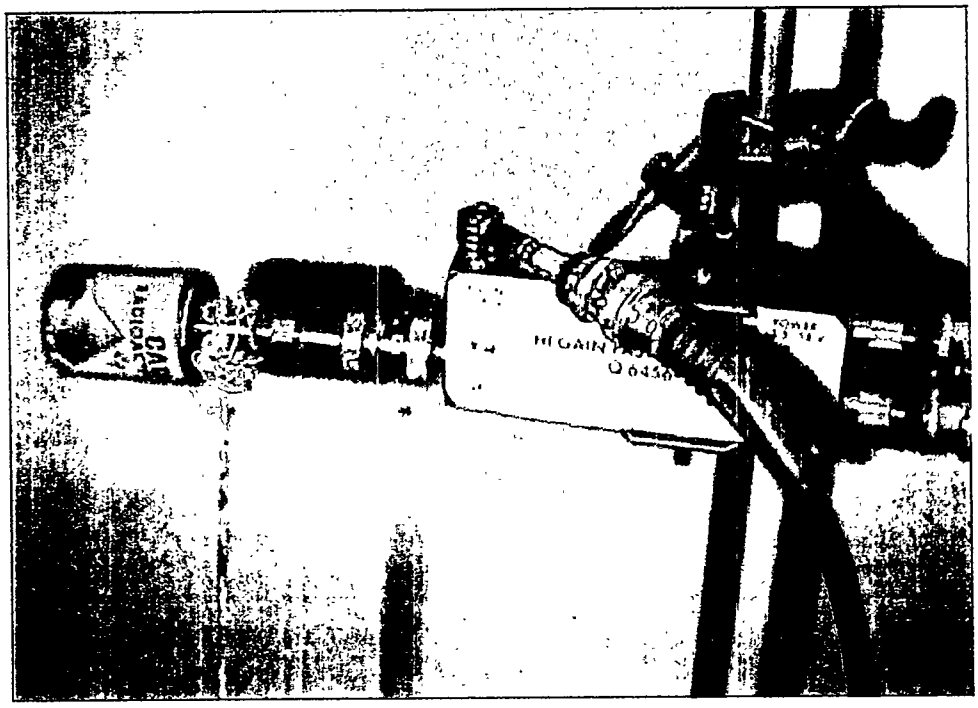

(b)

Fig. 2.6. (a) Sketch of ^{252}Cf fission source ionization chamber. (b) The ^{252}Cf fission source ionization chamber connected to the high-gain fast amplifier.

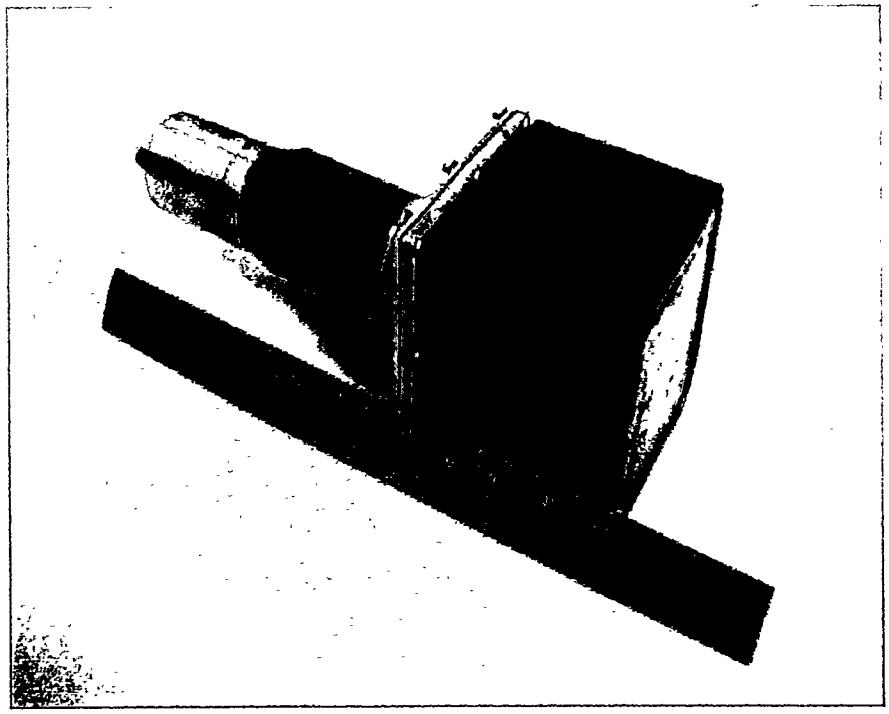

Fig. 2.7. Photograph of 4 × 4 in. plastic scintillation detector.

The NWIS data acquisition components consist of two electronic boards that are installed in a commercially available personal computer. The data capture and compression module is located on one of the electronics boards and is used to acquire the signals from the constant fraction discriminators. The output of the data capture and compression (DCC) module is input to a data-processing component that inputs the data to the computer. The computer is used to process the signals from the data acquisition components. The computer is also used to start and stop the data acquisition and is used process and display the data. A data acquisition driver is provided so that the computer can communicate with the data acquisition board. The computer's peripherals include a monitor, keyboard, mouse, and printer.

2.2. Measurements of Deposit Profile

The CFSDT deposit profile measurements were performed by placing the ^{252}Cf source on one side of the deposit pipe and one or more detectors on the other side as shown in Fig. 2.2. For the profile measurements, only the neutron TOF distribution is used. The measured intensity of neutrons $I(E)$ with energy E, transmitted through the process pipe, is given by the usual exponential attenuation law [Ref. 13]:

$$I(E) = I_{air}(E)\exp[-\Sigma_t(E)d - 2\Sigma_p w] = I_0\exp[-\Sigma_t(E)d], \quad (1)$$

where $I_{air}(E)$ is the intensity of neutrons measured in air, $\Sigma_t(E)$ and Σ_p are the total macroscopic neutron cross sections of the deposit and the pipe, respectively, d is the total deposit thickness along the measurement path as illustrated in Fig. 2.2, w is the thickness of the pipe. Here $I_0 = I_{air}(E)\exp[-2\Sigma_p w]$ is the intensity of neutrons transmitted through the empty process pipe. Both $I(E)$ and $I_0(E)$ are measured, $I(E)$ with the process pipe with the deposit and $I_0(E)$ with an empty process pipe.

The value of $\Sigma_t(E)$ for a hydrated UO_2F_2 deposit is known as a function of energy and for various values of H/U. The energy-dependent total macroscopic neutron cross section of a hydrated UO_2F_2 deposit for assumed H/U values ranging from 1 to 6 [Ref. 14] is shown in Fig. 2.8. At low neutron energies, Σ_t is sensitive to both changes in the hydration level and variations in the neutron energy, denoted by the large separation between the three neutron cross sections at the low energy (0.5, 1.0, and 1.5 MeV). At high energies (above 6 MeV),

the neutron cross sections are essentially constant with H/U. Moreover, the neutron cross sections are not strong functions of the neutron energy. This feature becomes important because it demonstrates that timing uncertainties (< 2 ns), which are related to the neutron energy, will not have a strong effect on the calculation of the deposit material properties.

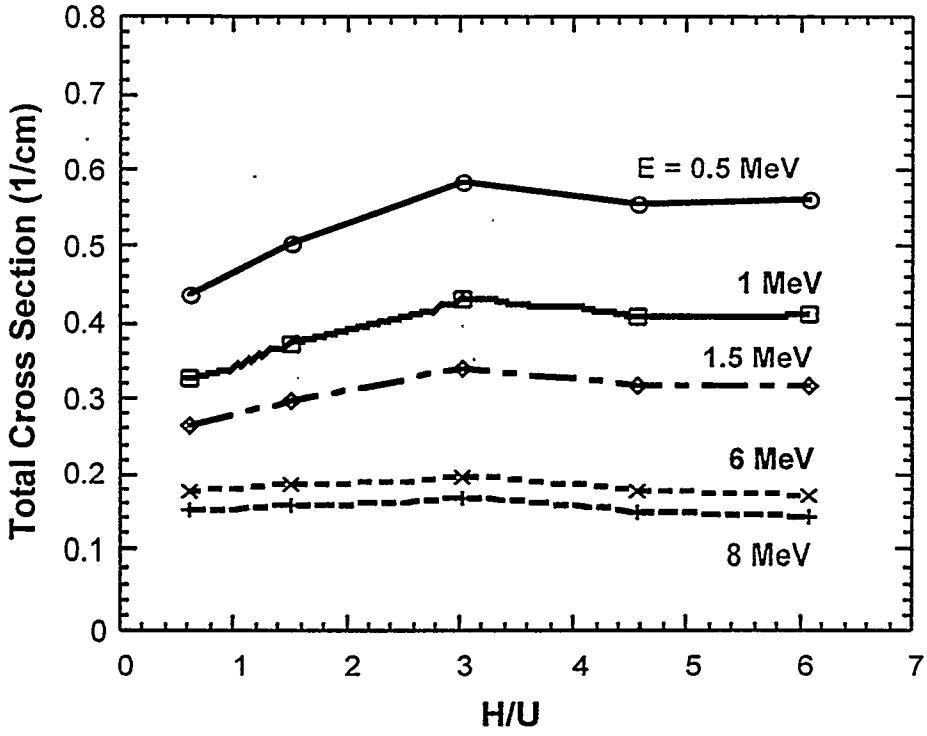

Fig. 2.8. Energy-dependent total macroscopic neutron cross section of a uranyl fluoride deposit as a function of H/U.

2.2.1. Effects of deposit geometry and scattering

For Eq. (1) to be valid, the total neutron cross section at high energy must be known and the scattering of neutrons from the surrounding deposit into the detectors must be minimized. This is accomplished by using relatively higher-energy neutrons ($E \sim$ 8 MeV) in the spectrum because scattering would reduce the neutron energy below 8 MeV so that neutrons that scatter into the detector would be counted higher than the time corresponding to 8 MeV. Furthermore, the population of the higher-energy neutrons from the ^{252}Cf fission is significantly lower (see Fig. 2.1).

MCNP-DSP Monte Carlo code calculations [Ref. 15] were used to verify the assumption that measurements of the deposit thickness from high-energy neutrons are not sensitive to geometry or scattering effects. MCNP-DSP models the stochastic nature of particle interactions in a medium in which space, angle, and energy are continuous variables. The code tracks both neutrons and photons in a manner that simulates the CFSDT measurements. Furthermore, the MCNP-DSP code utilizes a probability distribution for the number of prompt neutrons produced per ^{252}Cf fission to achieve the statistical fluctuations found in nature. The code also includes a dual-particle source that produces neutrons and photons having the multiplicities and energy distributions of ^{252}Cf. MCNP-DSP has been widely benchmarked and has shown to be an excellent tool for planning experiments in criticality safety, safeguards, NDA, and arms control verification [Ref. 16].

Figure 2.9 shows two potential measurement configurations for an assumed distribution of material in a process pipe having a 24-in. OD as in the Hockey Stick. Because the deposit distribution is unknown, it must be determined whether the measurement results will depend on the position of the source and detector with respect to the deposit. These configurations (shown in Fig. 2.10) were evaluated by three separate MCNP-DSP calculations to quantify potential sensitivities to geometry effects. All three calculations assumed a constant process pipe wall thickness (as in the Hockey Stick), a constant separation between source and detector, and a constant deposit thickness. The only parameter modified in the calculation is the location of the deposit in the process pipe: (1) close to the source, (2) close to the detector, or (3) splitting the distance between the two.

Figure 2.11 shows the time distribution calculated by MCNP-DSP of counts in the detector after the spontaneous fission of ^{252}Cf for each geometry studied. The data have been arbitrarily modified on the time axis so that the gamma-ray peak is placed at 25 ns for clarity of the figure. Based on a separation distance of 24 in. between the source and detector, the rising portion of the neutron response between 38 and 42 ns corresponds to the arrival of neutrons 13 to 17 ns after the source fission. This arrival time corresponds to neutron energies between 6.7 and 11.5 MeV with the midpoint of 15 ns corresponding to neutron energies of $E = 8.5$ MeV. The portion of the neutron response is essentially invariant to the deposit location, indicating that the assumptions are correct and that the measured data can be interpreted without having to determine absolutely the deposit location with respect to the source or detector.

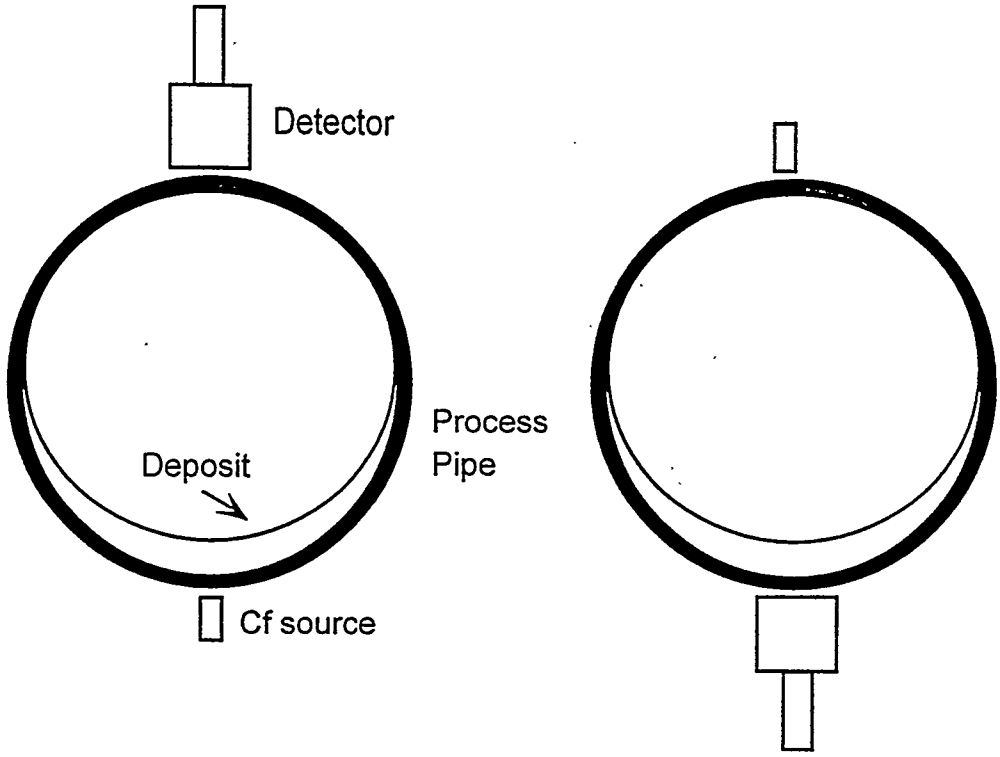

Fig. 2.9. Assumed deposit material profiles in the process pipe.

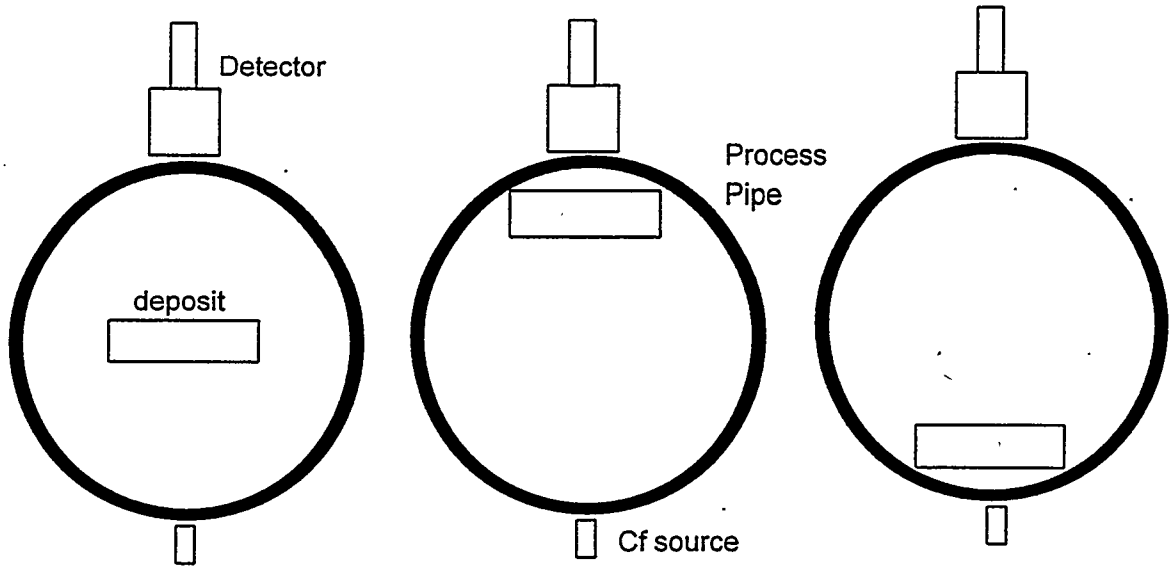

Fig. 2.10. Process pipe cross section view of the MCNP-DSP models for the study of geometry effects of source and detector locations with respect to pipe deposit.

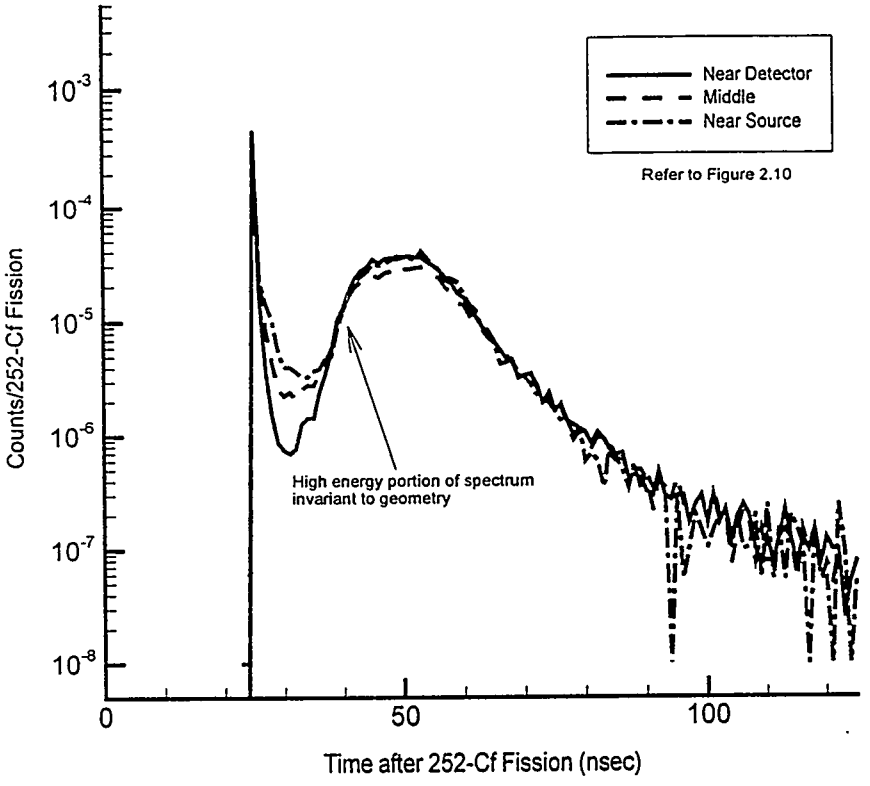

Fig. 2.11. Calculated TOF signatures of three deposit locations with respect to source and detector (Fig. 2.10), indicating that the rising part of the signature, the high energy neutron distribution, is invariant with the location of the deposit in the pipe.

2.2.2. Determination of deposit thickness and profile

With a neutron energy of 8.5 MeV selected, the approximations of Eq. (1) are valid and the total deposit thickness is obtained as

$$d = -\ln(I/I_O)/\Sigma_t \ , \qquad (2)$$

where Σ_t (E = 8.5 MeV) is given in Fig. 2.12 as a function of H/U [Ref. 14]. As seen from this figure, the variation of Σ_t is less than ±14% for a broad range of H/U values (0.6–16). To determine the deposit thickness from Eq. (2), the effects of the process pipe need to be eliminated by making use of the empty-pipe measurements for obtaining I_O. The measurement of I_O is referred as a "calibration measurement."

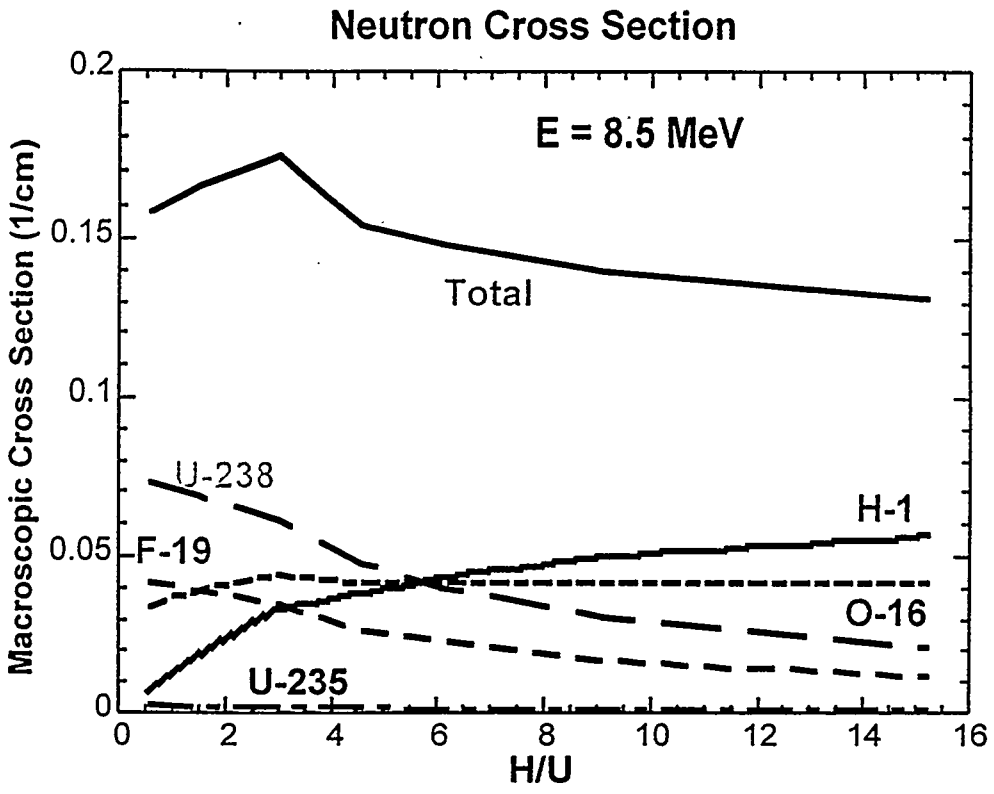

Fig. 2.12. Total macroscopic neutron cross section at $E = 8.5$ MeV for a uranyl fluoride deposit as a function of H/U.

The deposit thickness in a given location on the process pipe is measured as follows. The cross correlation function between the ^{252}Cf source and the detector #2 (see Fig. 2.2) is obtained from the NWIS measurements for the intensity of transmitted neutrons $I(E)$ through the process pipe containing the deposit. Similarly, $I_0(E)$ is obtained from the empty-pipe calibration measurements. Thus the value of I/I_0 at 8.5 MeV is obtained because the physical separation between the source and the detector is the same and known. In the case of detector #3 (see Fig. 2.2), the cross correlation function between detector #3 and the source is also utilized for the measurements. The deposit thickness at the measurement location is then determined from Eq. (2) using I/I_0 from this transmission measurements.

The deposit image (the spatial profile) for a given location on the process pipe is obtained by performing a number of vertical transmission measurements, in the direction of y-axis, and horizontal transmission measurements, in the direction of x-axis, by moving the position of the source and the detector simultaneously on the process pipe as shown in Fig. 2.13. The total deposit thickness in the horizontal direction $d_x(y)$ and the total deposit thickness in the

vertical direction $d_y(x)$ are estimated from these transmission measurements (I/I_O). The composite image of the deposit in the process pipe is constructed from $d_x(y)$ and $d_y(x)$. The result is further verified by the source and the detector rotation measurements, that give the total (radial) deposit thicknesses, around the process pipe, as shown in Fig. 2.1. Moreover, the information about in- ($x < 0$) and-out ($x > 0$) (or right-and-left), up- ($y > 0$) and-down ($y < 0$) [or top- ($y = D/2$) and-bottom ($y = -D/2$), where D is the diameter of the process pipe] symmetries of the deposit profile is immediately seen in the data from the vertical and horizontal transmission scans.

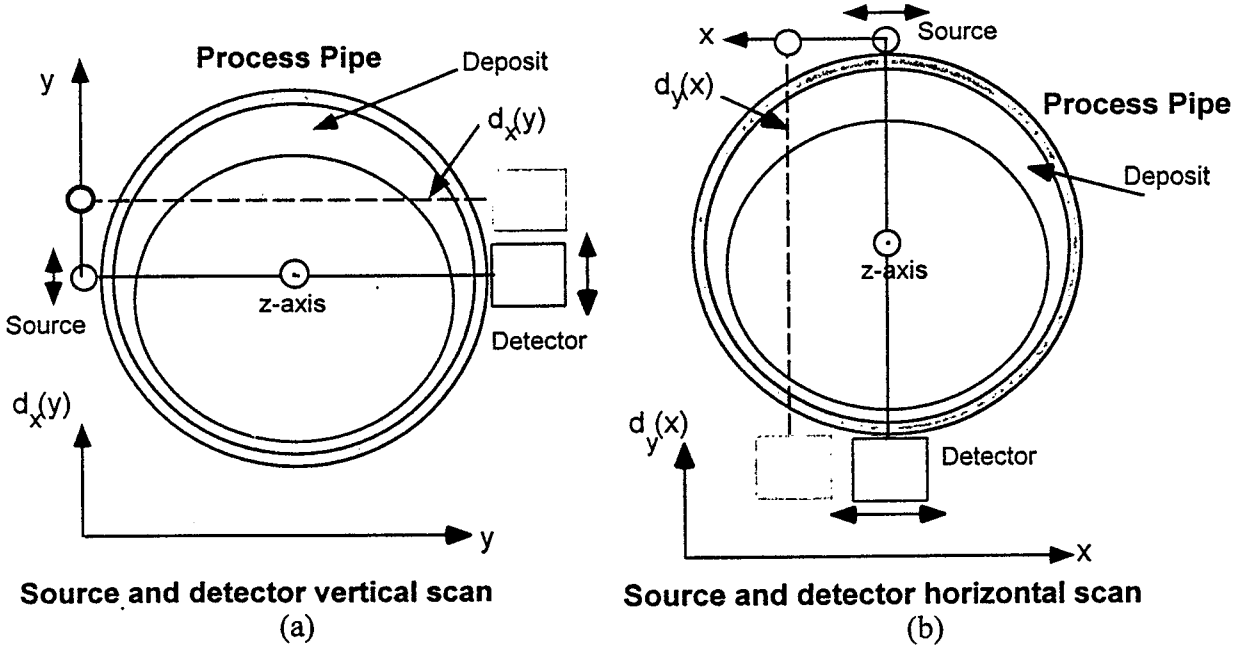

Fig. 2.13 (a) Vertical source and detector scan, (b) horizontal source and detector scan for mapping the deposit profile in the process pipe.

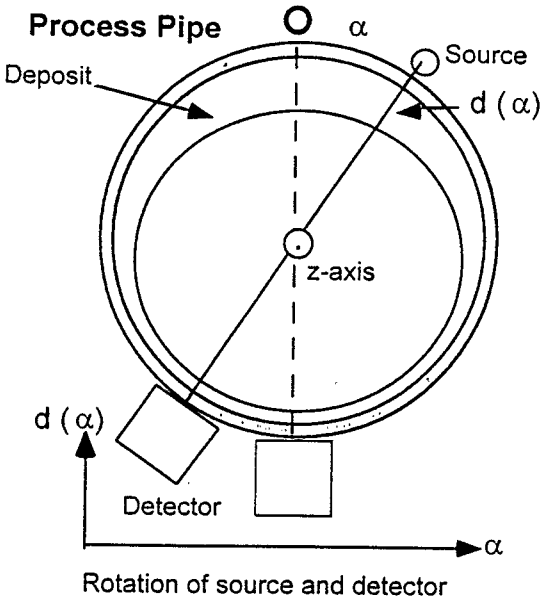

Fig. 2.14. Source and detector rotation measurements around the process pipe.

2.2.3. Measurements of thin deposits

If a very thin deposit or no deposit is present in the process pipe [i.e., if the deposit thickness is d ~ 0, or as seen from Eq. (2), $I/I_O \sim 1$], the accuracies of the deposit and calibration measurements play an important role in determining the thickness or presence of a thin film deposit. The uncertainty in deposit thickness due to the measurements is obtained from Eq. (2) as $\Delta d = \pm\sqrt{2} \times (\Delta I/I)/\Sigma_t$. Here $\Delta I_O/I_O = \Delta I/I$ is used for the relative uncertainties of the measurements. In Fig. 2.15, Δd is plotted as a function of $\Delta I/I$ with the total macroscopic neutron cross section of Σ_t (E = 8.5 MeV) $\approx$ 0.155 cm^{-1} averaged for H/U = 0.16–16 (see Fig. 2.12). If $\Delta I/I = \Delta I_O/I_O \leq \pm 5\%$ is taken as a typical value for the measurements, and if this value is used in Fig. 2.15, the expected uncertainty in deposit thickness is $\Delta d \leq \pm 0.2$ in. Depending upon the absolute value of $I/I_O \sim (1 \pm\sqrt{2} \times \Delta I/I)$ for the measurements of thin deposits, the inferred thickness can become negative due to the measurement uncertainty, especially for the calibration measurements I_O, so that $I/I_O > 1$. During the calibration measurements, even though an empty process pipe that is physically similar to the pipe containing deposits is used, the two pipes cannot be exactly the same. Moreover, locating the measurement system on the calibration pipe cannot match the deposit pipe measurement location exactly. These are possible contributors to the source of uncertainty for these measurements and can lead to nonphysical values of deposit thickness if I is within

uncertainty of I_O. As a result of this possibility only thick deposit measurements could be used for the H/U determination.

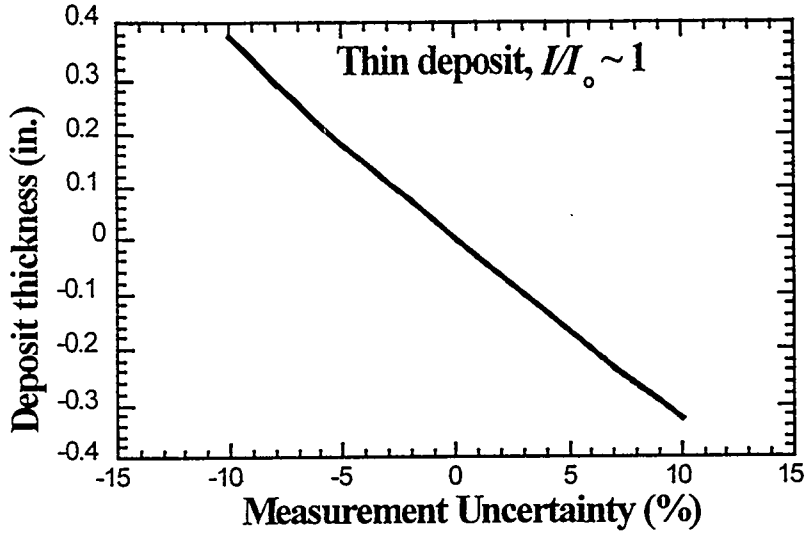

Fig. 2.15. Variations of measured deposit thickness in the presence of thin or no deposit as function of measurement uncertainty.

2.3. Measurements of H/U

The density of the $UO_2F_2 \cdot H_2O$ deposit mixture is directly related to the level of hydration (H/U), in the deposit compound. In general this deposit can be represented as, where H/U = $2n$. As discussed earlier, the interaction probabilities of gamma rays with the deposit is dependent on the density. Moreover, the attenuation of gamma rays also depends on the deposit thickness, which is obtained from the transmission measurements for the 8.5-MeV neutrons. The gamma rays from the ^{252}Cf source have the energy spectrum of $N^{\gamma}(E)$. The mass attenuation coefficient μ_i/ρ_i and the density ρ_i for the individual elements of the hydrated deposit compound are known. The intensity of the transmitted gamma rays through the deposit pipe is expressed as

$$I^{\gamma}(E) = C^{\gamma} N^{\gamma}(E) \exp[-2\mu_w w - \sum_i (\mu_i/\rho_i)\, \rho_i\, d] , \qquad (3)$$

where $N^{\gamma}(E)$ is normalized to unity so that C^{γ} is the number of source prompt gamma rays per fission, μ_w is the linear attenuation coefficient of the process pipe wall material, and w is the wall thickness of the process pipe.

In the ideal case, the time domain signature (the cross correlation function between detector #2 and the source) of the gamma rays is an impulse function, but because the time resolution of the measurement system is finite, the time signature will have a finite broadening in time. Therefore, the total counts for the transmitted gamma rays Γ are related to the total counts integrated over the gamma-ray peak in the cross correlation function between detector #2 and the source, which is the integral of Eq. (3) over the energy spectrum of the gamma rays. Thus the total gamma-ray counts Γ for the deposit pipe is

$$\Gamma_O = \int_O^{\infty} dE\, I^{\gamma}(E) = \int_O^{\infty} dE\, C^{\gamma} N^{\gamma}(E) \exp[-2\mu_w w - \sum_i (\mu_i/\rho_i)\, \rho_i\, d] \,. \qquad (4)$$

The measurement of the cross correlation function between detector #2 and the source for the empty pipe leads to the total counts under the gamma-ray peak as

$$\Gamma_O = \int_O^{\infty} dE\, I_O^{\gamma}(E) = \int_O^{\infty} dE\, C^{\gamma} N^{\gamma}(E) \exp[-2\mu_w w] \,. \qquad (5)$$

The ratio of the last two relations gives

$$\Gamma / \Gamma_O = \int_O^{\infty} dE\; N^{\gamma}(E) \exp[-2\mu_w w - \sum_i (\mu_i/\rho_i)\, \rho_i\, d] \;/\; \int_O^{\infty} dE\; N^{\gamma}(E) \exp[-2\mu_w w] \,,$$

$$\Gamma / \Gamma_O = F(\mathrm{H/U},\, d) \,. \qquad (6)$$

Given the known energy spectrum of ^{252}Cf gamma rays $N^{\gamma}(E)$ (Fig. 2.1), μ_w for the process pipe, and μ_i/ρ_i [Ref. 14] as given in Fig. 2.16 for the elements of the UO_2F_2 - H_2O mixture, the right-hand side of Eq. (6), $F(\mathrm{H/U},\, d)$, can be calculated for various values of H/U and the deposit thickness. A plot (Fig. 2.17) is produced for $(\Gamma/\Gamma_O) = F(\mathrm{H/U},\, d)$ as a function of deposit thickness and the values of H/U. The ratio of H to U for given deposit measurements is determined as follows. First, the deposit thickness is obtained from the intensity of the transmitted 8.5-MeV neutrons across the deposit pipe [Eq. (2)]. Then, the ratio of total

counts for the transmitted gamma rays (Γ/Γ_o), which is obtained from the measure of the cross correlation function between detector #2 and the source with and without the deposit, is utilized for determining the corresponding value of H/U (Fig. 2.17).

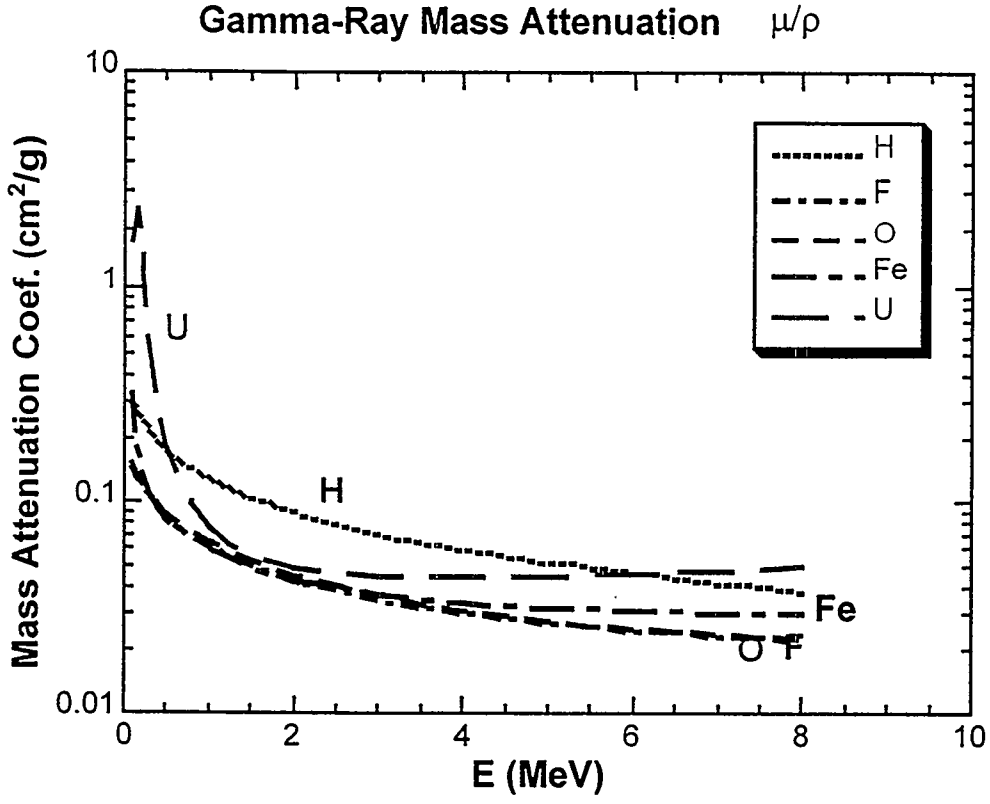

Fig. 2.16. Gamma-ray mass attenuation coefficient given for the elements hydrated deposit $UO_2F_2 - H_2O$ mixture.

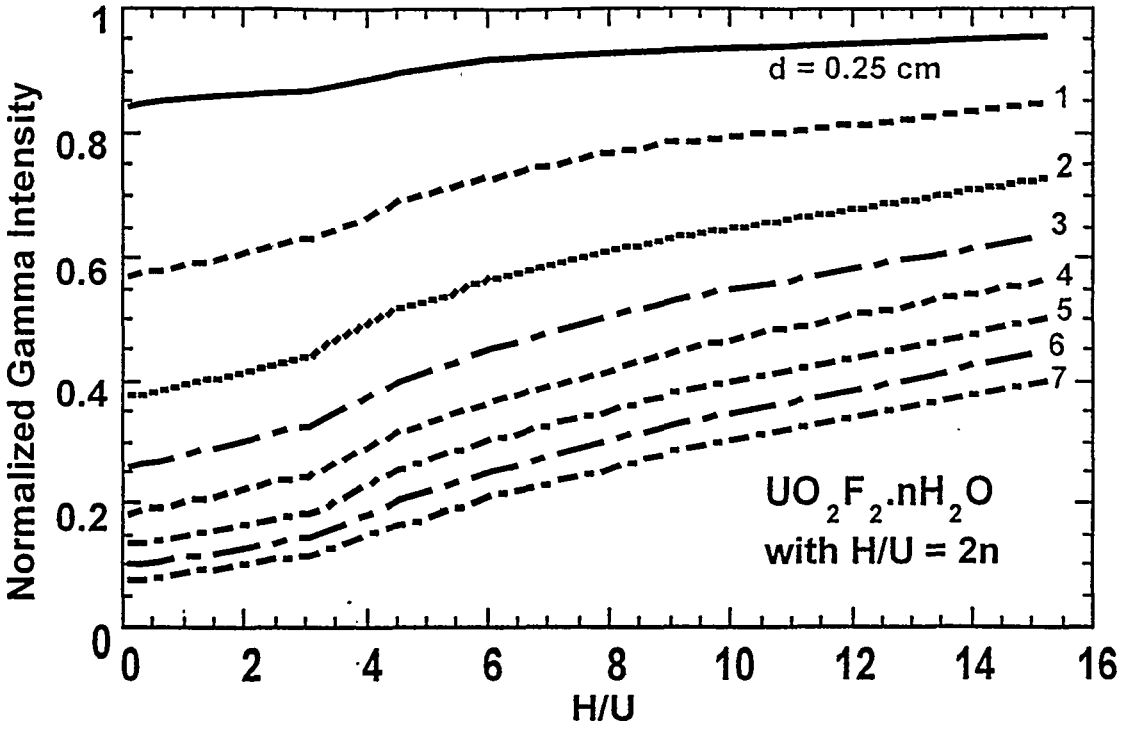

Fig. 2.17. Calculated [Eq. (6)] normalized gamma-ray attenuation for various values of deposit thickness as a function of H/U.

For thin deposits (approximately 2 cm or less) and the normalized gamma-ray ratio $(\Gamma/\Gamma_0) < 1$, the determination of H/U is very sensitive because of the flattening of the curves (Fig. 2.17). That is, for a thin deposit, an error of 0.5 cm can correspond to a large variation in the value of H/U for $(\Gamma/\Gamma_0) \sim 1$.

This data analysis description gives a first estimate of the deposit thickness d and the level of hydration, H/U. To determine the deposit characteristics from these measurements, a clean process pipe that is similar in physical and nuclear characteristics to the pipe containing deposits is required for the calibration measurements of I_0 for the neutrons and Γ_0 for the gamma rays.

2.4. Iterative Procedure for Deposit Thickness and H/U Improvements

The measurement results can be further improved by making a number of iterative calculations using the initial values of deposit thickness and H/U. As illustrated in Fig. 2.18, the following steps can be taken for this procedure:

1. From the neutron transmission measurements at E = 8.5 MeV, a first estimate of deposit thickness d is obtained by using a total macroscopic cross section Σ_t averaged over H/U because Σ_t only varies about ±15% for H/U = 0.6–16 (see Fig. 2.12). This approach is roughly equivalent to selecting an H/U of ~4 or $\Sigma_t \approx 0.155$ cm^{-1}.

2. By utilizing this initial value of the deposit thickness together with the gamma-ray transmission measurements and Fig. 2.17, the corresponding new H/U value is obtained.

3. The value of Σ_t can now be refined because a better estimate of H/U is known, and in turn, a refined deposit thickness can be recalculated from Eq. (2).

4. The process is repeated with this refined deposit thickness (Fig. 2.17) to further improve the value of H/U. This iterative process can continue until the improvements in the values of deposit thickness and H/U are negligible.

2.5. Total Uranium Mass of Deposit

The total uranium mass of the deposit can be calculated by using the results of the deposit profile obtained along the process pipe together with the measurements of H/U, which gives the uranium deposit density ρ_u. As shown in Fig. 2.19 [Ref. 17], H/U is directly related to ρ_u obtained for UO_2F_2 - H_2O mixtures for various values of uranium enrichment.

A section of the deposit pipe having a length of L_i is defined by the midpoints between measurement locations on either side of the measurement point L_m. As shown in Fig. 2.20, the deposit volume V_i of each measurement segment i is calculated from the measured

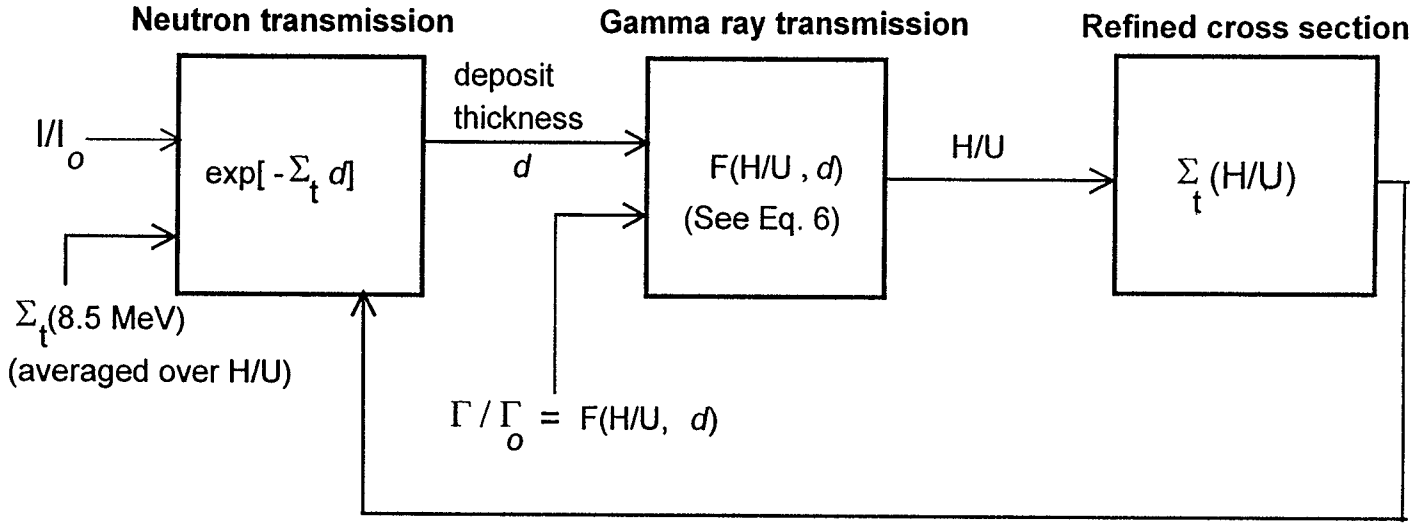

Fig. 2.18. Procedure for iterative refinement of the deposit thickness and the value of H/U.

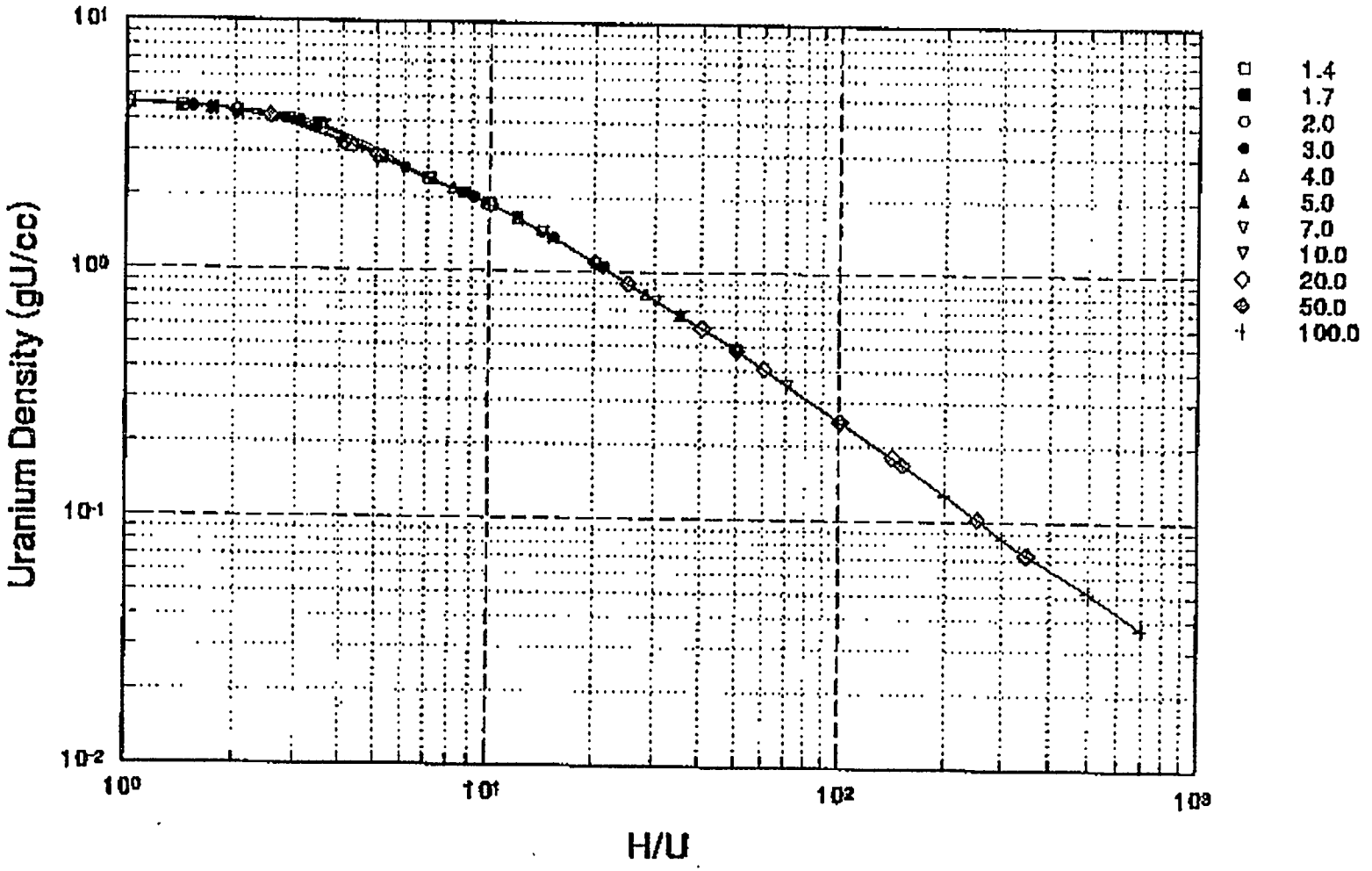

Fig. 2.19. Uranium deposit density calculated for UO_2F_2 - H_2O mixtures for values of uranium enrichment [Ref. 17].

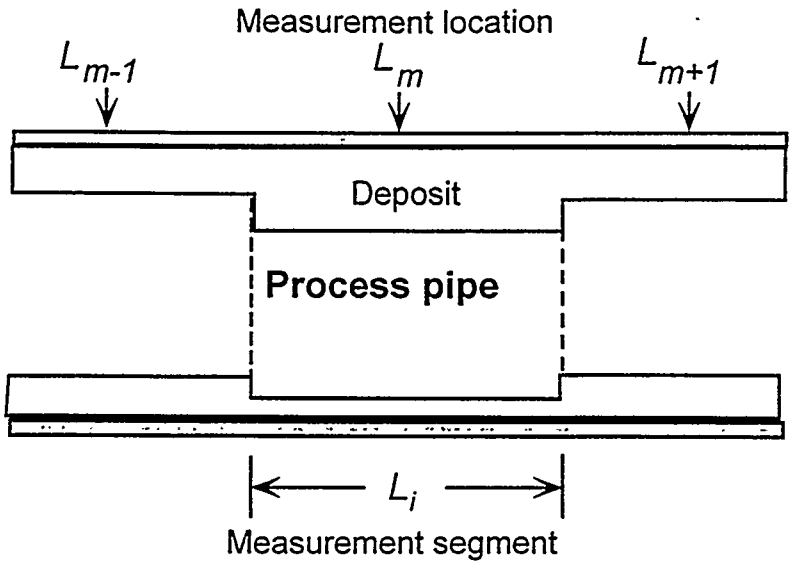

Fig. 2.20. Deposit volume is calculated from a measurement segment *i*, a section of the deposit pipe having a length of L_i, which is defined by the midpoints of either side of the measurement point L_m, where the deposit profile is measured, and assuming that within the measurement segment the deposit profile remains uniform.

deposit thickness and its shape, assuming that the deposit profile remains uniform within the measurement segment. The overall deposit volume V_d of the process pipe is then obtained by adding up the calculated deposit volumes of the segments such that the whole process pipe is well accounted for (i.e., $V_d = \sum_i V_i$, where the summation is over the total number of measurement segments). The total uranium mass of the deposit is then $\Delta M_u = \rho_u \times V_d$ with the associated relative uncertainty of

$$\Delta M_u / M_u = \pm[(\Delta \rho_u / \rho_u)^2 + (\Delta d / d)^2]^{0.5} , \qquad (7)$$

which is utilized later for the uncertainty assessment of the uranium mass of the deposit in the measured process pipes of Hockey Stick and Tee-Pipe. The assumption of a uniformly varying deposit is especially significant because nonuniformity was observed in the source-detector rotation measurements and because of the general nature of the deposit obtained from the intrusive view with the fiber-optic camera. This assumption was used because measurements were performed at only six locations along the Hockey Stick process pipe.

This page intentionally left blank.

3. UNIT 2, CELL 7, B-LINE OUTLET (HOCKEY STICK) DEPOSIT MEASUREMENTS

3.1. Description of the Measurements

Deposit characterization measurements were performed at a number of locations on the Unit 2, Cell 7, B-Line Outlet (Hockey Stick) process pipe located on the cell floor of the K-29 Building. As shown in Fig. 3.1, the Hockey Stick pipe has a D_O= 24 in. OD, and is about 17 ft long. It is made of a carbon steel and has a wall thickness of w = 0.375 in. The arrangement of the measurement system on the Hockey Stick and the locations of the NWIS processor and its associated electronics used on the operating floor of the building (the lower level) are schematically shown in Fig. 3.2. Photographs of the NWIS processor, which is located in the clean area of the operating floor separated by a boundary from the rest of the floor, and its associated electronics, which are located on the operating floor, are shown in Fig. 3.3. The electronics were connected to the NWIS processor by 425-ft-long cables and to the measurement system at the Hockey Stick by 75-ft-long cables, as shown in Fig. 3.2. Communication between the NWIS operator at the clean area and the measurement team on the cell floor was accomplished with a set of intercoms as indicated in Fig. 3.2.

The source and the detectors (detector #2 and detector #3 in Fig. 2.2) of NWIS were placed on the Hockey Stick with a fixture that allowed both the source and the detectors to scan the process pipe vertically and horizontally (Fig. 3.4). As shown schematically in Fig. 2.2, all detectors were placed side-by-side along the pipe (z-axis). (The coordinate system to be used throughout the discussions is indicated in Figs. 2.2 and 3.5.) Measurement locations were selected on the Hockey Stick to address (1) the primary concern of performing the measurements safely and (2) the need for enough clearance around the process pipe to place the detectors. Therefore, the measurement fixture was secured with a number of safety cables to the structure around the Hockey Stick to minimize any inadvertent movement on the process pipe.

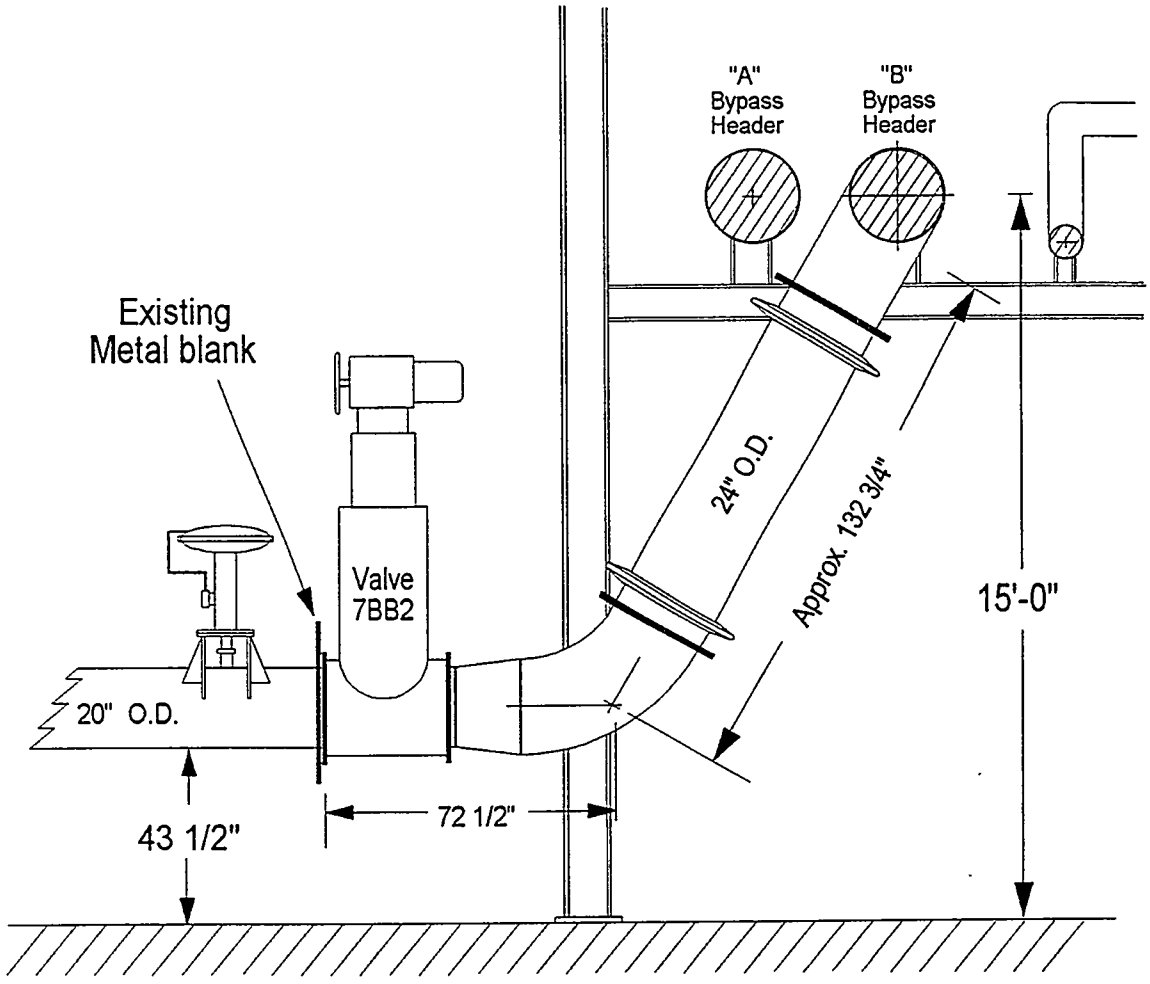

Fig. 3.1. Dimensions of Unit 2, Cell 7, B-Line Outlet process pipe (Hockey Stick).

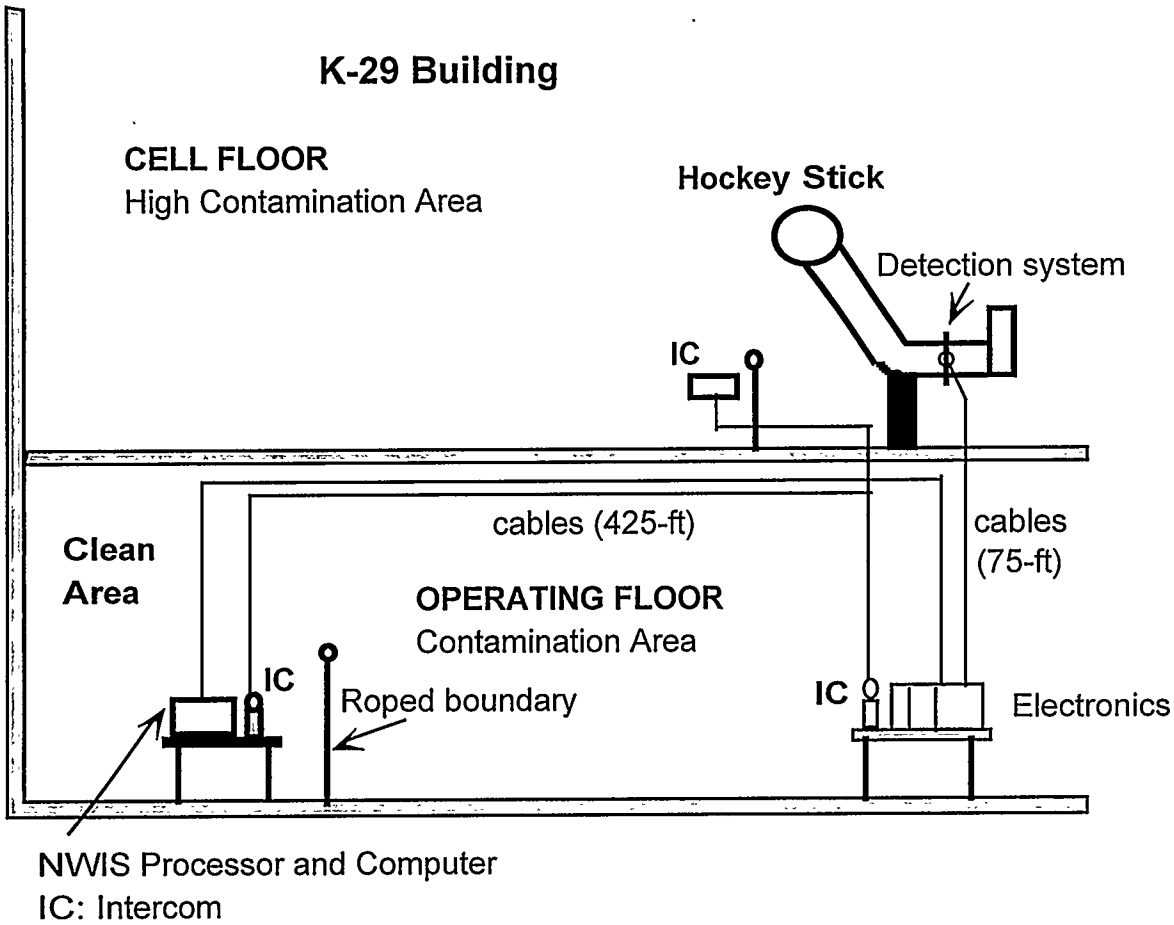

Fig. 3.2. Arrangement of the measurement system on the Hockey Stick, the locations of the electronics, and the location of NWIS processor in the K-29 Building.

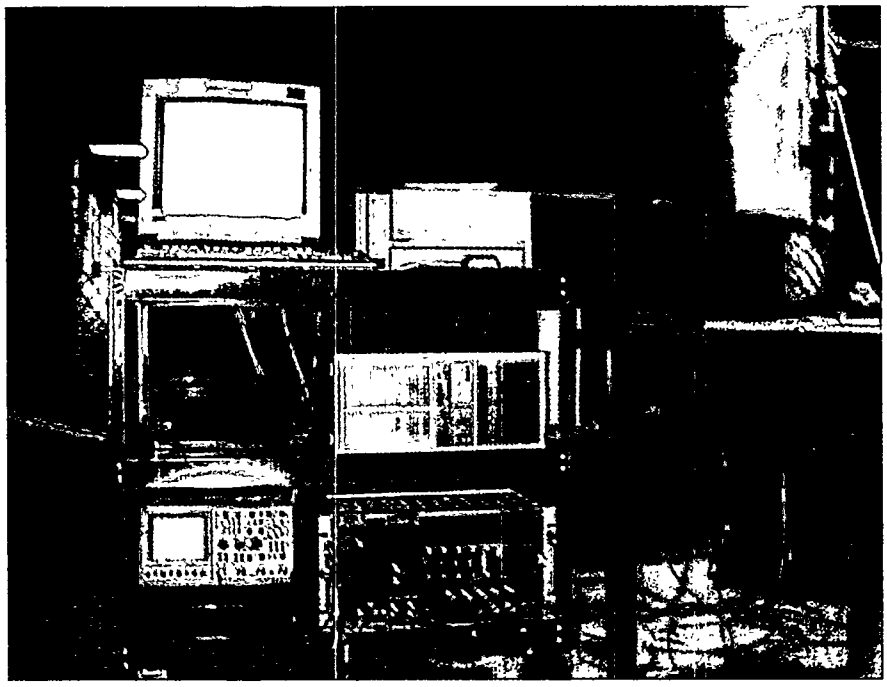

(a)

(b)

Fig. 3.3. (a) Photograph of the NWIS processor. (b) Photograph of NWIS processor associated electronics used for the measurements in the K-29 Building.

The measurement locations along the Hockey Stick process pipe are given with respect to the welded metal blank flange (L = 0) located by the left side of the block valve (7BB2), as shown in Fig. 3.5. These locations along the midplane of the Hockey Stick, as indicated in Fig. 3.5, are L = 40, 54, 80, 104, 133, and 163 in. In addition to these, the 7BB2 block valve was also measured axially and radially. As shown in Fig. 2.13, the measurements were performed by continually repositioning the ^{252}Cf source and the pair of detectors vertically and horizontally every 2 in. Moreover, in some of these locations, whenever enough clearance around the process pipe was available, the source and the detectors were rotated 360° in 30° intervals, as illustrated in Fig. 2.14. These locations were L = 54 in. and L = 104 in. In addition, the detector translation measurements were performed vertically (y) and horizontally (x) while fixing the source in various locations (that is, on the top side, on the midplane, and on the bottom side of the process pipe). The top of the Hockey Stick is defined as $y = D/2$. The bottom of the process pipe is defined as $y = -D/2$. (See Fig. 3.5.) Altogether, more than 300 measurements were performed on the Hockey Stick for the profile characterizations. During these measurements the cell floor temperature varied between 84 and 90° F, and the performance of the measurement system was stable.

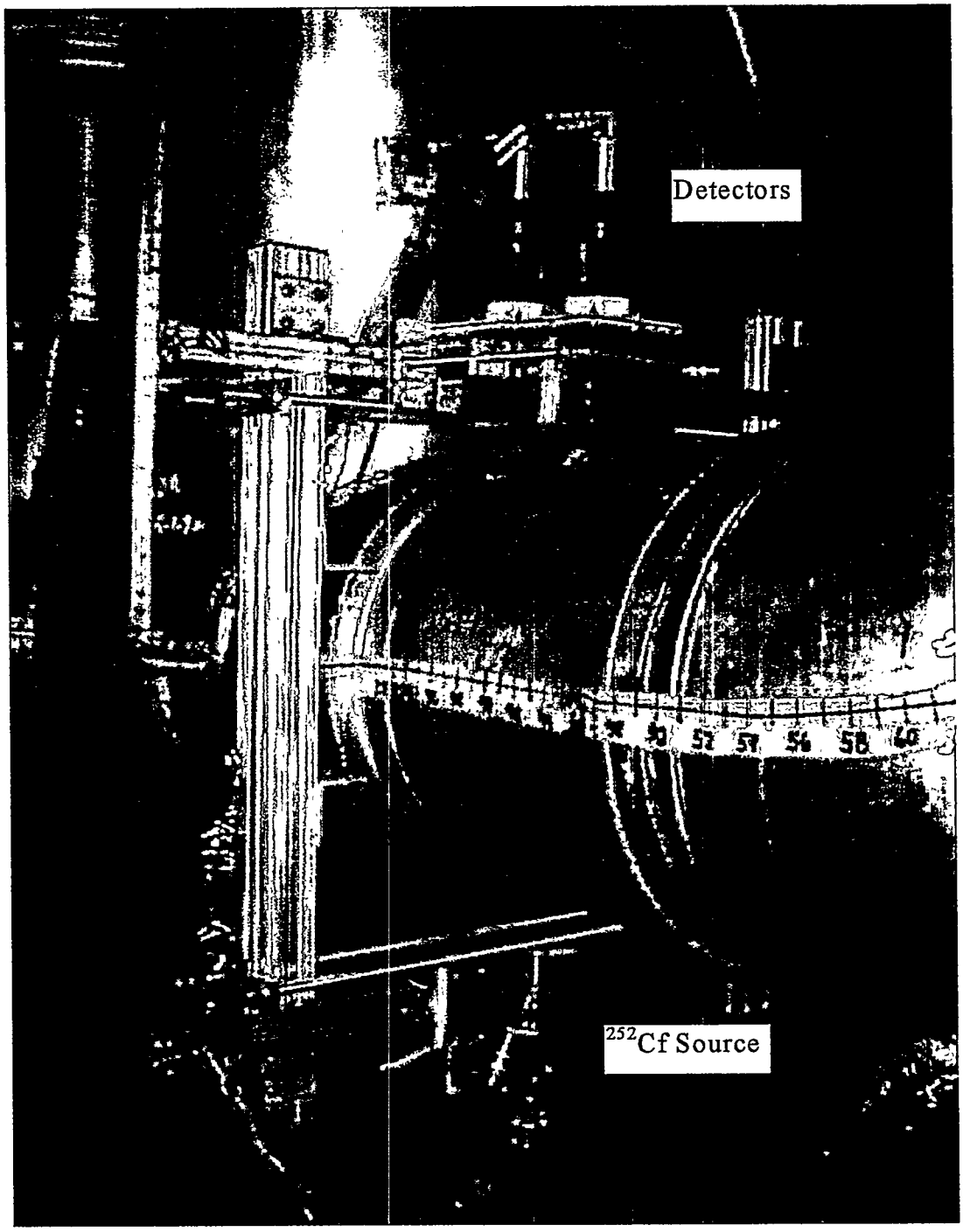

Fig. 3.4. The Cf source and the detectors placed on the Hockey Stick by means of a fixture for the deposit measurements.

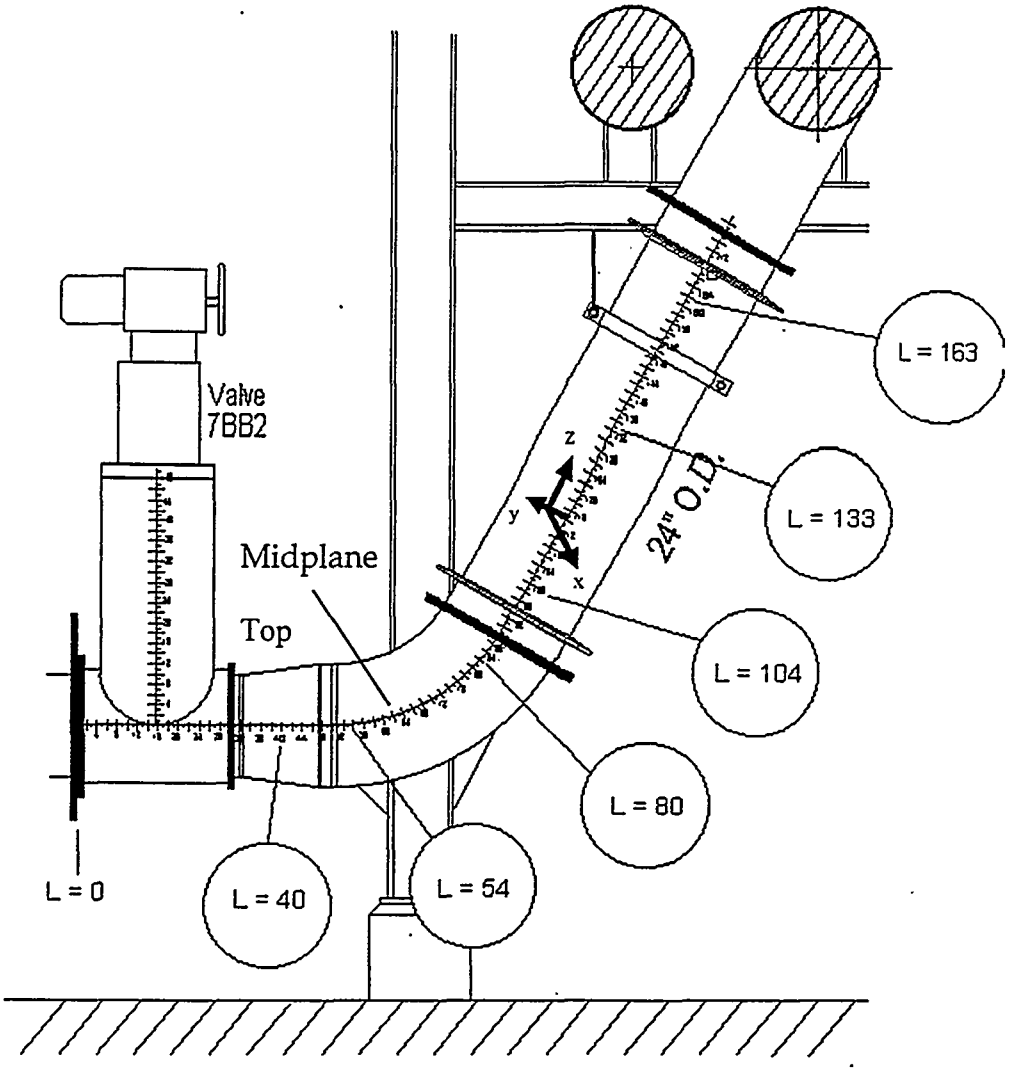

Fig. 3.5. Measurement locations along Hockey Stick given with respect to the welded metal blank flange ($L = 0$) located by the left side of the block valve (7BB2). Units are given in inches.

3.2. Measurement Reproducibility and Calibration

Before, during, and after the deposit characterization measurements each day, a number of TOF measurements in air were performed for detector efficiency measurements with the ^{252}Cf source and the two detectors 40 in. apart. Figure 3.6 shows the detector efficiency as a function of neutron energy. The peak efficiency is approximately 50%, and efficiency for 8.5-MeV neutrons is approximately 38%. The variations of the peak efficiency from the detector efficiency measurements are given in Table 3.1. Throughout the deposit characterization measurements detection efficiency was maintained within ±5% for detector

#2 and within ±1.5% for detector #3. This variation is inconsequential if the deposit thickness measurement and the calibration measurement were performed on the same day because they are relative measurements. Thus the detector efficiency cancels. These detector efficiency measurements were also used to verify the proper operation of the NWIS measurement hardware and to maintain repeatability of measurements from day to day. If needed, minor adjustments were made to the gain of the detectors. The threshold setting of the constant fraction discriminator was adjusted to set the lower energy threshold of the detectors at 1/3 the energy of the Compton edge for cesium-137 gamma rays to minimize effects on the counting system from some of the deposit background radiation. As seen from the detector efficiency measurement (Fig. 3.6), this corresponds to 1 MeV for the lowest-energy neutron that can be measured. For neutrons, the neutron threshold of 1.6 MeV is the energy point at which the detector efficiency for neutrons is half of its maximum value. The measurement precision was ensured by collecting 10^9 data blocks, having 512 time bins per block, within ~12 min of NWIS processing. The result was compared with 5×10^{10} data blocks taken during a 12-h overnight NWIS run for the same location, and no significant difference between the two measurements was observed (Fig. 3.7).

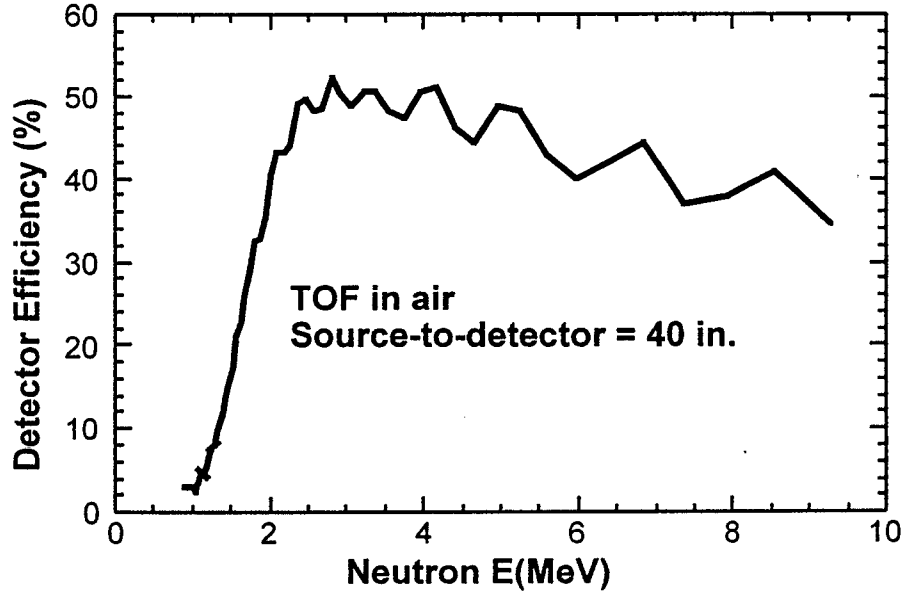

Fig. 3.6. Plot of detector efficiency given as function of neutron energy. This is obtained from CFSDT TOF measurements in air with ^{252}Cf source and detectors separated 40 in. in air.

Table 3.1. Variations of detector peak efficiency

	Peak detector efficiency (%)	
TOF filename	Detector #2	Detector #3
tf03r06	54	50
tf06r02	54	50
tf14r01	50	48
tf14r02	50	48
tf16r01	50	50
tf17r01	50	47
tf17r34	45	49
tf18r01	45	50
tf18r46	54	48
tf19r01	53	48
tf19r42	50	48
tf20r01	50	48
tf20r64	48	49
tf21r01	47	50

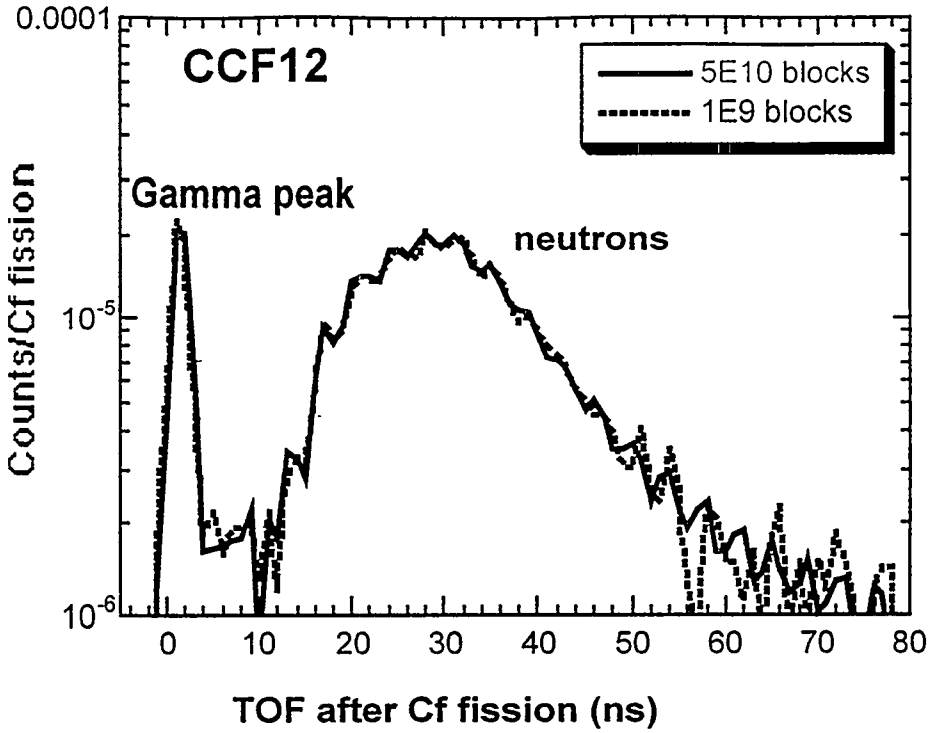

Fig. 3.7. Time distribution of counts after Cf fission for 10^9 data blocks, having 512 time bins per block, within ~12 min. of NWIS processing time, and 5×10^{10} data blocks taken during a 12-h overnight NWIS run for the same location.

The reproducibility of the measurements was determined by performing repeated measurements at each measurement location on the process pipes at different times. These repeated measurements were much less than 10% different. As illustrated in Fig. 3.8, two measurements were performed at the same location, one with the horizontal source detector scan and another with the source detector rotation measurements on the midplane of the Hockey Stick ($x = 0$) at $L = 104$ in. The data from these two measurements were within a few percent of each other.

The corresponding calibration measurements for removing the effects of the deposit process pipe were performed on an empty section of pipe (Fig. 3.9), which has similar physical characteristics to those of the Hockey Stick pipe. This is needed for the data analysis discussed in Sects. 2.1 and 2.2. The calibration pipe was placed the same height above the cell floor as the Hockey Stick to account for the effects of floor reflections. These calibration measurements were performed at 2-in. increments in a manner consistent with the Hockey Stick deposit measurements. The calibration measurements were used to remove the effects of the pipe so that the deposit thickness could be obtained.

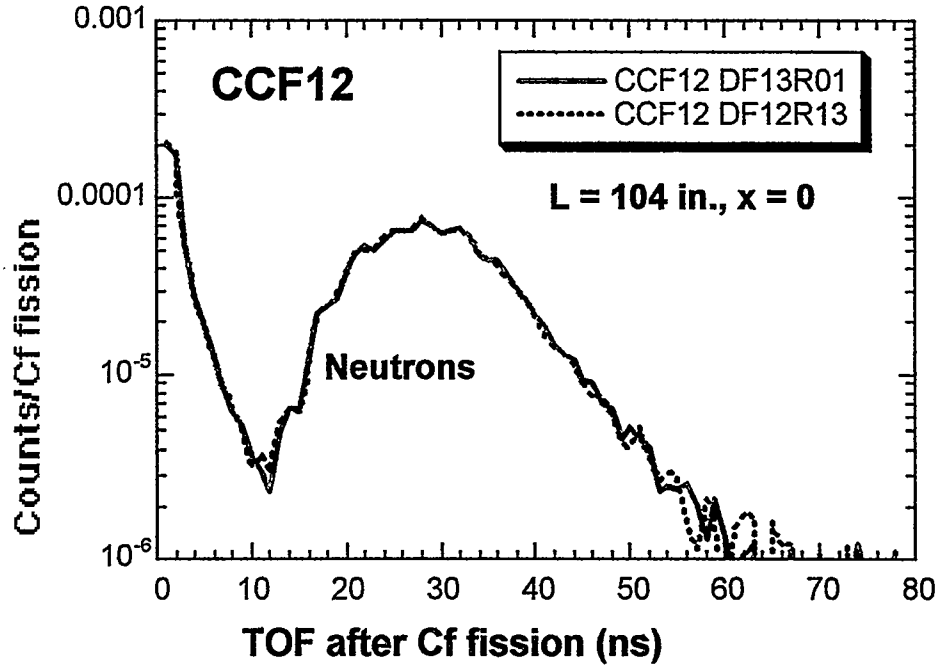

Fig. 3.8. Measurement reproducibility is shown for two measurements taken at the same location, one with the horizontal source detector scan (data file name: DF12R13) and the second one with the source detector rotation (data file name: DF13R01) measurements on the midplane, $x = 0$, of the Hockey Stick at $L = 104$ in.

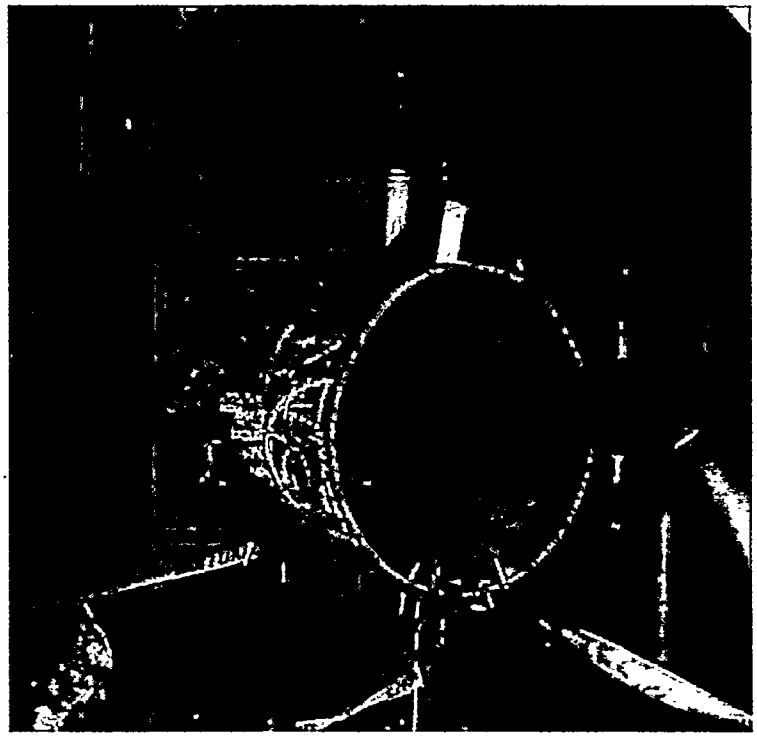

Fig. 3.9. Clean pipe section for calibration measurements for removing the pipe attenuation from the deposit measurements.

3.3. Hockey Stick Measurement Results

The following results were obtained from the Hockey Stick deposit characterization measurements obtained by detector #2 (see Fig. 2.2). The detailed results obtained from detector #3 (whose center is 4.5 in. further up the pipe from the center of detector #2) are presented in Appendix A, and the data are included in the tables of this section for comparison.

3.3.1. Deposit profile and its distribution along the Hockey Stick

The measurement and data analysis methods were discussed in Sect. 2. A typical cross correlation function between detector #2 and the source measured on the midplane at $L = 54$ in. is shown in Fig. 3.10. As indicated on the figure, the first peak represents the TOF ($\tau \sim 2$ ns) of prompt gamma rays from ^{252}Cf fission; the second peak ($\tau \sim 29$ ns) is mainly for fission neutrons having an average energy of $E = 2.13$ MeV (see Table 2.1). Counts for $\tau > 80$ ns represent the uncorrelated background contribution to the TOF spectrum. The 8.5-MeV neutrons occur at 15 ns in the TOF spectrum. These data are corrected for effects of the pipe by dividing by the I_0 value from the empty pipe calibration measurements. The deposit thickness is then found from Eq. (2) because Σ_t ($E = 8.5$ MeV), obtained from the value of H/U, is known.

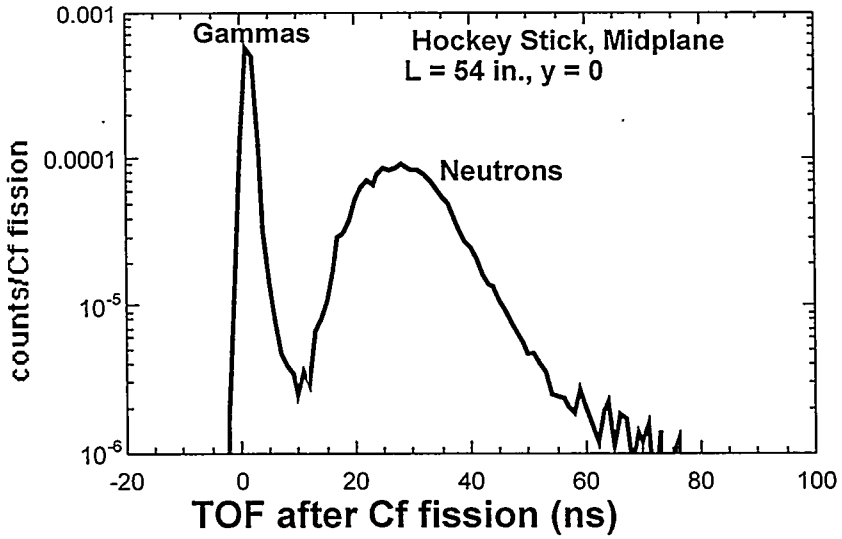

Fig. 3.10. Typical cross correlation function between detector #2 and the source measured on the midplane ($y = 0$) of $L = 54$ in. Here the first peak represents the TOF ($\tau \sim 2$ ns) of gamma rays while the second peak ($\tau \sim 29$ ns) is for the neutrons having an average energy of $E = 2.13$ MeV. Counts for $\tau > 80$ ns represent the uncorrelated background to the TOF spectrum.

The following measurement results, obtained from the Hockey Stick scans with the source and the detectors #2 and #3, are given in the form of data tables for comparing the measurements of the two detectors. The corresponding deposit profiles constructed from the measurements are given. The measurement results from the detector #2 for the deposit profiles along the Hockey Stick are presented for $L = 54$, 40, 80, 104, 133, and 163 in. measured along the midplane of the pipe from the flange ($L = 0$ in.) located by the left side of the block valve (Fig. 3.5). These results are discussed according to the order of the deposit measurements performed on the Hockey Stick.

3.3.1.1. Measurement results at $L = 54$ in.

Initial results at $L = 54$ in.

The $L = 54$ in. section of the 24-in.-OD process pipe is near the bottom of the Hockey Stick (see Fig. 3.5), near the 7BB2 block valve, where wet air was thought to have leaked in. As shown in Fig. 2.13, vertical and the horizontal source and detector scans were performed, as was a source-detector rotation (Fig. 2.14). Obstructions prevented measurements at 0° and 270° rotation. The neutron data were analyzed at 8.5 MeV, as discussed in Sect. 2.2. Initially, an average value of the total neutron interaction cross section corresponding to an H/U of 4 was used to calculate the deposit thickness from the transmission measurements of the neutrons, as discussed in Sect. 2.2. The first set of results of the measured deposit thickness, without iterative improvements, is presented in Table 3.2A and 3.2B for the total transmission thicknesses, and 3.2C for the total radial thicknesses at the measurement positions. These values are used to obtain the radial thickness of the deposit, i.e., the deposit profile. Contrary to expectation, the data in Table 3.2A immediately showed that the deposit at $L = 54$ in. existed on the top of the process pipe and that the bottom contained very little deposit material. Not more than 0.1 in. deposit thickness could be resolved with the measurements discussed in Sect. 2.2.3. The data also indicated that the deposit had an annular shape because increasing displacement from the midplane yielded an increasing measured deposit thickness. A comparison of values obtained at 2-in. increments from the midplane in Table 3.2B indicated that the deposit profile was fairly symmetric from left to right. Because the vertical scans revealed that very little deposit material existed in the bottom of the process pipe, the information from the horizontal scan could be used to calculate the deposit thickness at the top of the process pipe. The source-detector scans were limited to ±10 in. because at 12 in. part of the detector views the source directly.

Table 3.2A. Hockey Stick initial results of total transmission thickness from vertical source and detector scan at L = 54 in.

Position y (in.)	$-\text{Ln}(I / I_0)$	Thickness (in.)[a]
10	2.13	5.38
8	1.29	3.27
6	0.870	2.20
4	0.391	0.99
2	0.259	0.65
0	0.065	0.16
–2	0.287	0.73
–4	0.261	0.66
–6	0.200	0.51
–8	0.225	0.57
–10	0.070	0.18

[a] These values are vertical transmission thickness at the horizontal position given in column 1 and were obtained with neutron cross section data for H/U = 4.

Table 3.2B. Hockey Stick initial results of total transmission thickness from horizontal source and detector scan at L = 54 in.

Position x (in.)	$-\text{Ln}(I / I_0)$	Thickness (in.)[a]
10	0.506	1.28
8	0.713	1.80
6	0.858	2.17
4	0.978	2.47
2	0.987	2.50
0	0.769	1.94
–2	0.909	2.30
–4	0.819	2.07
–6	0.623	1.58
–8	0.649	1.64
–10	0.445	1.13

[a] These values are vertical transmission thickness at the horizontal position given in column 1 and were obtained with neutron cross section data for H/U = 4.

Table 3.2C. Hockey Stick initial results of total radial thickness from rotation of source and detector at $L = 54$ in.

Rotation α (Deg.)	$-\text{Ln}\ (I / I_0)$	Thickness (in.)[a]
30	0.782	1.98
60	0.409	1.03
90	0.360	0.91
120	0.585	1.48
150	0.929	2.35
180	1.19	3.00
210	0.907	2.29
240	0.573	1.45
300	0.494	1.25
330	0.823	2.08

[a] These values are the total thickness along a diameter at angle given in column 1 and were obtained with neutron cross section data for H/U = 4.

Additional information about the profile was obtained by the source-detector rotation data from Table 3.2C. Obstructions prevented measurements at the 0° and 270° positions. Ideally, measurement locations that are 180° apart should yield the same results, but slight differences within the uncertainty of the measurements were noted. Measurements with the detector located on the top of the process pipe indicated slightly more material than was indicated in the complementary measurements obtained with the source and the detector positions reversed. The slight increase (a few percent) when the detector is on the top of the process pipe may be attributed to its proximity to the deposit.

Results of the gamma-ray portion of the measured signature at $L = 54$ in. used to calculate the hydration level of the deposit (without iterative improvements) are summarized in Table 3.3. To avoid edge effects, deposit hydration was only measured near the horizontal and vertical midplane of the process pipe, corresponding to $y = 0$, ±2, and ±4 in. These results clearly reiterate the problem identified earlier for thin deposits. When data from the $y = -2$ in. location were compared with data from the –4 in. position for the vertical scan, the difference in $\ln (\Gamma/\Gamma_O)$ was only 0.01. In comparison, the difference in the deposit thickness estimated at the two locations was 0.07 in. However, because of the extreme sensitivity of the method to thin deposit materials, there was a large difference in estimation of the value for H/U; that is, H/U = 3.5 at $y = -2$ in. while H/U = 14.7 at $y = -4$ in. For this reason, only data for deposits thicker than 1.25 in. were used to determine deposit hydration level.

Table 3.3. Hockey Stick first estimate of deposit hydration at L = 54 in. from vertical and horizontal scan

Thickness (in.)	y (in.)	$-\text{Ln}(\Gamma/\Gamma_o)$	H/U
0.99	4	0.70	> 15
0.65	2	0.69	11.5
0.16	0	0.73	> 15
0.73	–2	0.74	3.5
0.66	–4	0.73	14.7
Thickness (in.)	x (in.)	$-\text{Ln}(\Gamma/\Gamma_o)$	H/U
2.47	4	0.21	5.5
2.50	2	0.21	5.5
1.94	0	0.18	2.0
2.30	–2	0.18	3.5
2.07	–4	0.19	3.0

Iterative improvements of measurement results at L = 54 in.

The method outlined in Sect. 2.3 was used to obtain the iterative refinement of the deposit thickness and the hydration presented in Table 3.4 for the deposit profile at L = 54 in. During the iterative process, it was assumed that in a narrow region between the detector and the source (such as a vertical or horizontal scan) the deposit material properties were relatively constant, and an average H/U and a new corresponding total neutron cross section was determined. This new value of Σ_t was then used to improve the estimate of the deposit thickness and the H/U value. The iterative scheme continues until the average H/U value had converged and was only changing slowly. Small variations in H/U do not significantly affect the value of Σ_t so that the estimated deposit thickness did not change and the iteration process was completed. For this case, the acceptable convergence was reached in three iterations. The second iteration resulted in an average H/U value of 3.7, and the third iteration resulted in an average value of 3.8. These small changes in H/U did not significantly affect the neutron cross-section values (see Fig. 2.12), so that the estimated thickness did not change and the solution converged.

The data in Table 3.4 indicate that the deposit thickness in the radial direction varied from $d(x = 0)$ = 1.83 in. to d (x = 2 in.) = 2.35 in. The average value of H/U at this location determined from the horizontal scan was 3.8. As discussed in Sect. 3.3.3, to better quantify the value of H/U for the Hockey Stick, the remainder of the deposit profiles were included in the data analysis. Fig. 3.11 presents the estimated deposit profile at L = 54 in. These results

incorporate data from the vertical (Table 3.5A), horizontal (Table 3.5B), and rotation (Table 3.5C) scans. In these tables the results obtained from the second NWIS detector (denoted as detector #3 in Fig. 2.2; and located at L = 58.5 in.) are also included in parenthesis for comparison between the two detector results. A comparison of the results from both detectors indicated the existence of strong spatial deposit irregularities. Over a distance change of only 4.5 in. the average deposit thickness varied by a factor of 2 and at some locations, by much more or much less. As discussed in Sect. 5, the intrusive observations showed that the deposit was not smooth in this region but consisted of large, closely grouped nodules and that the deposit was very irregular in thicknesses. The deposit thicknesses and the hydration levels reported are average results based on the region covered by the 4 × 4 in. detectors. The measurement results for the obtained with detector #2, with iterative improvement as described in Sect. 2.3, are presented for the rest of the measurement locations of L = 40, 80, 104, and 163 in. The profiles and more detailed discussion of the results for detector #3 are given in Appendix A.

Table 3.4. Hockey Stick iterative results at L = 54 in. using measurement data from source and detector horizontal scan

Location	Initial Results		Iteration #1		Iteration #2		Iteration #3	
Horizontal scan, in.	Thickness (in.)[a]	H/U[a]	Thickness (in.)[a]	H/U[a]	Thickness (in.)[a]	H/U[a]	Thickness (in.)[a]	H/U[a]
x = 4	2.47	5.5	2.21	4.5	2.30	4.8	2.33	4.9
x = 2	2.50	5.5	2.23	4.5	2.30	4.8	2.35	4.9
x = 0	1.94	2.0	1.74	1.5	1.80	2.1	1.83	2.3
x = –2	2.30	3.5	2.05	3.5	2.12	3.6	2.17	3.7
x = –4	2.07	3.0	1.85	3.0	1.92	3.2	1.96	3.3
Average[b] H/U		3.9		3.4		3.7		3.8

[a] Average transmission thickness and hydration of region seen by 4 × 4 in. detectors.
[b] Average H/U is used for determining the value of the neutron cross section (Fig. 2.12) for next iteration.

Table 3.5A. Hockey Stick iterative results of total transmission thickness from vertical dource and detector scan at $L = 54$ in.

Position y (in.)	$-\text{Ln}\ (I / I_0)$	Thickness (in.)[a]	
10	2.13	5.24	(3.06)
8	1.29	3.17	(2.92)
6	0.870	2.14	(1.50)
4	0.391	0.96	(0.79)
2	0.259	0.63	(0.78)
0	0.065	0.15	(0.70)
–2	0.287	0.70	(0.49)
–4	0.261	0.64	(0.34)
–6	0.200	0.49	(0.38)
–8	0.225	0.55	(0.36)
–10	0.070	0.17	NP[b]

[a] Results from detector #3 are given in parentheses. The center of detector #3 was located 4.5 in. further up the pipe than the distance given in the table title (54 + 4.5 = 58.5 in. for location of detector #3). Values not in parentheses are from the data of detector #2, which was centered 54 in. along the pipe. These thicknesses are along a line of sight between the source and the detector.

[b] Not physical (NP); see Section 2.2.3 for discussion.

Table 3.5B. Hockey Stick iterative results of total transmission thickness from horizontal source and detector scan at $L = 54$ in.

Position x (in.)	$-\text{Ln}\ (I / I_0)$	Thickness (in.)[a]	
10	0.506	1.24	(1.58)
8	0.713	1.75	(2.21)
6	0.858	2.11	(2.36)
4	0.978	2.40	(2.86)
2	0.987	2.42	(3.02)
0	0.769	1.89	(2.41)
–2	0.909	2.23	(2.90)
–4	0.819	2.01	(2.02)
–6	0.623	1.53	(1.68)
–8	0.649	1.59	(1.69)
–10	0.445	1.09	(0.62)

[a] Results from detector #3 are given in parentheses. The center of detector #3 was located 4.5 in. further up the pipe than the distance given in the table title (54 + 4.5 = 58.5 in. for location of detector #3). Values not in parentheses are from the data of detector #2, which was centered 54 in. along the pipe. These thicknesses are along a line of sight between the source and the detector.

Table 3.5C. Hockey Stick iterative results of total radial thickness from rotation of source and detector at $L = 54$ in.

Rotation α (Deg.)	$-\text{Ln}(I / I_o)$	Thickness (in.)[a]	
30	0.782	1.92	(1.24)
60	0.409	1.00	(0.86)
90	0.360	0.88	(0.60)
120	0.585	1.43	(0.87)
150	0.929	2.28	(2.10)
180	1.19	2.92	(2.58)
210	0.907	2.23	(2.39)
240	0.573	1.40	(1.12)
300	0.494	1.21	(0.92)
330	0.823	2.02	(1.64)

[a] Results from detector #3 are given in parentheses. The center of detector #3 was located 4.5 in. further up the pipe than the distance given in the table title (54 + 4.5 = 58.5 in. for location of detector #3). Values not in parentheses are from the data of detector #2, which was centered 54 in. along the pipe. These thicknesses are along a line of sight between the source and the detector and in this case are along a diameter.

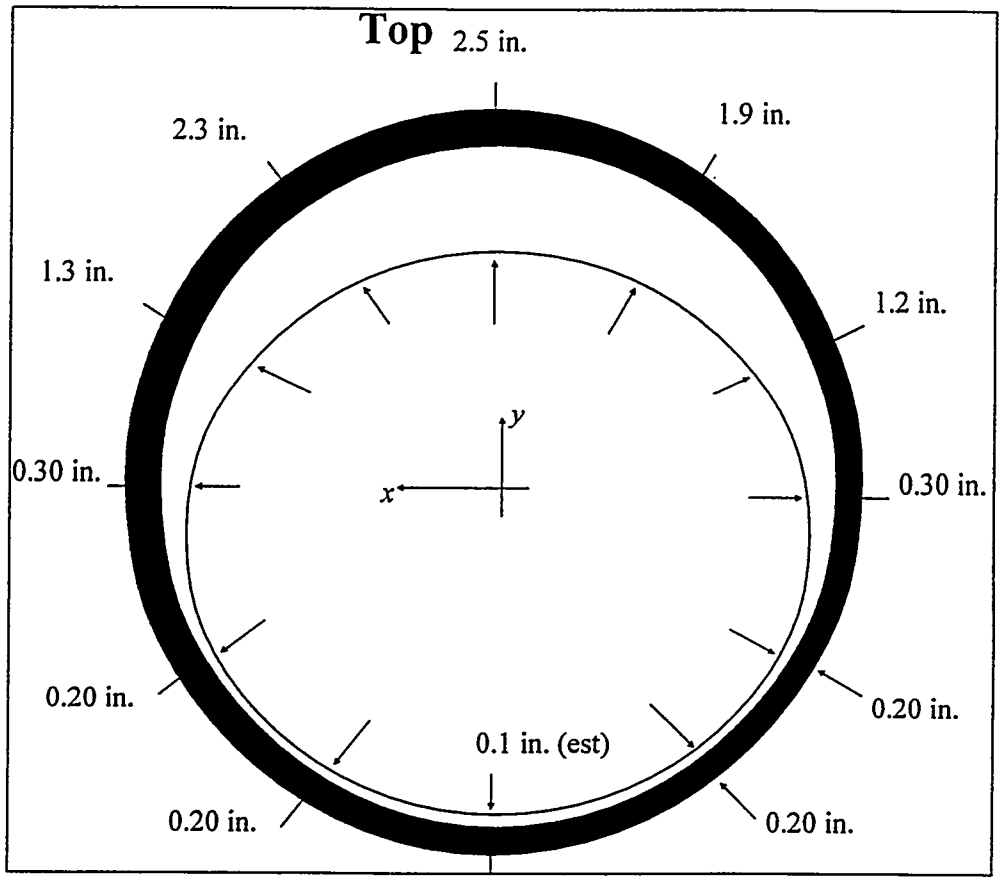

Figure 3.11. Hockey Stick deposit profile at $L = 54$ in.

3.3.1.2. Measurement results at $L = 40$ in.

This location is a transition section of the Hockey Stick connecting to the 20-in.-OD pipe, which is a part of the 24-in.-OD valve body, and the 24-in.-OD process pipe (see Fig. 3.5). At the location of the measurements, $L = 40$ in. (note that detector #3 is at $L = 44.5$ in.), the transition section has 22-in. OD. Because of this smaller diameter, the transition section could not be measured at x or $y = \pm 10$ in. source-detector locations. Calibration measurements were performed on a nearby identical transition section already determined to contain no deposits. Data from the vertical and horizontal source and detector scans are given in Tables 3.6A and 3.6B, respectively. The deposit profile was similar to that of $L = 54$ in.; most of the deposit was on the top of the process pipe. Detector #3 indicated a slightly thicker deposit and some large deposit variations in thickness with a change in location of 4.5 in. Figure 3.12 presents the estimated deposit profile, which was also assumed to be smoothly varying. The average H/U obtained from the iterative procedure was 3.5 and was used for determining the neutron cross section (Fig. 2.2) for determining the deposit thickness.

Table 3.6A. Hockey Stick iterative results of total transmission thickness from vertical source and detector scan at $L = 40$ in.

Position y (in.)	$-\text{Ln}\,(I/I_0)$	Thickness (in.)[a]	
8	1.79	4.10	(2.72)
6	1.18	2.71	(2.27)
4	0.51	1.18	(1.45)
2	0.51	1.17	(1.12)
0	0.20	0.47	(0.94)
−2	0.28	0.64	(0.67)
−4	0.17	0.39	(0.81)
−6	0.14	0.31	(0.84)
−8	0.12	0.28	(0.62)

[a] Results from detector #3 are given in parentheses. The center of detector # 3 was located 4.5 in. further up the pipe than the distance given in the table title (40 + 4.5 = 44.5 in. for location of detector #3). Values not in parentheses are from the data of detector #2, which was centered 40 in. along the pipe. These thicknesses are along a line of sight between the source and the detector.

Table 3.6B. Hockey Stick iterative results of total transmission thickness from horizontal source and detector scan at $L = 40$ in.

Position x (in.)	$-\text{Ln}(I/I_0)$	Thickness (in.)[a]	
8	0.20	0.46	(0.57)
6	0.14	0.31	(1.10)
4	0.32	0.72	(1.16)
2	0.41	0.93	(1.86)
0	0.41	0.93	(1.97)
–2	0.43	0.99	(1.70)
–4	0.25	0.57	(1.10)
–6	0.24	0.55	(0.91)
–8	0.19	0.43	(0.34)

[a] Results from detector #3 are given in parentheses. The center of detector # 3 was located 4.5 in. further up the pipe than the distance given in the table title (40 + 4.5 = 44.5 in. for location of detector #3). Values not in parentheses are from the data of detector #2, which was centered 40 in. along the pipe. These thicknesses are along a line of sight between the source and the detector.

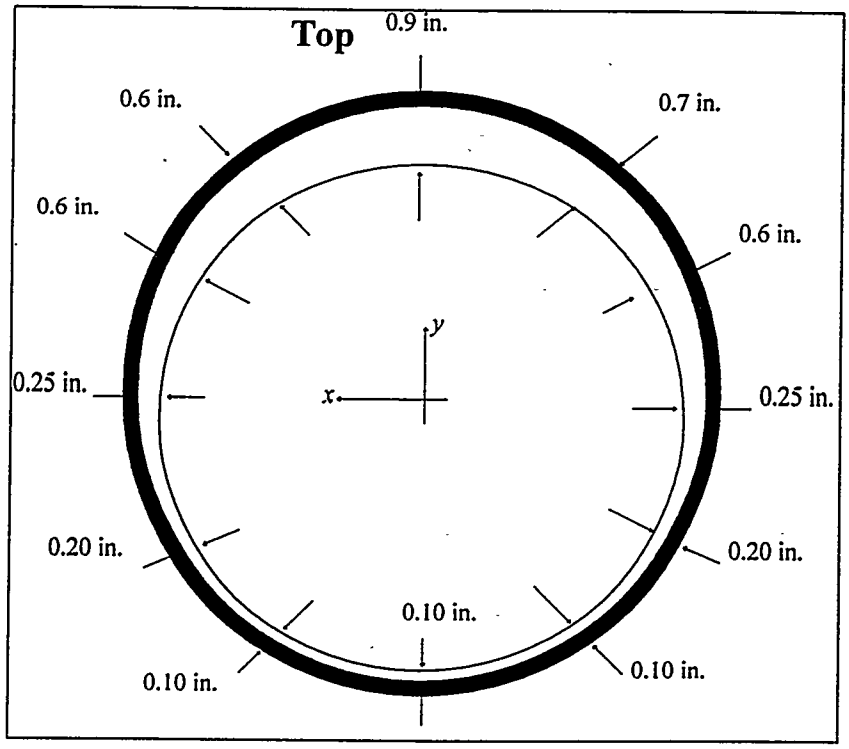

Fig. 3.12. Hockey Stick deposit profile at $L = 40$ in.

3.3.1.3. Measurement results at $L = 80$ in.

This position corresponds to the curved elbow section of the process pipe directly below the expansion joint (see Fig. 3.5). This location was extremely difficult to measure because the expansion joint interferes with the fixture that holds the detector and the source. Consequently, only a single vertical source and detector scan was performed. The measurement results from this scan are given in Table 3.7 together with the results obtained from the detector #3 (which is located at L = 84.5 in.). The estimated deposit profile is presented in Fig. 3.13. The top to bottom deposit variations obtained from these two detectors are similar to each other; however, differences for the same position are large, indicating a very nonuniform deposit. Results from the vertical scan alone indicate that the deposit exists primarily on the upper part of the process pipe. By comparing the thickness of the deposit near the edges with the thickness at a similar location that is well characterized, such as L = 54 in., an estimated thickness for the remainder of the deposit profile can be inferred. The average H/U obtained from the iterative procedure is 5.

Table 3.7. Hockey Stick iterative results of total transmission thickness from vertical source and detector scan at $L = 80$ in.

Position y (in.)	$-\text{Ln}\,(I / I_o)$	Thickness (in.)[a]	
10	1.97	5.07	(3.74)
8	1.13	2.90	(3.29)
6	0.79	2.02	(1.89)
4	0.45	1.15	(1.05)
2	0.63	1.62	(1.11)
0	0.35	0.91	(1.03)
−2	0.45	1.16	(1.13)
−4	0.45	1.16	(1.03)
−6	0.52	1.33	(0.96)
−8	0.45	1.16	(1.31)
−10	0.29	0.76	(0.88)

[a] Results from detector #3 are given in parentheses. The center of detector # 3 was located 4.5 in. further up the pipe than the distance given in the table title (80 + 4.5 = 84.5 in. for location of detector #3). Values not in parentheses are from the data of detector #2, which was centered 80 in. along the pipe. These thicknesses are along a line of sight between the source and the detector.

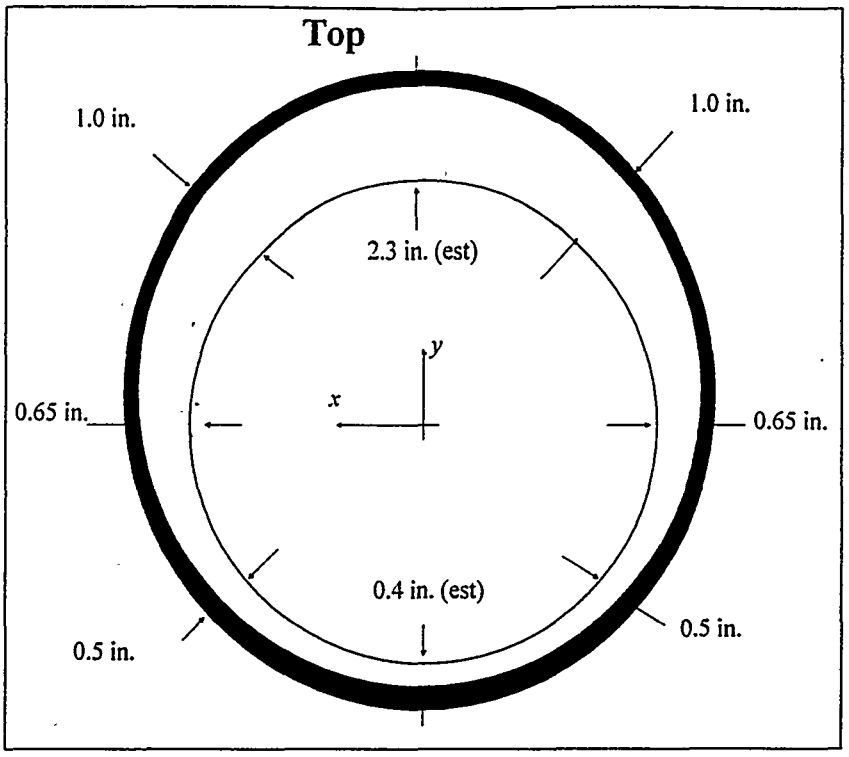

Fig. 3.13. Hockey Stick deposit profile at $L = 80$ in.

3.3.1.4. Measurement results at $L = 104$ in.

This deposit measurement location is on the vertical riser, immediately above the expansion joint (see Fig. 3.5). The average H/U value of ~2.2 is obtained from the iterative procedure. As evidenced from data obtained from the vertical and the horizontal source and detector scans (see Tables 3.8A and 3.8B), the deposit is more symmetric in this location, with deposit material now appearing in the lower (bottom) half of the process pipe, where none had been seen in previous locations. Data obtained from the source-detector rotation measurements (see Table 3.7C) show that there is a lack of material at one angular position on the pipe, as indicated by sudden dips in the estimated deposit thickness at 60° and 240°. This seems to be confirmed by corresponding dips at the $x = -4$ in. and -6 in. positions on the horizontal scan. The estimated deposit profile for this location is given in Fig. 3.14. The results from detector #3, which is located at $L = 108.4$ in., are also included in the data tables and are considerably different for the same x or y position. The comparison of the two detector measurements show similar variations and large irregularities in the measured deposit thicknesses.

Table 3.8A. Hockey Stick iterative results of total transmission thickness from vertical source and detector scan at L = 104 in.

Position y (in.)	–Ln (I / I_o)	Thickness (in.)[a]	
10	1.17	2.87	(2.59)
8	0.68	1.68	(2.14)
6	0.39	0.95	(1.25)
4	0.33	0.81	(1.13)
2	0.42	1.02	(0.58)
0	0.42	1.02	(1.19)
–2	0.23	0.57	(1.12)
–4	0.19	0.47	(1.20)
–6	0.29	0.71	(0.52)
–8	0.26	0.65	(0.79)
–10	0.35	0.87	(0.66)

[a] Results from detector #3 are given in parentheses. The center of detector # 3 was located 4.5 in. further up the pipe than the distance given in the table title (104 + 4.5 = 108.5 in. for location of detector #3). Values not in parentheses are from the data of detector #2, which was centered 104 in. along the pipe. These thicknesses are along a line of sight between the source and the detector.

Table 3.8B. Hockey Stick iterative results of total transmission thickness from horizontal source and detector scan at L = 104 in.

Position x (in.)	–Ln (I / I_o)	Thickness (in.)[a]	
10	0.69	1.70	(1.74)
8	0.71	1.75	(1.84)
6	0.63	1.54	(1.45)
4	0.51	1.24	(1.83)
2	0.64	1.57	(1.36)
0	0.52	1.27	(1.60)
–2	0.49	1.21	(1.49)
–4	0.38	0.92	(0.72)
–6	0.39	0.95	(0.92)
–8	0.60	1.47	(0.88)
–10	0.68	1.67	(0.31)

[a] Results from detector #3 are given in parentheses. The center of detector # 3 was located 4.5 in. further up the pipe than the distance given in the table title (104 + 4.5 = 108.5 in. for location of detector #3). Values not in parentheses are from the data of detector #2, which was centered 104 in. along the pipe. These thicknesses are along a line of sight between the source and the detector.

Table 3.8C. Hockey Stick iterative results of total radial thickness from source and detector rotation at L = 104 in.

Rotation α (Deg.)	$-\text{Ln}\,(I/I_0)$	Thickness (in.)[a]	
0	0.45	1.11	(1.18)
30	0.44	1.08	(0.62)
60	0.21	0.51	(0.26)
90	0.52	1.27	(0.66)
120	0.45	1.11	(0.67)
150	0.68	1.67	(1.51)
180	0.63	1.55	(1.60)
210	0.40	0.98	(0.88)
240	0.28	0.68	(0.75)
270	0.64	1.58	(1.21)
300	0.77	1.88	(1.17)
330	0.63	1.55	(0.93)

[a] Results from detector #3 are given in parentheses. The center of detector # 3 was located 4.5 in. further up the pipe than the distance given in the table title (104 + 4.5 = 108.5 in. for location of detector #3). Values not in parentheses are from the data of detector #2, which was centered 104 in. along the pipe. These thicknesses are along a line of sight between the source and the detector and in this case are along a diameter.

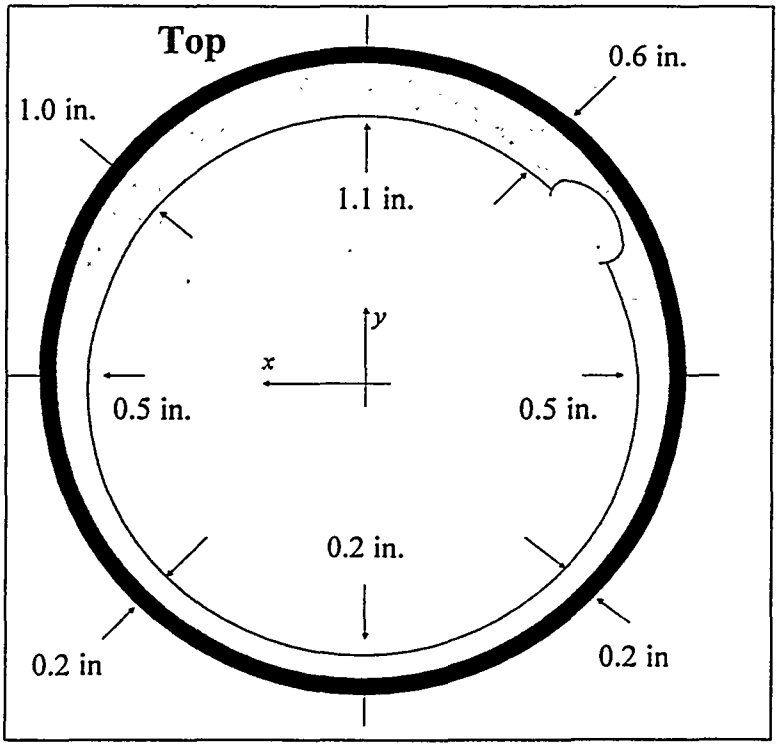

Fig. 3.14. Hockey Stick deposit profile at L = 104 in.

3.3.1.5. Measurement results at L = 133 in.

As shown in Fig. 3.5, this measurement location is approximately halfway up the inclined riser, midway between the two expansion joints. The measurement results from the vertical and the horizontal source and detector scans are presented in Tables 3.9A and 3.9B, respectively, and the estimated deposit profile is given in Fig. 3.15. The measured thicknesses have less irregularity from location to location at the top of the riser of the Hockey Stick, in contrast to the data at L = 54 in. The deposit profile becomes increasingly symmetric further up the vertical riser, although there is still a slight tendency for more deposit material to exist in the upper half of the process pipe than in the lower region. Detector #3 (which is located at L = 137.5 in.) results have a trend similar to detector #2 results, but the deposit is less thick, especially on the midplane. The average H/U obtained from the iterative procedure is ~5.25 at this measurement location.

Table 3.9A. Hockey Stick iterative results of total transmission thickness from vertical source and detector scan at L = 133 in.

Position y (in.)	$-\text{Ln}\ (I / I_o)$	Thickness (in.)[a]	
10	1.06	2.94	(0.79)
8	0.91	2.51	(0.97)
6	0.62	1.73	(0.76)
4	0.51	1.42	(0.66)
2	0.60	1.65	(0.79)
0	0.41	1.12	(0.90)
−2	0.63	1.74	(1.01)
−4	0.44	1.21	(0.72)
−6	0.58	1.60	(0.74)
−8	0.61	1.68	(0.89)
−10	0.73	2.01	(0.94)

[a] Results from detector #3 are given in parentheses. The center of detector # 3 was located 4.5 in. further up the pipe than the distance given in the table title (133 + 4.5 = 137.5 in. for location of detector #3). Values not in parentheses are from the data of detector #2, which was centered 133 in. along the pipe. These thicknesses are along a line of sight between the source and the detector.

Table 3.9B. Hockey Stick iterative results of total transmission thickness from horizontal source and detector scan at L = 133 in.

Position x (in.)	$-\text{Ln}\,(I / I_o)$	Thickness (in.)[a]	
10	0.63	1.62	(0.62)
8	0.88	2.29	(1.32)
6	0.76	1.97	(1.46)
4	0.93	2.42	(1.67)
2	1.21	3.14	(1.89)
0	0.63	1.62	(1.50)
−2	0.83	2.15	(1.69)
−4	0.90	2.34	(1.51)
−6	0.77	2.00	(1.30)
−8	0.65	1.68	(1.69)
−10	0.61	1.59	(1.19)

[a] Results from detector #3 are given in parentheses. The center of detector # 3 was located 4.5 in. further up the pipe than the distance given in the table title (133 + 4.5 = 137.5 in. for location of detector #3). Values not in parentheses are from the data of detector #2, which was centered 133 in. along the pipe. These thicknesses are along a line of sight between the source and the detector.

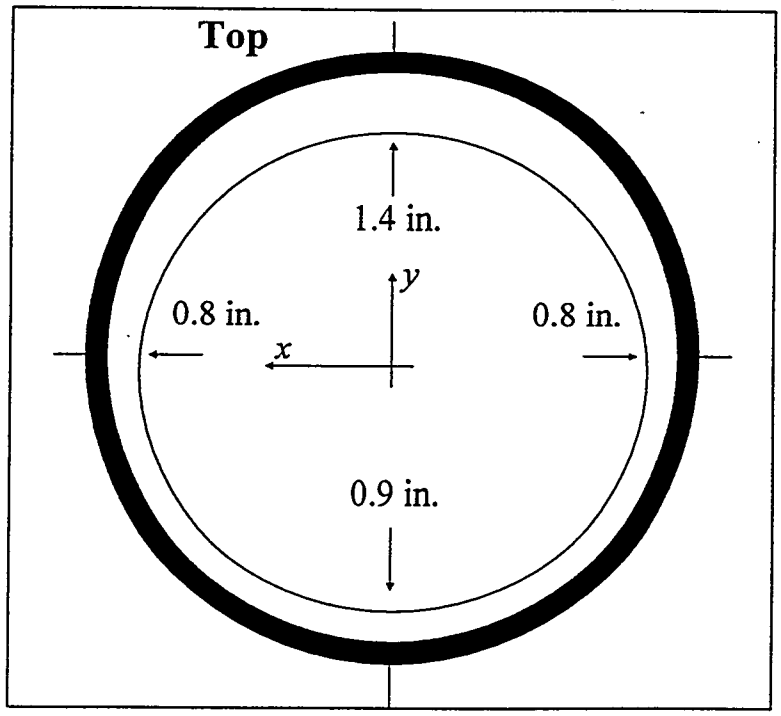

Fig. 3.15. Hockey Stick deposit profile at L = 133 in.

3.3.1.6. Measurement results at L = 163 in.

L = 163 in. is the last measurement location and corresponds to the highest position on the vertical riser, about 10 ft from the cell floor. Table 3.10A and 3.10B, respectively, present the measured vertical and the horizontal source and detector scan deposit data for this location together with the results from detector #3, located at L = 167.5 in. The estimated deposit profile is given in Fig. 3.16. The measured deposit is very symmetric compared with those measured at the rest of the locations and is somewhat thinner than the deposit at L = 133 in. The second detector also shows slightly less deposit material in this location. The both detectors indicate that the measured data appear to vary much more smoothly than the results measured at L = 54 in. and L = 80 in. The average H/U found from the iterative procedure is 4.6.

Table 3.10A. Hockey Stick iterative results of total transmission thickness from vertical source and detector scan at L = 163 in.

Position y (in.)	$-\text{Ln}(I/I_o)$	Thickness (in.)[a]	
10	0.27	0.74	(0.45)
8	0.42	1.13	(0.70)
6	0.38	1.05	(0.85)
4	0.46	1.24	(0.68)
2	0.57	1.56	(1.03)
0	0.45	1.22	(0.93)
–2	0.57	1.56	(0.82)
–4	0.60	1.62	(0.83)
–6	0.48	1.29	(0.83)
–8	0.49	1.32	(1.01)
–10	0.41	1.12	(0.48)

[a] Results from detector #3 are given in parentheses. The center of detector # 3 was located 4.5 in. further up the pipe than the distance given in the table title (163 + 4.5 = 167.5 in. for location of detector #3). Values not in parentheses are from the data of detector #2, which was centered 163 in. along the pipe. These thicknesses are along a line of sight between the source and the detector.

Table 3.10B. Hockey Stick iterative results of total transmission thickness from horizontal source and detector scan at L = 163 in.

Position x (in.)	$-\text{Ln}\,(I / I_o)$	Thickness (in.)[a]	
10	0.34	0.93	(1.05)
8	0.52	1.41	(1.08)
6	0.68	1.84	(1.10)
4	0.60	1.63	(1.33)
2	0.67	1.83	(1.37)
0	0.59	1.59	(1.38)
−2	0.73	1.98	(1.79)
−4	0.74	2.02	(1.35)
−6	0.70	1.89	(1.15)
−8	0.66	1.80	(1.50)
−10	0.74	2.02	(0.49)

[a] Results from detector #3 are given in parentheses. The center of detector # 3 was located 4.5 in. further up the pipe than the distance given in the table title (163 + 4.5 = 167.5 in. for location of detector #3). Values not in parentheses are from the data of detector #2, which was centered 163 in. along the pipe. These thicknesses are along a line of sight between the source and the detector.

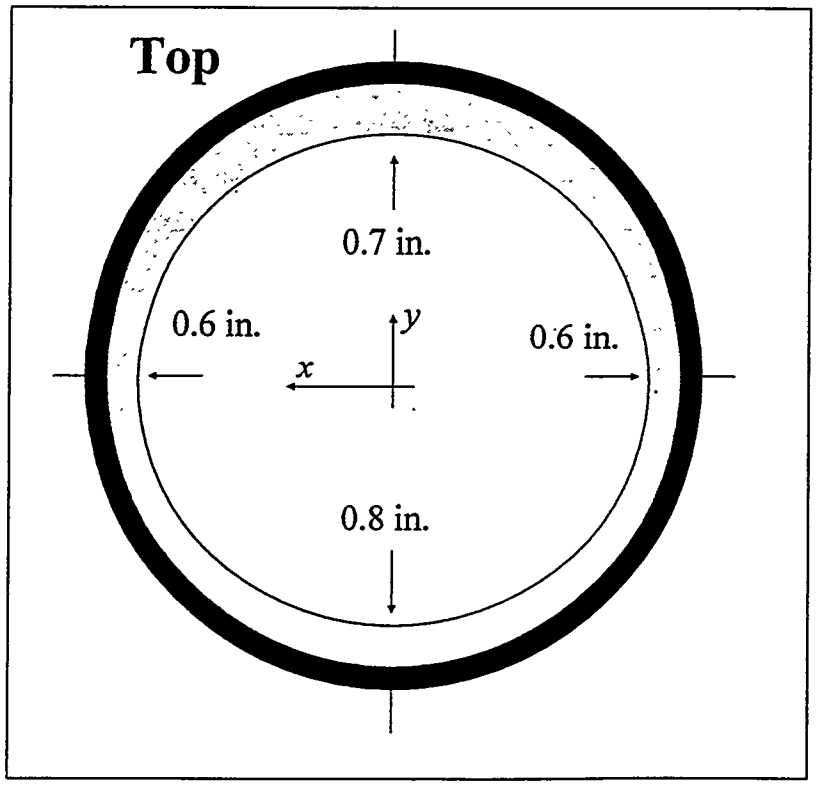

Fig. 3.16. Hockey Stick deposit profile at L = 163 in.

3.3.1.7. Summary of deposit distribution

The Hockey Stick deposit profile findings can be briefly summarized as follows. The deposit is annular in shape and mostly located on the top of the Hockey Stick process pipe up to $L = 104$ in. An asymmetric deposit was found around the elbow region of the process pipe. Comparison of the results obtained from the two NWIS detectors, which are 4.5 in. apart along the process pipe, indicate strong irregularities in the deposit material over small distances. This observation was later confirmed from the intrusive look inside the process pipe discussed in Sect. 5. The deposit distribution becomes more uniform with distance up the riser section of the Hockey Stick; that is, for $L > 104$ in. In general, the deposit varies from a very asymmetric distribution at the bottom of the Hockey Stick near the outlet 7BB2 block valve to an increasingly symmetric deposit at the top of riser. The deposit loading (kilogram per foot) or thickness decreases along the process pipe, and the deposit material distribution appears to become more smoothly varying.

3.3.2. H/U for Hockey Stick deposit

The method of obtaining H/U was discussed in detail in Sect. 2.2. The values of H/U are obtained from the deposit profile results together with the measurements of the gamma-ray attenuation results in Fig. 2.17. To avoid the extreme sensitivity of thin deposits for resolving the value of H/U satisfactorily, the deposits that are less than 1 in. thick were not used in this data analysis. About 64 measurements satisfied the criterion. The values of H/U from measurements obtained from the iterative procedure are given in Tables 3.11 and A.7. The frequency distribution of the H/U data from these iterated values for detector #2 is given in Fig. 3.17. The mean value of H/U is obtained from Table 3.11 as H/U $\doteq$ 3.5; a standard deviation of the mean value is 0.20 for these 64 measurement results. Thus the measured value of H/U for the Hockey Stick has an average value H/U = 3.5 $\pm$ 0.20. The average value for detector #2 was H/U = 3.4 $\pm$ 0.25, obtained from Table 3.10B. The average value from detector #3 was H/U = 3.6 $\pm$ 0.24, obtained from Table A.7.

Table 3.11. Hockey Stick iterated values of H/U from measurements with detector #2

0.5	2.3	3.5	4.2	4.9
0.5	2.8	3.7	4.2	5.1
0.5	2.9	3.7	4.5	5.1
1.5	3.0	3.8	4.5	5.7
1.5	3.0	3.9	4.7	
2.0	3.3	4.0	4.8	
2.2	3.3	4.0	4.9	

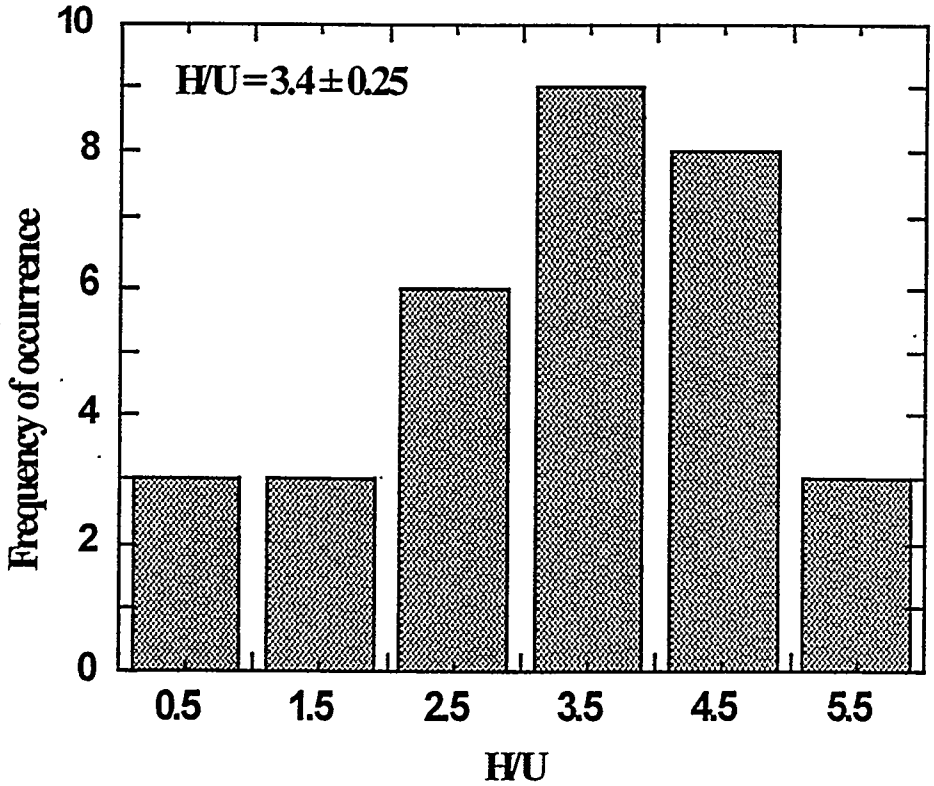

Fig. 3.17. Hockey Stick frequency distribution for iterated values of H/U from measurements.

3.3.3. Uncertainty for the deposit thickness measurements

The uncertainty for the deposit thickness $\Delta d/d$ can be estimated for the measurements from Eq. (2) by making use of the method of error propagation. From the partial derivatives of Eq. (2) taken with respect to the each variable in the equation, and after arranging the variables in the form of relative error, $\Delta d/d$ can be calculated as

$$\Delta d/d = \pm\{(\Delta\Sigma_t / \Sigma_t)^2 + [(\Delta I_O / I_O)^2 + (\Delta I/I)^2] / (d\,\Sigma_t)^2\}^{0.5} . \qquad (8)$$

The upper bound of $\Delta d/d$ can be estimated by using a relatively thinner deposit thickness of $d \sim 1$ in. Taking $\Delta I_O / I_O = \Delta I/I \approx \pm 5\%$ as a typical value for the measurements, and $\Delta\Sigma_t / \Sigma_t \approx \pm 3\%$, which is obtained from the measured value of H/U = 3.4 ± 0.25 in the neutron cross section data (Fig. 2.12), and also taking Σ_t (H/U = 3.4) ≈ 0.165 cm^{-1} from Fig. 2.12 and using these in Eq. (8), leads to $\Delta d/d \approx \pm 17\%$. Therefore, the Hockey Stick deposit profile results presented here have a typical uncertainly of $\leq \pm 17\%$.

3.3.4. Hockey Stick total uranium mass

As discussed in Sect. 2.4, the total uranium mass of a deposit is calculated from the deposit profile, its distribution obtained along Hockey Stick, and the measurements of the H/U ratio needed for determining the uranium density. The total mass of each measurement segment i can be obtained from the measured deposit thickness and its shape. However, these calculations were simplified by assuming a uniform deposit profile within the measurement segment, as defined in Sect. 2.5, having an average deposit thickness $\bar{d}_i$, which can be obtained by averaging the thicknesses given on the deposit profile, thus,

$$\bar{d}_i = (1/N_i) \sum_j d_j, \qquad \text{with } j = 1, N_i , \qquad (9)$$

where d_j is the deposit thickness given for each point (indicated with an arrow) on the profile, and N_i is the total number of points on the profile, as shown in Figs. 3.11 through 3.16. This approach is equivalent to averaging the deposit profile over the surface area as discussed in Appendix C. The total deposit volume V_d of the Hockey Stick can then be estimated from the volume of the each deposit segment V_i as

$$V_d = \sum_i V_i = \sum_i \pi L_i \, \bar{d}_i \, (D - \bar{d}_i), \quad \text{with } i = 1, N \,, \tag{10}$$

where L_i is the length of the measurement segment, measured on the midplane of the pipe (see Fig 3.18), as defined in Sect. 2.4, such that $L_t = \sum_i L_i = 163$ in. is the total length of the Hockey Stick on which the deposit distribution is characterized, N is the number of measurement locations (which is also the number of measurement segments), and $D = (D_O - 2w)$ is the inner diameter of the process pipe. The limited number of measurement positions preceded any other choice for estimating the volume of the deposit. The deposit volume for the 15-in.-long transition section (see Fig. 3.18) is calculated with a 22-in. diameter that corresponds to the center of the transition section where the deposit measurements were performed ($L = 40$ in.). The measured deposit profile results presented in Figs 3.11 through 3.16, and taking $N = 6$ as the total number of measurement segments in Eq. (10), the estimated results of the deposit volume of the each measurement segment are presented in Table 3.12, and the locations of these segments are shown in Fig. 3.18. The total deposit volume then is $V_d \approx 0.142$ m^3 for detector #2 and $V_d \approx 0.140$ m^3 for detector #3. An assumption is made when Eq. (10) is used that the thickness along the pipe varies linearly, although the data show that the deposit is highly irregular. With only six measurement locations, this is all that could be done. However, it is reassuring to observe that the numbers obtained for the data of two different detectors are in close agreement when using Eq. (10).

The density of the uranium in the Hockey Stick deposit is obtained from Fig. 2.17, or Barber's relationship of

$$\rho_u = 4.96 - 0.32 \times (\mathrm{H/U}) \,, \tag{11}$$

which is valid for H/U ≤ 4 in the water-moderated mixtures of uranyl fluoride [Ref. 17]. Using Eq. (11) for the uranium density of the deposit and its associated error, $\Delta\rho_u = 0.32 \times \Delta(\mathrm{H/U})$, $\rho_u = (3.87 \pm 0.08)$ g/cc is obtained for the measured moderation level of H/U = 3.4 ± 0.25. The total uranium mass in the deposit $M_u = \rho_u \times V_d$, and the associated error calculated from Eq. (7) lead to $M_u = 552 \pm 93$ kg. The enrichment of 3.34% (± 50% uncertainty) [Ref. 1], gives a total mass of ^{235}U of about 18 ± 2.3 kg. Similar results for the data of detector #3 are: H/U = 3.6 ± 0.24, $M_u = 532 \pm 90$ kg (see Appendix A).

The agreement between the two detector channels is quite good even though the adjacent detectors showed local variations. This result is consistent with the NDA measurements on the removed Hockey Stick deposit (Table 3.13).

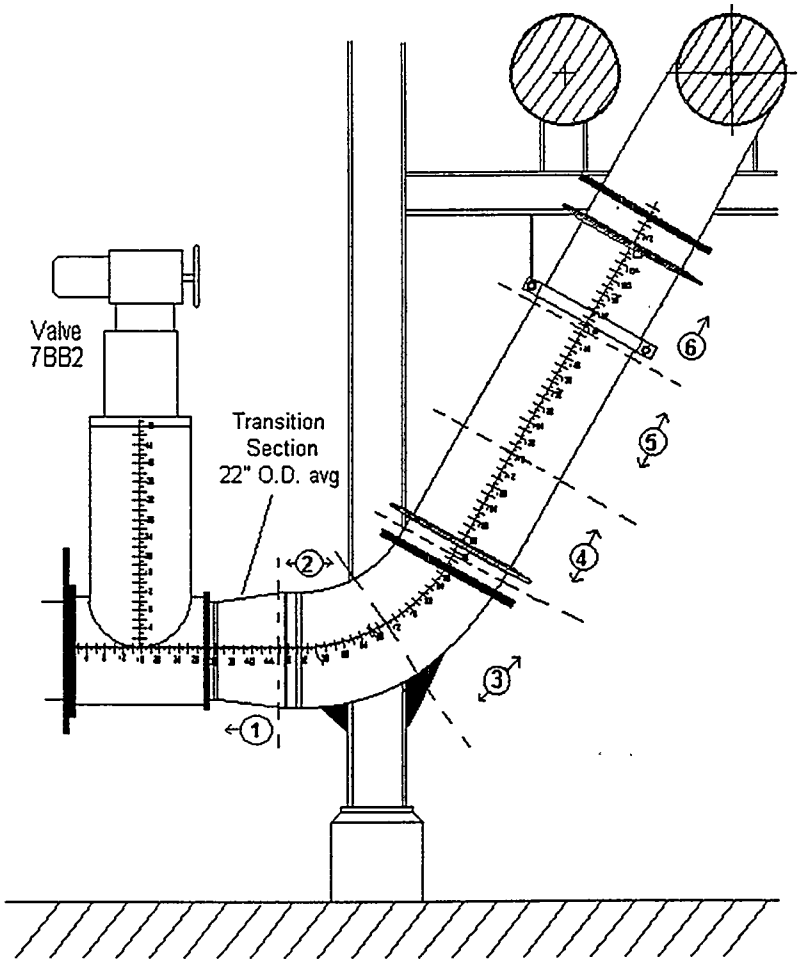

Fig. 3.18. Location of Hockey Stick measurement segments (see Table 3.11) used for calculation of deposit volume.

Table 3.12. Hockey Stick measurement deposit segments for obtaining the deposit volume from detector #2 results

Measurement location L (in.)	Deposit profile figure	Segment location (in.)	Measurement segment length L_i (in.)[a]	Segment average deposit thickness $\bar{d}_i$ (in.)	Segment volume V_i (in.^{3})[b]
40	3.11	0 – 47	47	0.38	1247[c]
54	3.12	47 – 67	20	0.89	1250
80	3.13	67 – 92	25	0.87	1529
104	3.14	92 – 118.5	26.5	0.53	1002
133	3.15	118.5 – 148	29.5	0.97	2003
163	3.16	148 – 163	15	0.67	1675[d]

[a] Measured on the midplane of the pipe (see Fig. 3.18).

[b] Total deposit volume: $V_d = \sum_i V_i = 8706$ in.^{3}

[c] Includes 15-in.-long transition section with an average diameter of 22 in. (see Fig. 3.18).

[d] Includes up to the top of the Hockey Stick, assuming that the deposit thickness varies linearly to the 0.1-in.-thickness at the top.

Table 3.13. Hockey Stick and Tee-Pipe NDA deposit removal results

Item	Post-Removal NDA Results			Reference (Appendix D)
	Total U[a] (kg)	^{235}U[b] (wt %)	^{235}U[a] (kg)	
Hockey Stick—Deposit material in fissile cans	425	2.73 to 3.44	12.8	NDA98-011
Hockey Stick—Removed pipe segments	25.1	3.0	0.754	NDA98-001
Hockey Stick—Pipe sections remaining in place	28.5		0.94	NDA97-423
Hockey Stick totals	478.6		14.5	
Valve 7BB2 (no fissile cans were generated; no pipe sections were removed)	----	-----	-----	
Valve 7BB2—remaining in place	14.8	3.3 (assumed)	0.49	NDA97-423
Valve 7BB2 Totals	14.8		0.49	
Tee-Pipe—Deposit material in fissile cans	84.4	2.78 to 3.13	2.53	NDA97-353 NDA97-370
Tee-Pipe—Removed pipe segments (none generated)	----	----	----	-----
Tee-Pipe—Pipe section remaining in place	14.05	3.01	0.42	NDA97-373
Tee-Pipe totals	98.5	-----	2.95	

[a] Uncertainty on NDA mass values is ± 50% of mass value.

[b] Uncertainty on NDA measured enrichments is ± 20% of enrichment value.

3.3.5. 7BB2 block valve deposit distribution measurement results

Deposit measurements were performed along the 7BB2 block valve (Fig. 3.19). The height of the valve body is L_V = 36 in., as indicated in the figure, and has a D_V = 24 in. OD. The measurements were performed for L = 9, 15, and 21 in. by scanning the source and detectors vertically, along the valve body, in 6-in. increments up to the height of H = 40 in. measured from the vertical midplane of the Hockey Stick (see Fig. 3.19). The empty valve calibration measurements were performed on a clean identical block valve located on a clean Hockey Stick process pipe. The initial deposit thickness results indicated the presence of a very thin deposit or no deposit at all. Therefore, it was not possible to determine an H/U value for the valve deposit. Thus, as discussed in Sect. 3.3.3, the deposit thickness was estimated from Eq. (2) by using Σ_t (H/U = 3.4) $\approx$ 0.165 cm^{-1}, obtained from the average measured value of H/U = 3.4 from the previous Hockey Stick deposit measurements. The deposit thickness measurement results are presented in Tables 3.14, 3.15, and 3.16 for L = 9 in., L = 15 in., and L = 21 in., respectively. As shown from these results, no deposit was measured except at the L = 21 in. measurement location. As seen from Table 3.14 (for L = 9 in.) and Table 3.15 (for L = 15 in.), most of the measured deposit thickness values are negative because of the precision of the measurement. The negative values are not physical, and result from the presence of a very thin deposit or no deposit at all, as discussed in Sect. 2.2.3. The thickness of the deposit was well within the uncertainty of the measurement, and thus led to nonphysical results.

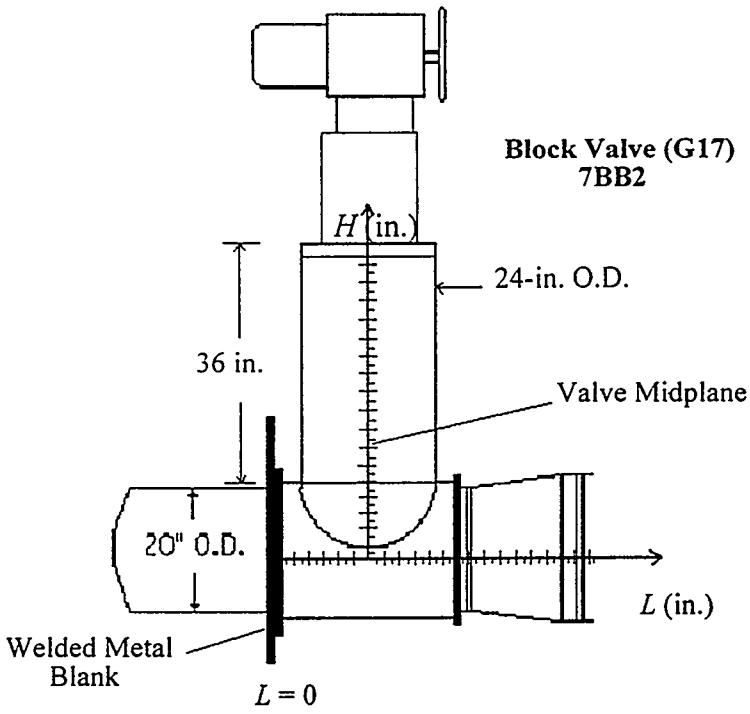

Figure 3.19. Unit 2, Cell 7, G-17 block valve (7BB2), showing the measurement path along the valve body measured from the Hockey Stick midplane, $H = 0$.

Table 3.14. Hockey Stick block valve results of total thickness from vertical source and detector scan at $L = 9$ in.

Position H (in.)	$-\text{Ln}\,(I / I_o)$	Thickness (in.)[a]
10	−0.064	NP
16	−0.119	NP
22	−0.088	NP
28	−0.088	NP
34	−0.047	NP
40	−0.040	NP

[a] Note: Not physical (NP). Please see Sect. 2.2.3 for the discussions of measurements of thin deposits.

Table 3.15. Hockey Stick block valve results of total thickness from vertical source and detector scan at $L = 15$ in.

Position H (in.)	$-\text{Ln}\,(I/I_0)$	Thickness (in.)[a]
10	−0.017	NP
16	−0.003	0.00
22	−0.083	NP
28	−0.199	NP
34	−0.012	NP
40	0.064	0.15

[a]Note: Not physical (NP). Please see Sect. 2.2.3 for the discussions of measurements of thin deposits.

Table 3.16. Hockey Stick block valve results of total thickness from vertical source and detector scan at $L = 21$ in.

Position H (in.)	$-\text{Ln}\,(I/I_0)$	Thickness (in.)[a]
10	−0.475	NP
16	0.582	1.43
22	0.754	1.85
28	0.734	1.80
34	0.194	0.47
40	0.242	0.59

[a]Note: Not physical (NP). Please see Sect. 2.2.3 for the discussions of measurements of thin deposits.

The block valve measurement results, obtained from $L = 21$ in., for the normalized deposit distribution along the valve are summarized in Fig. 3.20. The maximum deposit thickness (about 1 in.) is located at the middle of the valve toward the right of the process pipe. From that point on, the deposit thickness drops to about 0.3 in. at the top of the valve and about 0.1 in. on the bottom part of the valve. No deposit was measured on the left side of the valve. An average deposit thickness for the right halve of the valve body can be estimated from Table 3.16 (given for $L = 21$ in.) by averaging the data for all measurement locations, and $\bar{d}_a = 0.5$ in. is obtained from the average total deposit thickness of 1.0 in. A color photograph of the inside of the Hockey Stick looking toward the block valve and its surroundings is given in Fig. 3.21.

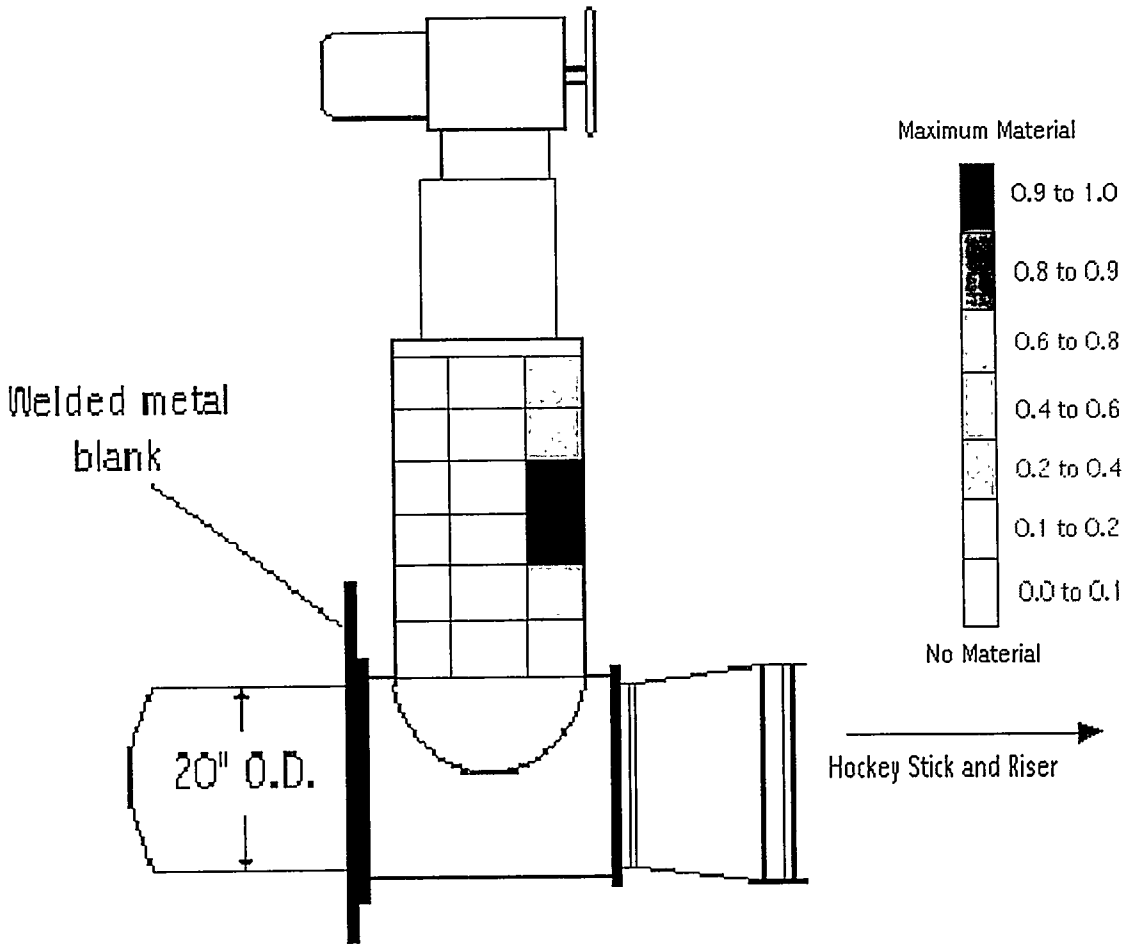

Fig. 3.20. Relative deposit distribution in the Unit 2, Cell 7, G-17 block valve.

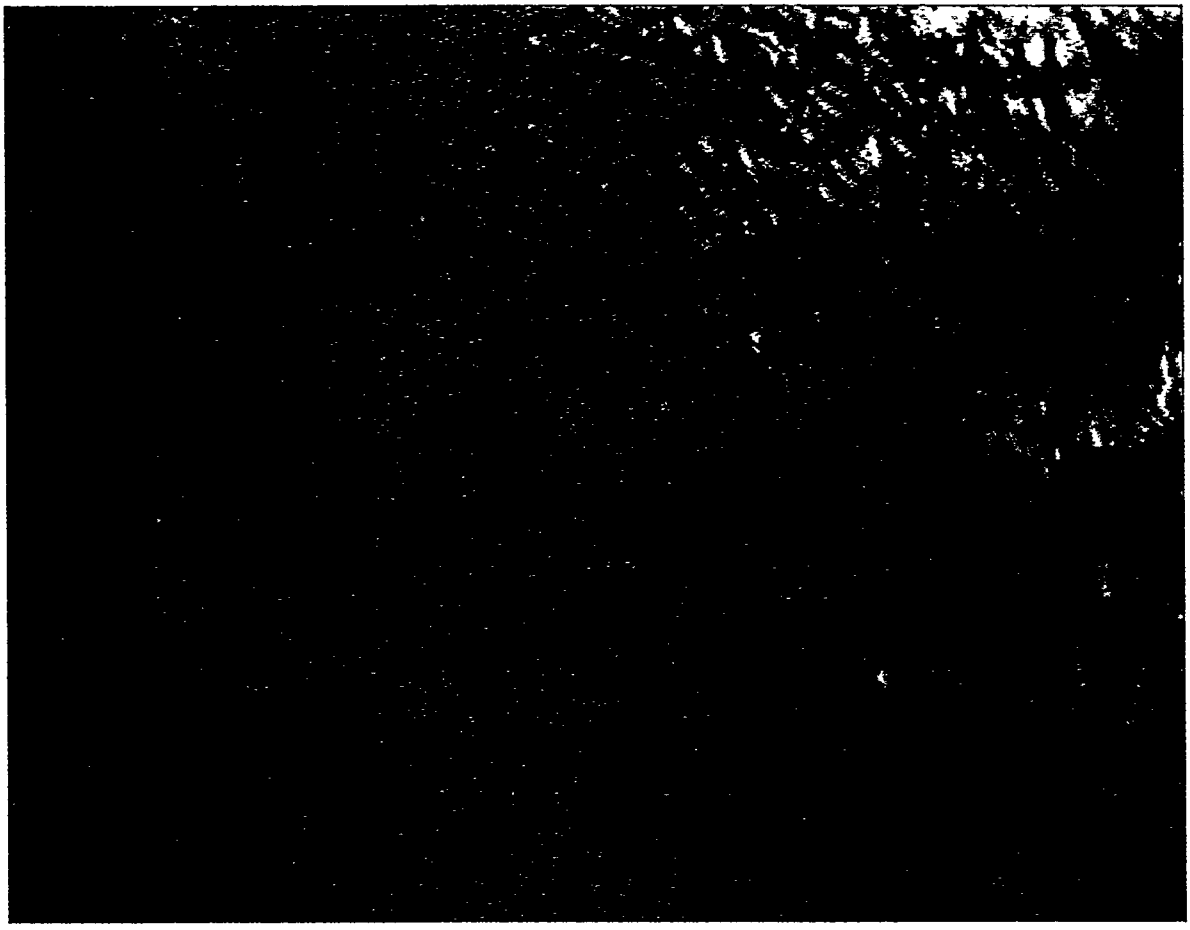

Fig. 3.21. Photograph of the Hockey Stick block valve deposit distribution obtained with the fiber-optic camera inserted into the pipe.

3.3.6 7BB2 block valve total uranium mass

The total uranium mass in the 7BB2 block valve was estimated by making using the average deposit thickness $\bar{d}_a$ = 0.5 in. obtained in Sect. 3.3.5. As shown in Fig. 3.20 that the measured deposit distribution in the valve body is located on the right half of the valve at L = 21 in., which is half way up the valve body. Thus the deposit is present mostly at about 1/6 of the valve peripheral. Therefore, the deposit volume can be estimated as

$$V_d = \pi L_V \, \bar{d}_a \times (D_V - 2w - \bar{d}_a)/6. \qquad (12)$$

Taking L_V = 36 in. for the length of the valve body, and D_V = 24 in. for the diameter of the valve in Eq. (12), the deposit volume then becomes $V_d = 3.4 \times 10^{-3}$ m^3. Using H/U ~ 3.5 and the corresponding ρ_u = 3.87 g/cc from the previous Hockey Stick measurements, the block valve total uranium mass of $M_u = \rho_u \times V_d \approx 13$ kg is estimated as an upper bound value.

3.4. Summary of Hockey Stick and 7BB2 Block Valve Deposit Measurements

The deposit characterization measurement results for the Hockey Stick and the 7BB2 block valve can be summarized as follows:

- The overall shape of the deposit in the Hockey Stick is annular; i.e., it is not solid. The distribution of the deposit along the Hockey Stick is summarized in Fig. 3.22.
- Spatially asymmetric (top-to-bottom) deposits are located below L = 104 in.
- The asymmetric deposit is thicker on the top of the Hockey Stick process pipe.
- The asymmetric deposit is mostly located around the pipe elbow (L = 40–104 in.) as seen in Fig. 3.22.
- The Hockey Stick deposits have thickness irregularities (that is, holes and bumps) along the process pipe periphery.
- The average measured H/U = 3.5 ± 0.20.

- The total measured uranium mass in the Hockey Stick is 542 ± 92 kg.

- The 7BB2 block valve deposit is located at the vertical center of the valve body toward the right, and the maximum thickness is about 1 in.

- The average deposit thickness on the wall along the valve body at location $L = 21$ in. is about 0.5 in. (The total deposit thickness at this location was 1.0 in.)

- The total measured uranium deposit mass of ~13 kg in the valve body is estimated as an upper bound value.

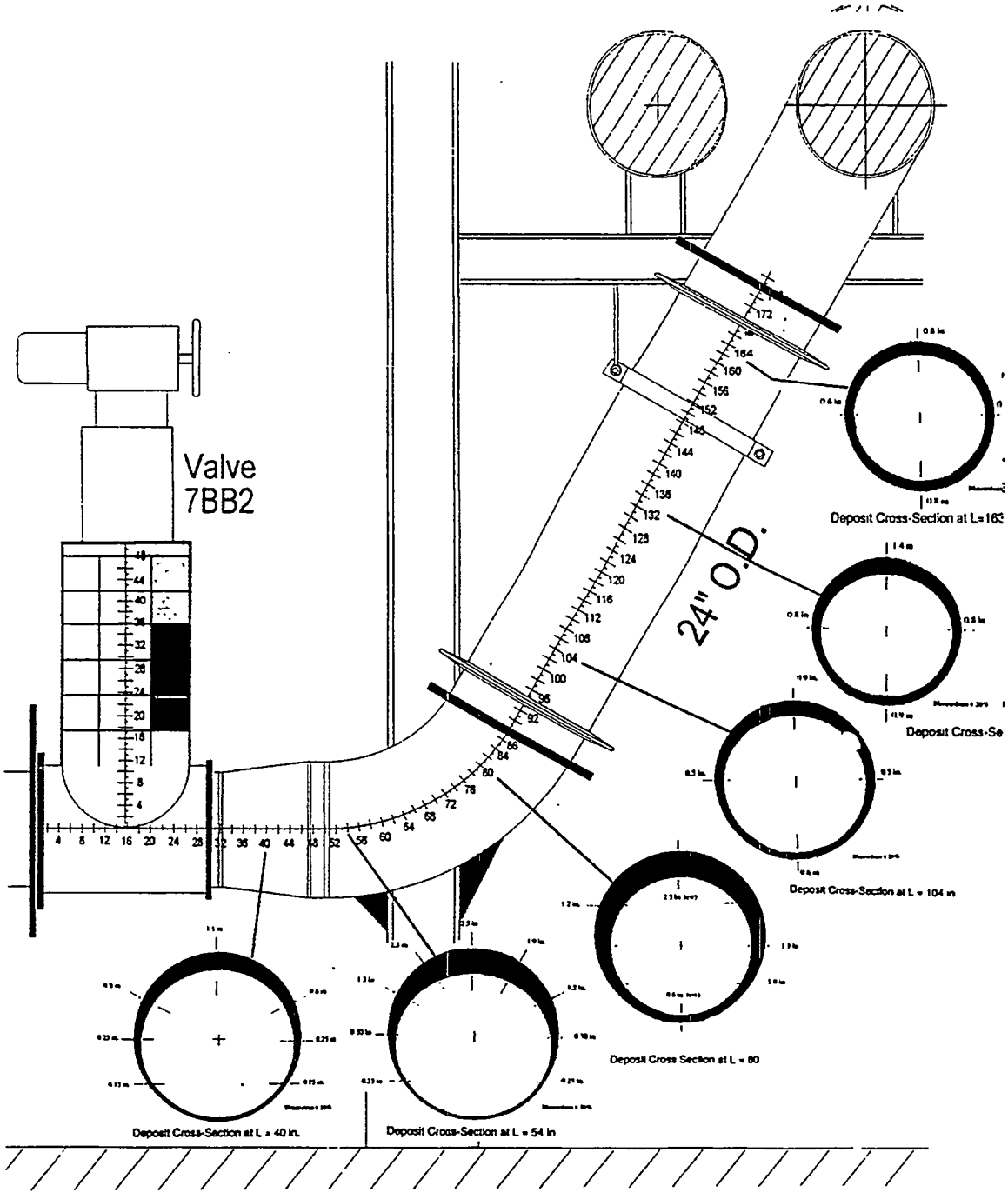

Fig. 3.22. Distribution of the deposit profile along the Hockey Stick.

4. UNIT 2, CELL 6 A-LINE OUTLET (TEE-PIPE) DEPOSIT MEASUREMENTS

4.1. Description of the Measurements

The deposit characterization measurements were performed at a number of locations on the Unit 2, Cell 6, A-Line Outlet process pipe, the Tee-Pipe similarly to the previous measurements on Hockey Stick. Figure 4.1 shows the Tee-Pipe, which consists of a horizontal section, D_h = 30 in. OD, about 10 ft long, and a riser section, D_r = 24 in. OD and about 12 ft long. These two sections are connected through a transition section that has flat surfaces on the front and the back of the process pipe. As shown in the figure, the Tee-Pipe has a massive support structure underneath the horizontal section that limited the ability of performing measurements around that region. Therefore, the equipment used to measure the Hockey Stick was modified to measure the Tee-Pipe. Only one detector (detector #2) was used to suit the shape of the Tee-Pipe and the limited clearances around it. In addition, a new fixture was fabricated to place the source and detector on the transition section of the Tee-Pipe, as shown in Fig. 4.2. Moreover, as in the Hockey Stick measurements, the same safety precautions were followed for securing the measurement fixture around the Tee-Pipe structure by using safety cables to eliminate the movement of the fixture inadvertently on the process pipe. Safety concerns were constantly considered for selecting and locating the measurement system on the process pipe so that the measurements would be performed safely. Altogether, more than 300 measurements were performed on the Tee-Pipe. During these measurements only one detector (detector #2 as shown in Fig. 2.2) was utilized because of constraints from the physical shape of the Tee-Pipe as well as limited clearance between the pipe and structures around it.

As discussed in Sect. 3.2, the measurement reproducibility and calibration procedures were also used for the Tee-Pipe deposit characterization. The detector efficiency was maintained, the measurement precision was ensured by taking 10^9 data blocks, and the reproducibility of the measurements was verified by performing repeated measurements at the same locations. The empty process pipe calibration measurements were also performed on a nearby Tee-Pipe that had no holdup material.

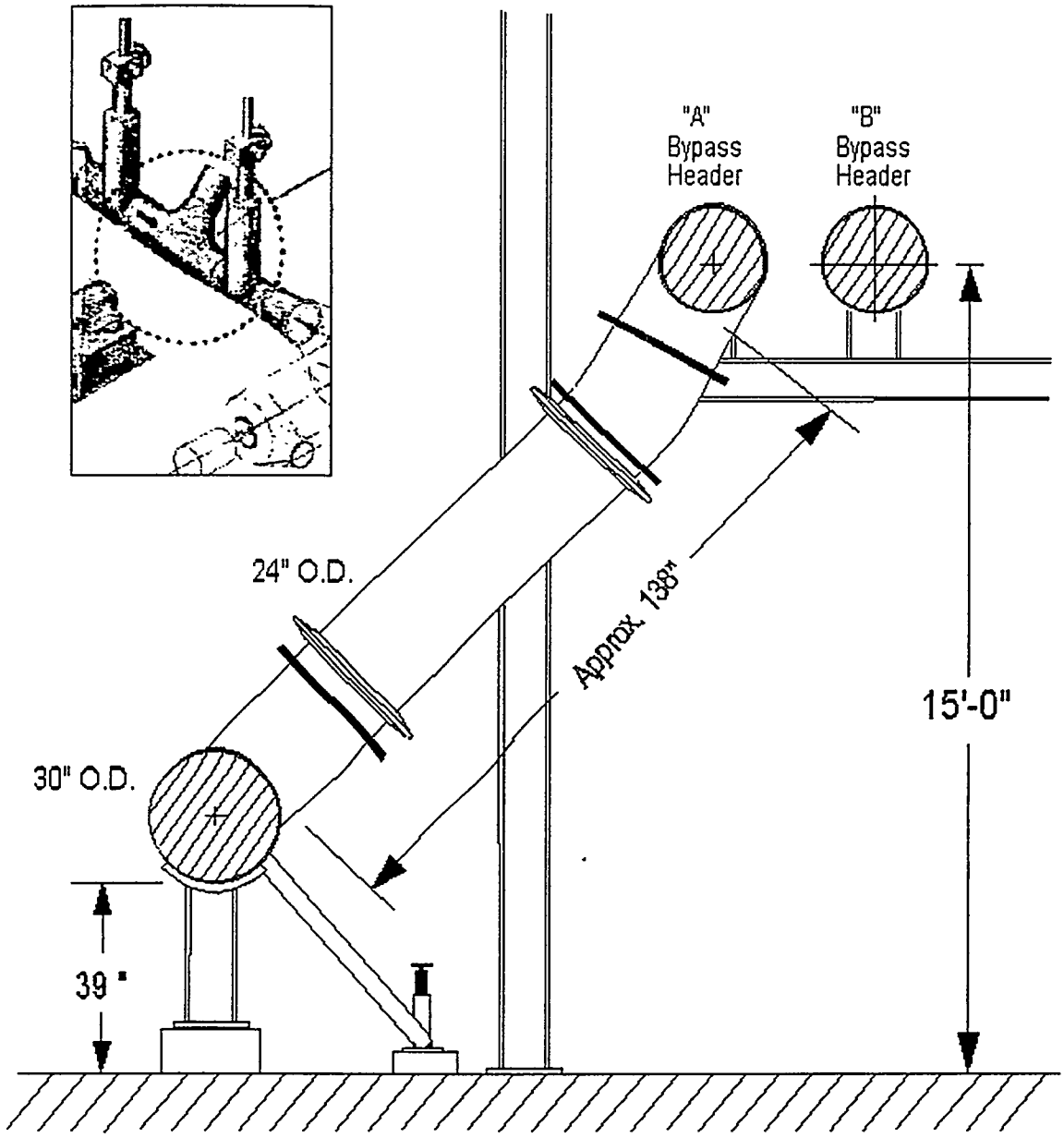

Fig. 4.1. Dimensions of Unit 2, Cell 6, A-Line Outlet process Tee-Pipe.

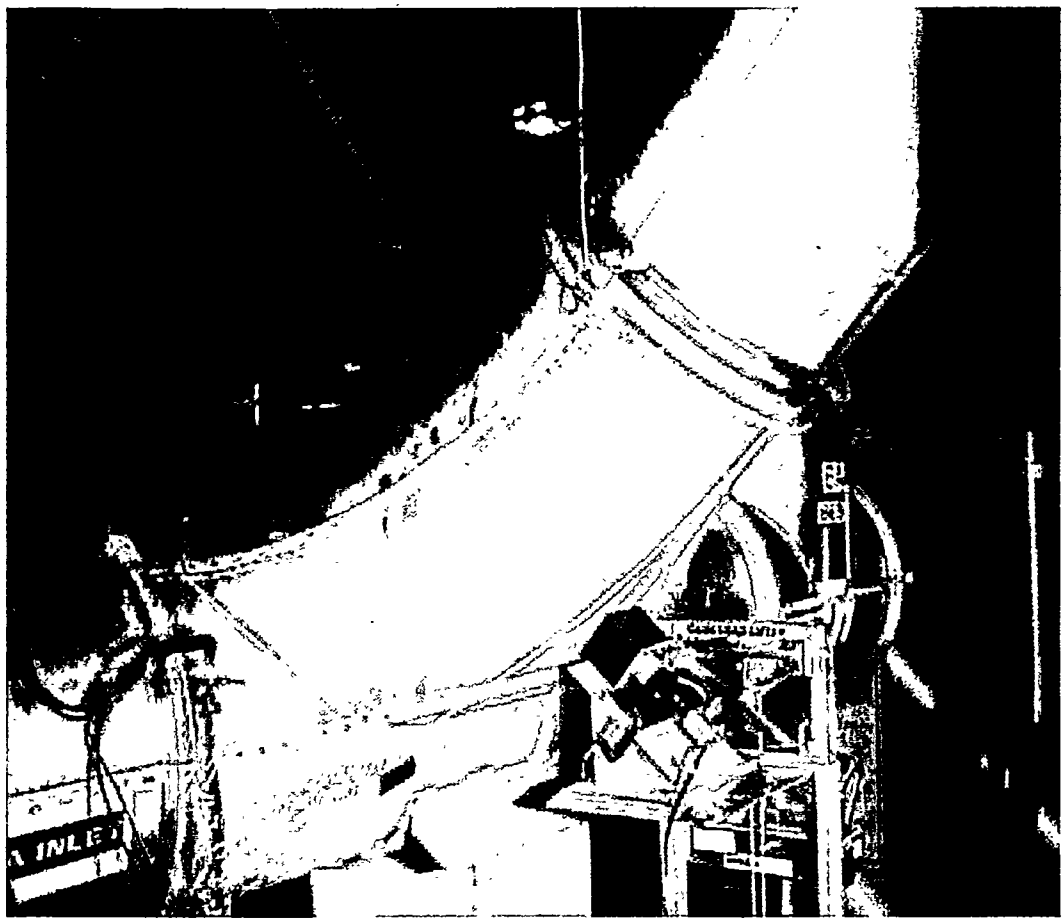

Fig. 4.2. Placement of source and detector on Tee-Pipe transition section by means of a wedge-shaped fixture.

4.2. Tee-Pipe Measurement Results

The Tee-Pipe measurements were performed on the horizontal, riser, and transition sections of the Tee-Pipe, as indicated on Fig. 4.3. The measurement locations on the horizontal section are given with respect to the center of the block valve (right side), $L = 0$, as shown on the figure. For the riser section, the measurement locations are indicated on the shoulder of the process pipe measured from the block valve (left side), $I = 0$, when the Tee-Pipe is observed from the floor in front of it, as indicated in Fig. 4.3, and this side of the Tee-Pipe is designated the "front side." The measurements on the transition section are given from the midplane of the horizontal section, indicated as $T = 0$ on Fig. 4.3.

The same measurement technique and data analysis were used for these deposit characterization measurements as were used for Hockey Stick. The deposit thickness was

estimated from Eq. (2). However, the measurements indicated that overall there was a very thin deposit of material distributed on the this process pipe, much less than 1 in., as a minimum value to get an accurate estimate of H/U, which is needed to determine Σ_t. Therefore, H/U = 3.4 ± 0.25, found from the Hockey Stick measurements, was assumed for the Tee-Pipe deposit and Σ_t (H/U = 3.4) ≈ 0.165 cm^{-1}, obtained from Fig. 2.12, was used for the calculations of the deposit thickness. The empty process pipe calibration measurements for I_0 were performed on a similar clean Tee-Pipe, right after or before the deposit measurements were performed.

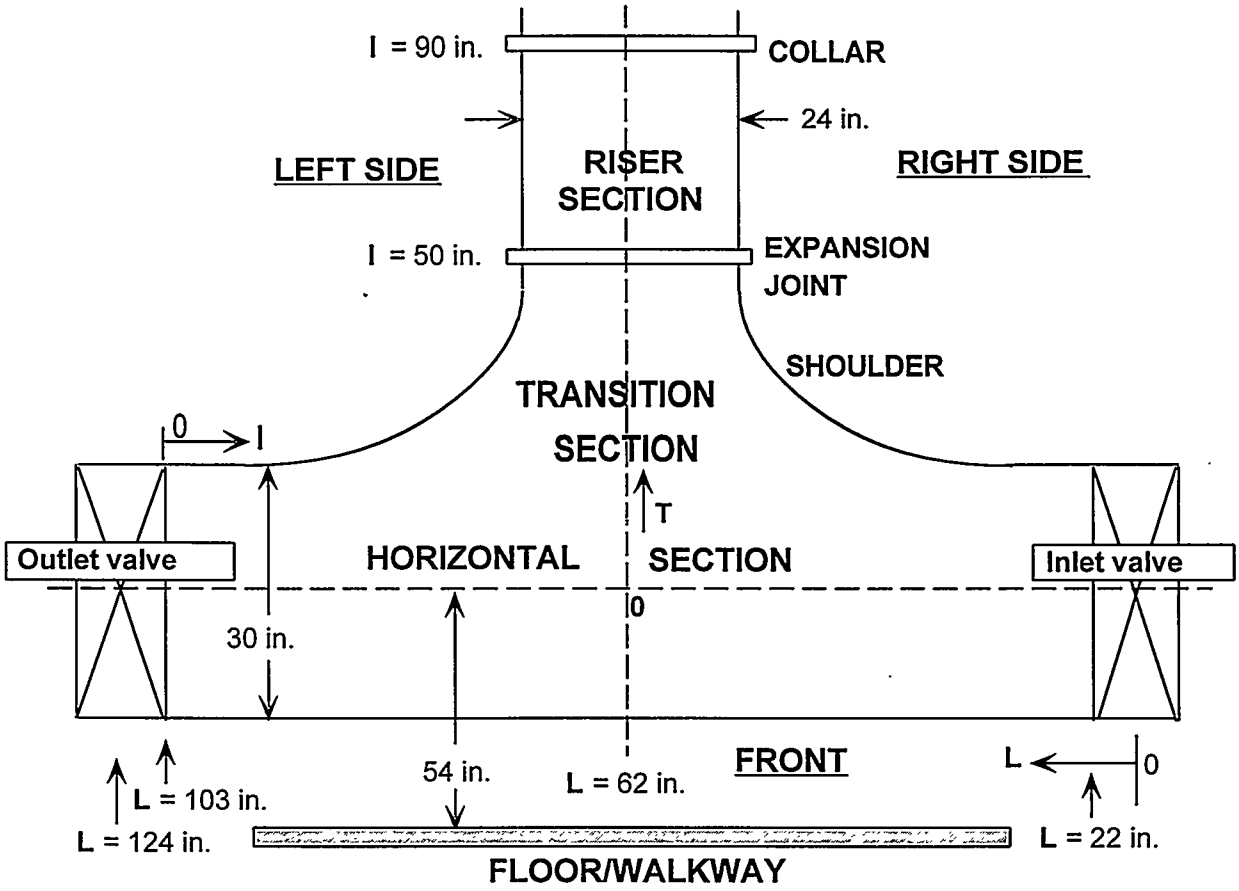

Fig. 4.3. Sketch of Tee-Pipe showing sections with measurement references (i.e., $L = 0$, $I = 0$, $T = 0$).

4.2.1. Tee-Pipe horizontal section deposit profile distribution

A series of measurements was performed on the horizontal section of the pipe as follows.

(a) The ^{252}Cf source was placed on one side (back) while only one detector was placed on the on other side (front) on the midplane of the pipe (see Fig. 4.3). The horizontal source and detector scans were performed on the midplane from L = 16 to L = 108 in. with the increments that were given in Table 4.1 together with the measurement results on the total deposit thickness. These results indicate the existence of a thin deposit on the right part of the section, in the neighborhood of L = 32 in., where the maximum deposit thickness is about 0.34 in.

(b) The vertical source and detector scans were performed at L = 32 in., which is located on the right part of the horizontal section (see Fig. 4.3). The measurement results are given in Table. 4.2. The measured total deposit thickness on the midplane was about d_x = 0.5 in. At the same location, the detector was placed on the top of the pipe while the source was on the bottom; the measured deposit was about d_y = 0.57 in. These two results indicate that the deposit profile is about uniform and has an average deposit thickness of $(d_x/2 + d_y/2)/2 \sim 0.26$ in.

(c) The vertical source and detector scans were performed at L = 92 in., which is located on the left part of the horizontal section (see Fig. 4.3). This location is symmetric to the previous measurement location, L = 32 in. The results of the deposit thickness measurements are given in Table. 4.3. The measured total deposit thickness on the midplane was about d_x = 0.338 in., which is about 35% lower than the thickness at L = 32 in. If it is assumed that the deposit is distributed uniformly, this result suggests that the deposit material on the wall is about 0.16 in. thick.

(d) Horizontal source and detector scans were also performed at the bottom of the pipe, 13 in. below the midplane of the horizontal section (see Fig. 4.3). The results presented in Table 4.4 indicate the existence of a very thin deposit throughout the bottom of the pipe, except around the right half of the section, described in paragraph b, where there is slightly more.

The reproducibility of the Tee-Pipe measurements was checked by performing repeated measurements on the deposit pipe at different times. As shown in Fig. 4.4, two measurements were performed at the same location (L = 32 in. at the midplane), one with the case discussed in part (a) (data file name: DH06R04), and the other with the vertical source detector scan (data file name: DH07R07) discussed previously. The results of these repeated measurements were within ±2% for the high-energy (E > 2-MeV) distribution of neutrons, where the TOF is less than 30 ns, as shown in Fig. 4.4.

Table 4.1. Tee-Pipe results for total thickness from horizontal source and detector scan along midplane of horizontal section (See Fig. 4.3)

Position L (in.)	$-\text{Ln}\,(I / I_0)$	Thickness (in.)[a]
16	0.042	0.10
24	0.142	0.35
32	0.137	0.33
42	0.055	0.13
52	–0.038	NP
62	–0.064	NP
72	–0.006	NP
82	–0.067	NP
92	0.063	0.15
101	0.016	0.04
108	–0.052	NP

[a] Note: Not physical (NP). Please see Sect. 2.2.3 for the discussions of measurements of thin deposits.

Table 4.2. Tee-Pipe results for total thickness from vertical source and detector scan at $L = 32$ in. (See Fig. 4.3)

Position y (in.)	$-\text{Ln}\ (I / I_0)$	Thickness (in.)
14	0.420	1.03
12	0.391	0.96
9	0.260	0.64
6	0.295	0.72
3	0.165	0.40
0	0.204	0.50
–3	0.195	0.48
–4	0.292	0.71
–6	0.270	0.66
–9	0.415	1.02
–14	0.454	1.11

Table 4.3. Tee-Pipe results for total thickness from vertical source and detector scan at $L = 92$ in. (See Fig. 4.3)

Position y (in.)	$-\text{Ln}\ (I / I_0)$	Thickness (in.)
14	0.208	0.51
12	0.194	0.47
9	0.161	0.39
6	0.194	0.47
3	0.157	0.38
0	0.133	0.32
–3	0.150	0.37
–6	0.145	0.35
–9	0.238	0.58
–12	0.138	0.33
–14	0.116	0.28

Table 4.4. Tee-Pipe results for total thickness from horizontal source and detector scan along horizontal section at y = –13 in. from midplane (See Fig. 4.3)

Position L (in.)	–Ln (I / I_0)	Thickness (in.)[a]
32	0.304	0.75
37	0.426	1.04
42	0.126	0.31
47	0.263	0.64
52	0.021	0.05
57	0.037	0.09
62	0.097	0.24
67	–0.042	NP
72	0.064	0.15
77	0.042	0.10
82	–0.178	NP
87	–0.065	NP
92	0.099	0.24

[a] Note: Not physical (NP). Please see Sect. 2.2.3 for the discussions of measurements of thin deposits.

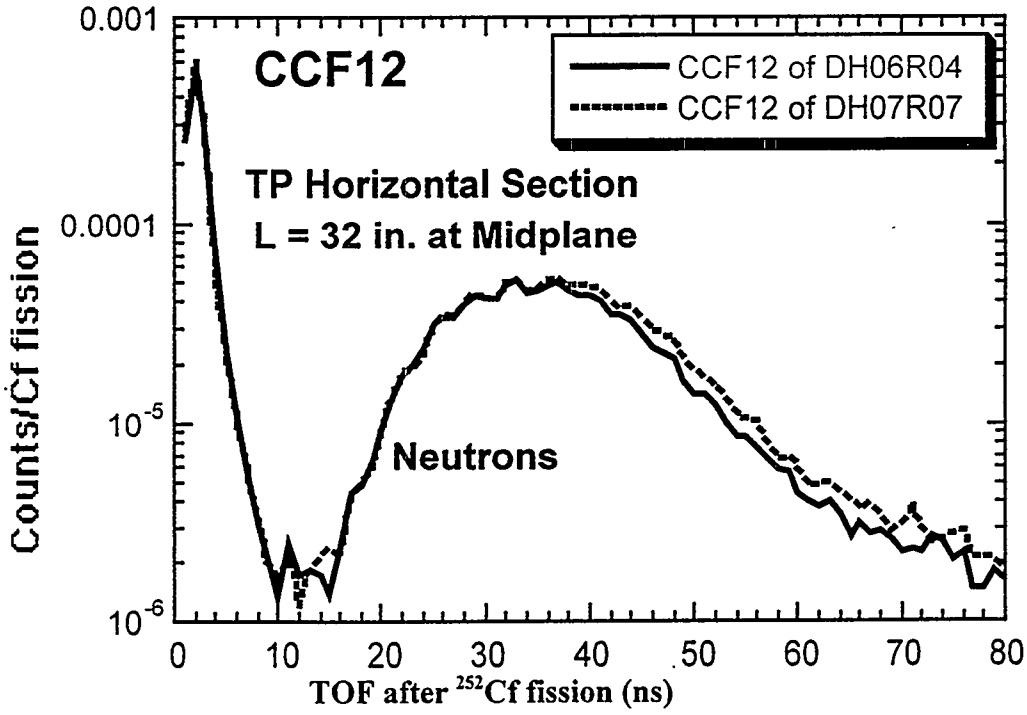

Fig. 4.4. Reproducibility of the Tee-Pipe measurements: two measurements taken at L = 32 in. at the midplane of the horizontal section at different times. These measurements were within ±2% for the high-energy (E>2-MeV) distribution of neutrons, where the TOF is less than 30 ns.

4.2.2. Tee-Pipe riser section deposit profile distribution

Measurements were performed by scanning the source and the detectors in the following configurations along the riser section of the Tee-Pipe.

(a) The ^{252}Cf source was placed on the left side (see Fig. 4.3) while the detector was on the right side of the pipe. The measurement results for the total deposit thickness across the midplane of the pipe are presented in Table 4.5. These results indicate a presence of a thin deposit of material, about 0.1 in. or less.

(b) The ^{252}Cf source was on the back side, and the detector was placed on the front side of the pipe. The corresponding measurement results are given in Table 4.6 for the total deposit thickness across the midplane of the riser section. Almost no appreciable deposit was observed from these measurements.

Table 4.5. Tee-Pipe results for total thickness from source (on left) and detector (on right) scan on midplane of riser section (see Fig. 4.3)

Position I (in.)	$-\text{Ln}\,(I/I_0)$	Thickness (in.)
36	0.061	0.15
58	0.0	0.0
74	0.053	0.13
90	0.061	0.15

Table 4.6. Tee-Pipe results for total thickness from source (on back) and detector (on front) scan on midplane of riser section (see Fig. 4.3)

Position I (in.)	$-\text{Ln}\,(I/I_0)$	Thickness (in.)[a]
36	0.049	0.12
58	−0.053	NP
74	−0.044	NP
89	0.031	0.07

[a] Note: Not physical (NP). Please see Sect. 2.2.3 for the discussions of measurements of thin deposits.

4.2.3. Tee-Pipe transition section deposit profile distribution

Deposit measurements were performed on two parts of this section of the pipe.

(a) A spatial fixture was made in a wedge shape for aligning the detector with the front face of the transition section. The source and detector scans were performed along the midplane of the pipe (see Fig. 4.3). Table 4.7 gives the measurement results for the total deposit thickness across the pipe. Almost none or a very thin deposit material was found, except at T = 25 in., where a slight amount of material (~0.3 in. of total deposit thickness) was measured. This location is close to where the expansion joint is located (see Fig. 4.3).

(b) Scans were performed with the source on the right and detector on the left of the shoulder part (see Fig. 4.2) of the transition section. The measurement results are presented in Table 4.8. As observed with the previous measurements, some deposit material (0.3 in. to 0.4 in. in total thickness) were measured near the expansion joint between the riser and the transition sections.

Table 4.7. Tee-Pipe results for total thickness from source and detector scan along midplane of transition section (see Fig. 4.3)

Position T (in.)	$-\text{Ln}\,(I / I_o)$	Thickness (in.)[a]
0	0.045	0.11
5	–0.017	NP
10	–0.045	NP
15	–0.020	NP
20	0.049	0.12
25	0.125	0.30

[a] Note: Not physical (NP). Please see Sect. 2.2.3 for the discussions of measurements of thin deposits.

Table 4.8. Tee-Pipe results for total thickness from source and detector scan on shoulder of transition section (see Fig. 4.3)

Position I (in.)	$-\text{Ln}\,(I / I_o)$	Thickness (in.)[a]
20	−0.074	NP
26	0.126	0.31
32	0.170	0.41

[a] Note: Not physical (NP). Please see Sect. 2.2.3 for the discussions of measurements of thin deposits.

4.2.4. Summary of deposit profile and its distribution on the Tee-Pipe

In general, the Tee-Pipe measurement results can be summarized as follows (see Fig. 4.5):

- Horizontal section left: No significant material was present in this location. At most, there is an annularly distributed thin-film deposit, approximately 0.16 in. thick.

- Horizontal section middle: No significant deposit material was present in this location. A thin film, approximately 0.1 in. thick, was estimated at the midplane and the bottom of the process pipe.

- Horizontal section right: A slightly larger amount of deposit was present. It appeared to be roughly annular and had a thickness of 0.25 to 0.29 in.

- Transition section: No significant deposit material was found on the front and rear flat surfaces. Some deposit was noted on the shoulders (curved sides) that was approximately 0.2 in. thick.

- Riser section: A slight amount of deposit was present, approximately 0.1 to 0.2 in. thick.

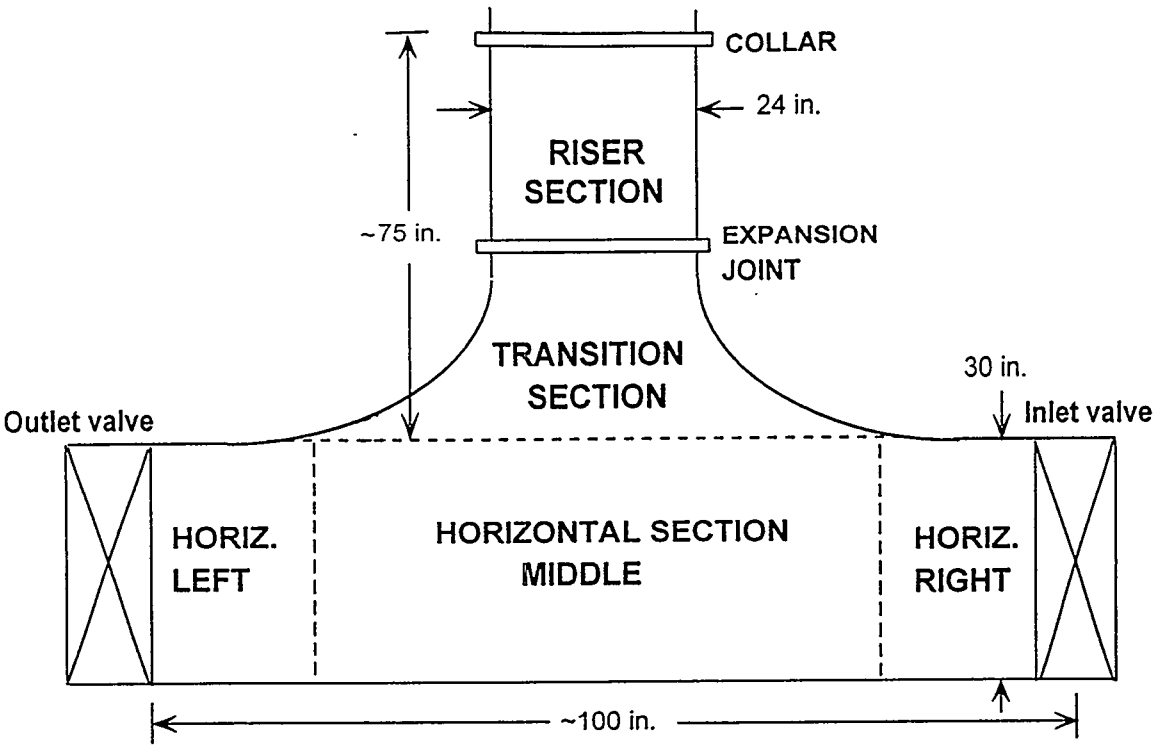

Figure 4.5. Deposit measurement locations and sections on Unit 2, Cell 6, A-Line Outlet, Tee-Pipe.

4.2.5. H/U for Tee-Pipe deposit

Because a very thin deposit was distributed on the this process pipe, the determination of the H/U was not possible. To get an accurate estimate of this ratio, a minimum deposit thickness of 1 in. is required.

4.2.6. Tee-Pipe total uranium mass

The total deposit volume in the Tee-Pipe can be estimated with a method similar to that used on the Hockey Stick. Equation (9) applies to the sections of the Tee-Pipe with appropriate pipe parameters of the horizontal and riser sections. For this estimate, the transition section is ignored but instead the riser section is extended to the midplane of the horizontal section. With these assumptions only two straight cylinders are considered for the Tee-Pipe, and the following relationship for the deposit volume is then obtained:

$$V_d = \pi L_h\, d_a\, (D_h - 2w - d_a) + \pi L_r\, d_a\, (D_r - 2w - d_a)\ . \qquad (13)$$

The measured length of the horizontal section is about L_h = 100 in., and for the riser section is about L_r = 75 in. A very thin deposit of material was distributed in the Tee-Pipe; however, a deposit thickness less than 0.1 in. can not be resolved reliably with the Tee-Pipe measurements performed within 5% uncertainty or less (see Fig. 2.15). Therefore, to have an upper-bound estimate for the uranium mass, the deposit thickness of d_a = 0.1 in. can be used in Eq. (13) as an average value for calculating the total deposit volume, and this leads to V_d = 0.024m^3. The total uranium mass of the Tee-Pipe deposit can then be estimated by taking H/U of 3.4 from the Hockey Stick measurements for determining the uranium density. Thus, given that ρ_u= 3.87 g/cc, the total uranium mass of M_u = 93 kg is estimated. This result is consistent with the NDA measurements on the removed Tee-Pipe deposit (Table 3.13). This estimated maximum uranium mass, in turn, with 2.95% enrichment, gives about 2.75 kg of ^{235}U at most; the earlier estimate for gamma-ray spectrometry was about 8.27 kg [Ref. 1].

4.3. Summary of the Tee-Pipe Deposit Measurements

The overall Tee-Pipe deposit measurements showed a very thin layer of deposit material (≤ 0.1 in.) distributed on the this process pipe, except in the horizontal section close to the block valve. A slight amount of deposit was present and appeared roughly annular with thickness of 0.25 to 0.29 in. The total uranium mass of 93 kg is obtained as an upper bound from the measurements.

This page intentionally left blank.

5. VISUAL OBSERVATIONS AND DISCUSSION

5.1 Intrusive Visual Observations

The Deposit Removal Project team wanted to survey the inside of these deposit pipes intrusively and to prepare a work plan according to the assessment of the nuclear criticality and safety of the deposits before the actual deposits were removed. Therefore, the DRP team made use of the results of the deposit distribution measurements for selecting the locations on the process pipes for visual observations. An articulated fiber-optic camera was inserted into the Hockey Stick at the top of the riser, and also from L = 68 in. on the side of the pipe about 5 in. below the midplane. At the same time, a special tool, as shown in Fig. 5.1, was also inserted for measuring the deposit thickness from the bottom of the Hockey Stick at L = 41 in. located at the transition section, and at L = 74 in., located around the elbow region (see Fig. 3.22).

Fig. 5.1. A spatial tool inserted into the deposit pipes for measuring the deposit thickness.

In general, the intrusive camera observations were in good agreement with the deposit measurements. For example, in the Hockey Stick, most of the deposit material was on the top of the process pipe (see Fig. 5.2), located from the block valve to the elbow region; that is, L = 40 to 80 in. The deposit in this region was not smooth, but mostly consisted of large,

closely grouped nodules, as shown in Figs. 5.3 and 5.4. As discussed in Appendix A, the data obtained from the second NWIS detector, which is 4.5-in. further up from the first detector along the pipe, indicated the existence of a structure and irregularities in the deposit within the 4.5-in. section between the two detector locations. The intrusively measured apparent deposit thicknesses at $L = 41$ in. and 74 in., which are given in Table 5.1, were also consistent with the deposit profile measurements throughout the Hockey Stick. The articulated fiber-optic camera showed that the deposit profile became more smooth and symmetrical up the riser section of the Hockey Stick, again correlating well with the CFSDT measurement results.

Table 5.1. Hockey Stick intrusive deposit measurement results

Measurement location, L (in.)	Deposit thickness (in.)	
	Top	Bottom
41	1.5	0.125
74	0.875	0.125

The dominant orange and green-yellow colors, which are related to the hydration level of the deposits [Ref. 11], as shown in the photographs of the Hockey Stick obtained with a fiber-optic camera (Figs. 5.2 and 5.3), indicate H/U ~ 3 to 4 [Refs. 18, 19]. This observation is consistent with the deposit measurements (H/U = 3.5 ± 0.20).

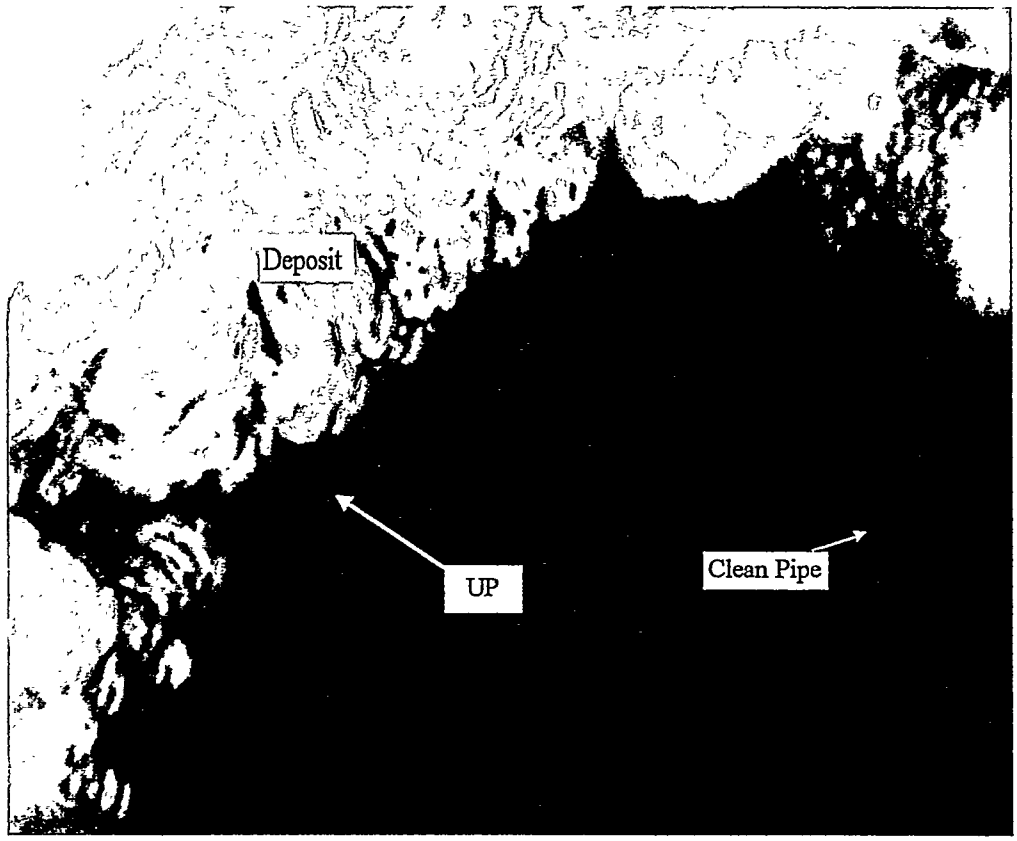

Fig. 5.2. Intrusive look into the Hockey Stick in the region at L = 40 to 80 in.

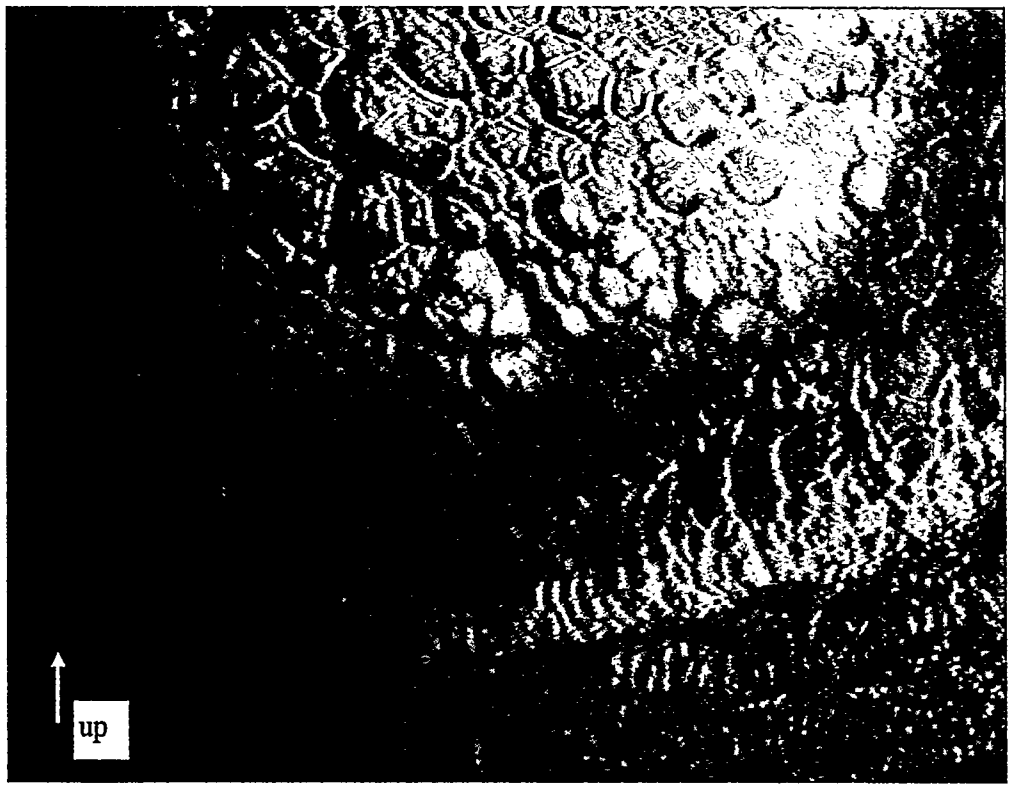

Fig. 5.3. Deposit nodules formed on the upper hemisphere of the Hockey Stick.

Fig. 5.4. Large deposit nodule observed in the vicinity of L = 70 in. in the Hockey Stick.

Similarly, intrusive visual observations on the Tee-Pipe were also performed by inserting the fiber-optic camera from the back of the pipe at the center of the horizontal section. As shown in Fig. 5.5, the observations were in good agreement with the Tee-Pipe deposit measurements. As seen from this photograph, the color of the deposit around the riser section of pipe, where the deposit is thin and uniform, is predominantly orange, which indicates that H/U ~ 3 to 4 [Refs. 18, 19] (see Sect. 4.2). Therefore, the use of H/U = 3.4 (the value obtained from the hockey stick measurements used in the Tee-Pipe data analysis was consistent with the observations made during the invasive examination of the Tee-Pipe. No deposit was observed at the bottom of the horizontal section (except some material flakes as shown in Fig. 5.6), and the color of the pipe material.

Fig. 5.5. Intrusive look into the Tee-Pipe in the region toward to the riser section.

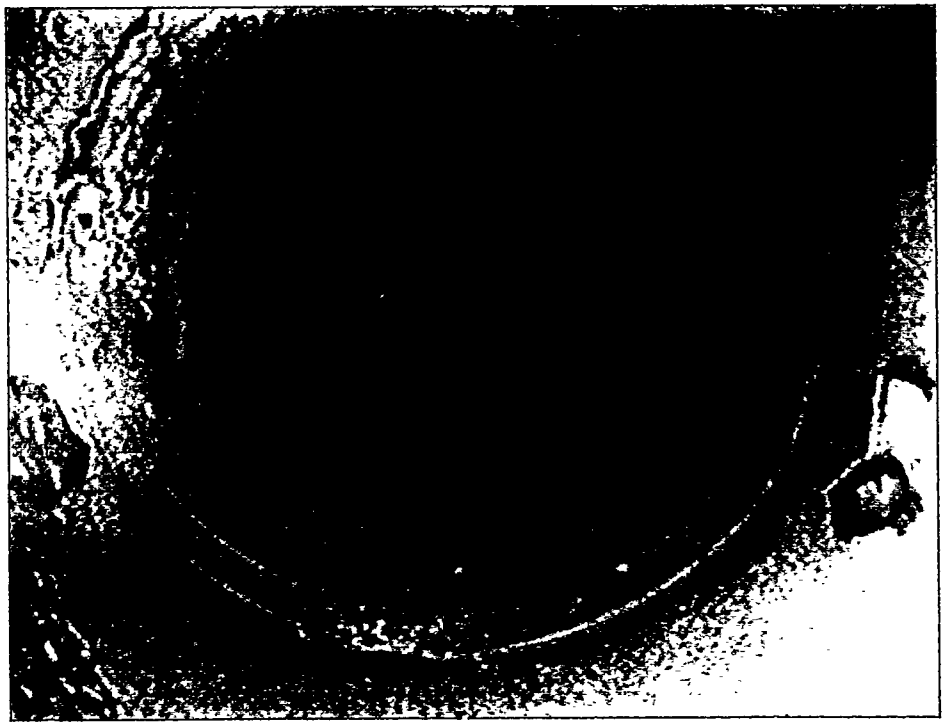

Fig. 5.6. Intrusive look into the Tee-Pipe looking down the riser to the horizontal section.

5.2 Observations During Deposit Removal

After the visual observations discussed in the previous section the Hockey Stick and the Tee-Pipe were cut, and the deposits have been successfully removed by the Deposit Removal Project team [Ref. 20]. Figure 5.7 shows the disassembly of the Hockey Stick after the torch cut at existing flanges (see Fig. 3.1) on either side of the elbow section. The following photographs (Figs. 5.8 through 5.10) were taken during these deposit removal activities on the Hockey Stick. As seen from the figures, the visual observations of the deposit profiles are consistent with the deposit measurement results, which are included in these figures for direct comparison. Figure 5.11, the cut Hockey Stick deposit pipe right after the elbow section, $L \sim 104$ in., shows the deposit irregularities (as measured, $L = 104$ in.), and the dominant orange and yellow-green colors that indicate H/U $\approx$ (3–4), as measured.

The Tee-Pipe deposit was removed from a large window piece opened at the back side of the T intersection as shown in Fig. 5.12. As indicated with the deposit measurements, very little deposit material was found at the bottom part of the horizontal section of the pipe. Figure 5.13 shows the photograph of the area inside the cut Tee-Pipe. This visual observation confirms the deposit measurement results discussed earlier and the color of the pipe wall material indicates lack of deposit material.

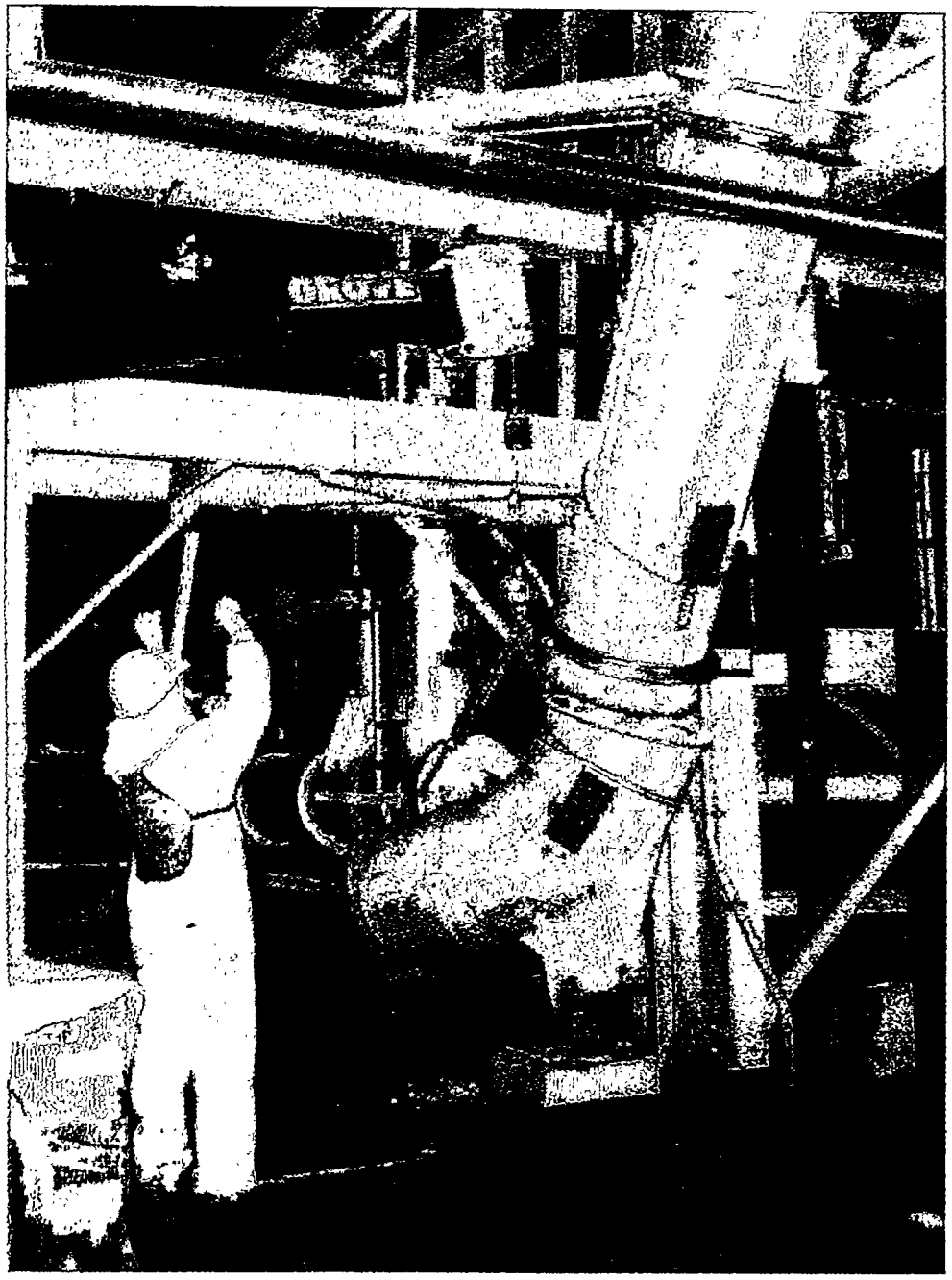

Fig. 5.7. Disassembly of the Hockey Stick deposit process pipe.

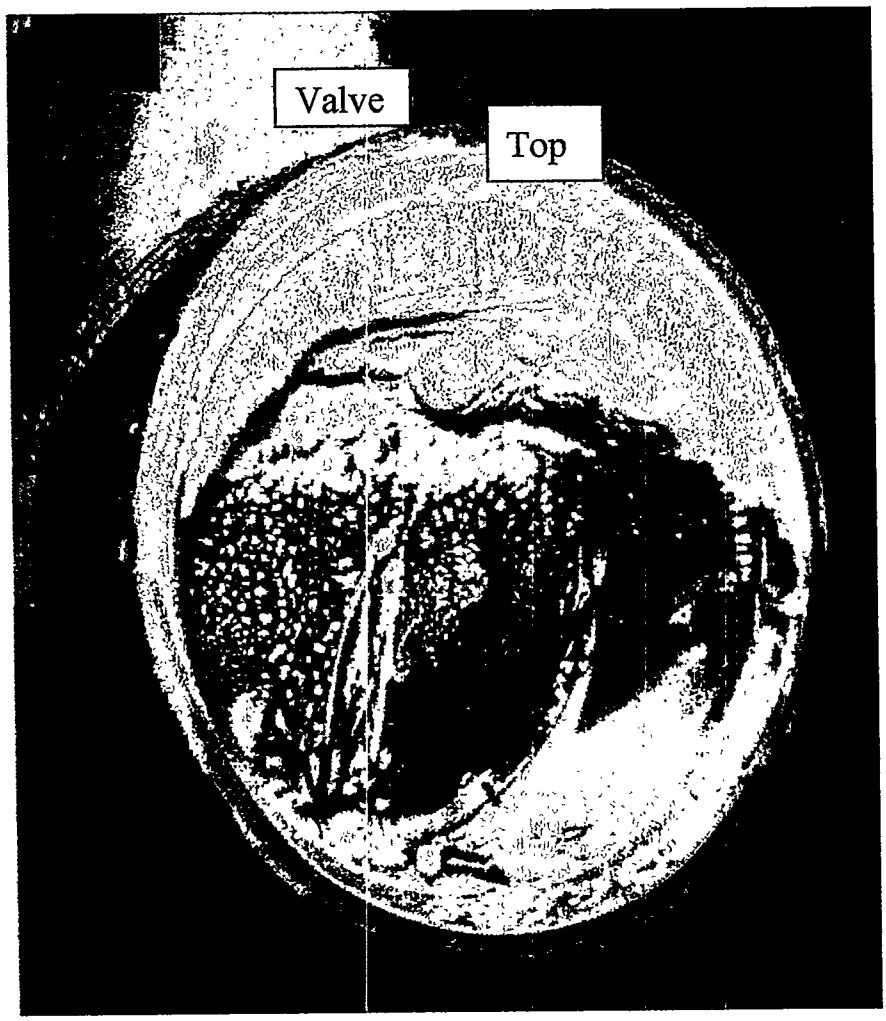

(a)

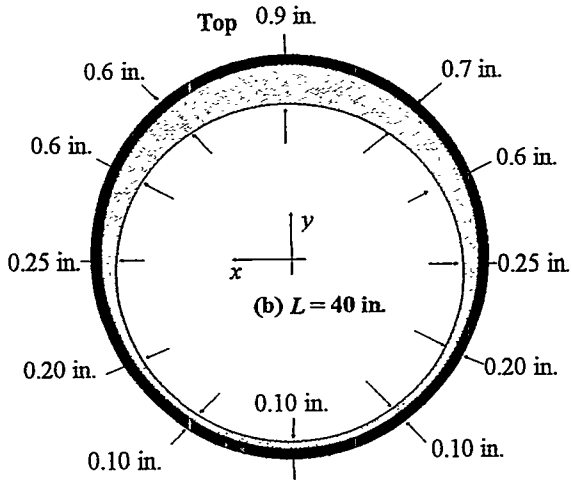

Fig. 5.8 (a) Deposit and irregularities on the upper part of the deposit pipe looking toward the inlet block valve from the transition section, $L = 40$ in., when the Hockey Stick was cut. (b) Non-intrusive radiation measurements by NWIS.

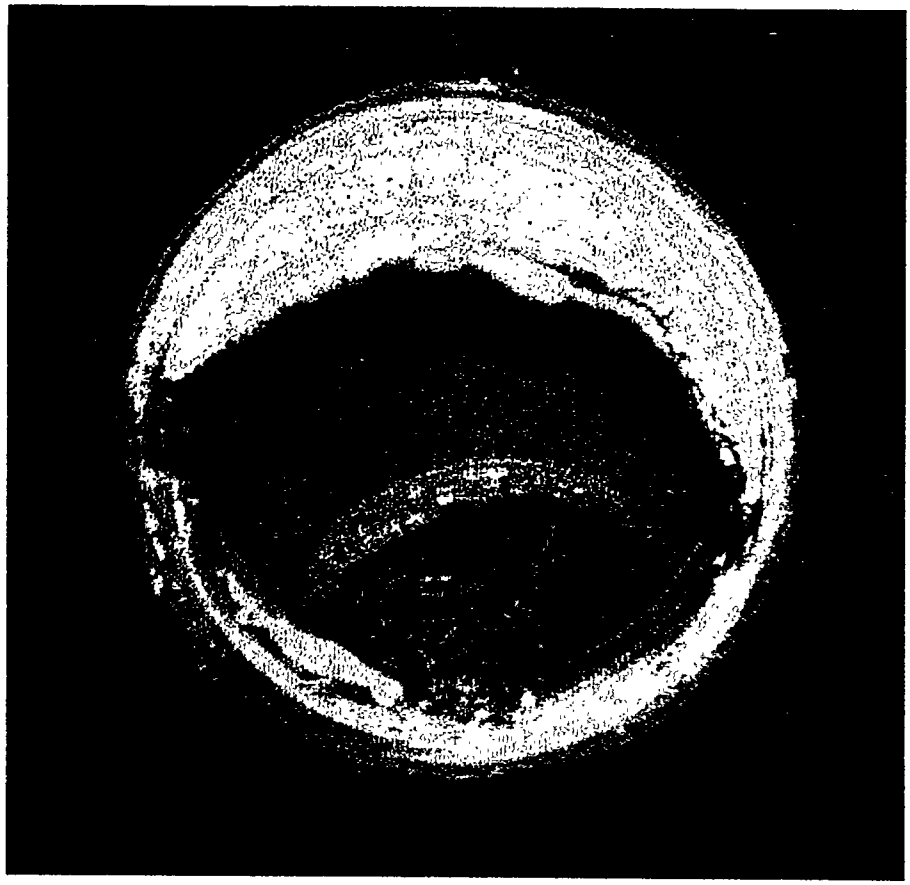

(a)

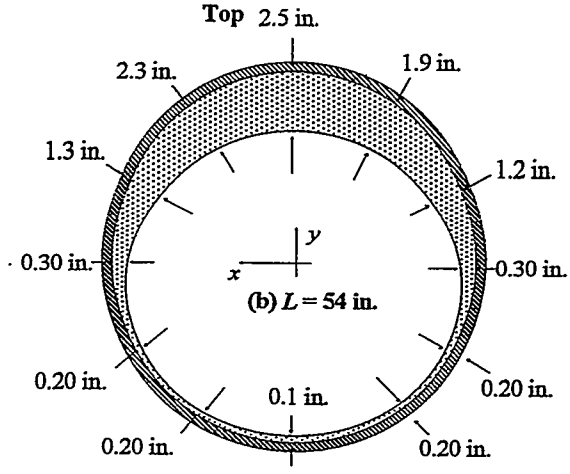

Fig. 5.9 (a) Crescent shape of deposit on the upper part of the pipe (L = 36–46 in.) obtained when the Hockey Stick was cut. (b) Non-intrusive radiation measurements by NWIS.

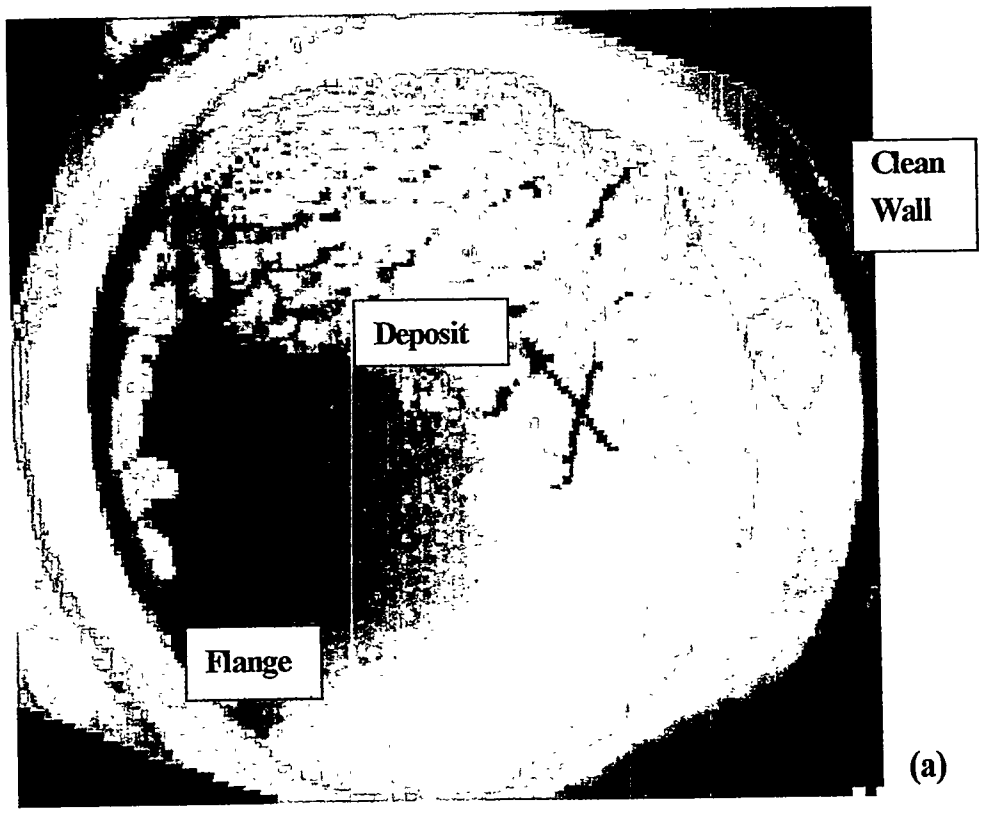

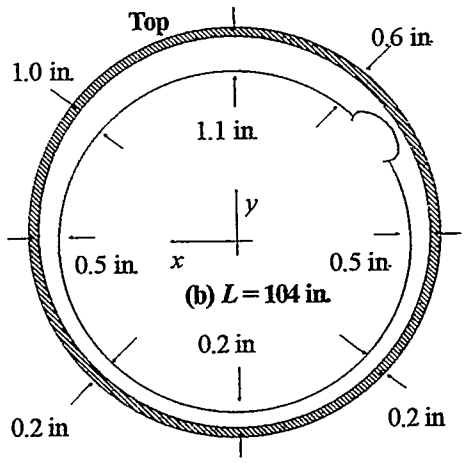

Fig. 5.10 (a) Deposit nodules and irregularities are shown on the upper part of the Hockey Stick together with the lack of material (shown with arrow) for L = 104 in. (b) Non-intrusive measurements by NWIS.

Fig. 5.11. Cut Hockey Stick deposit pipe showing the deposit irregularities and dominant orange color that indicates H/U ≈ (3–4), as measured. Visual observations confirmed the measurements at L = 104 in.

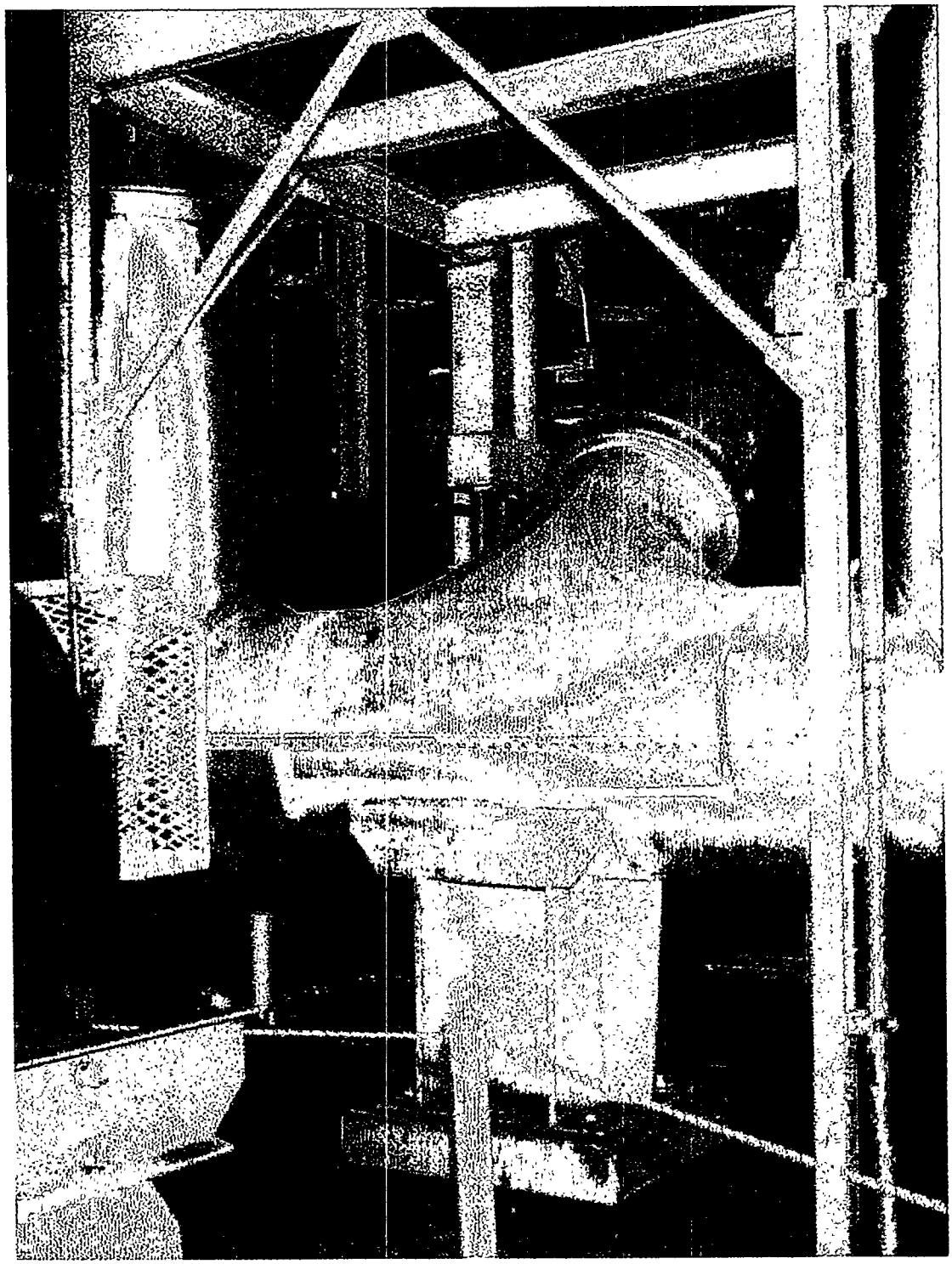

Fig. 5.12. Preparations for the Tee-Pipe deposit removal. A large window piece was opened at the back side of the T intersection as marked in the figure.

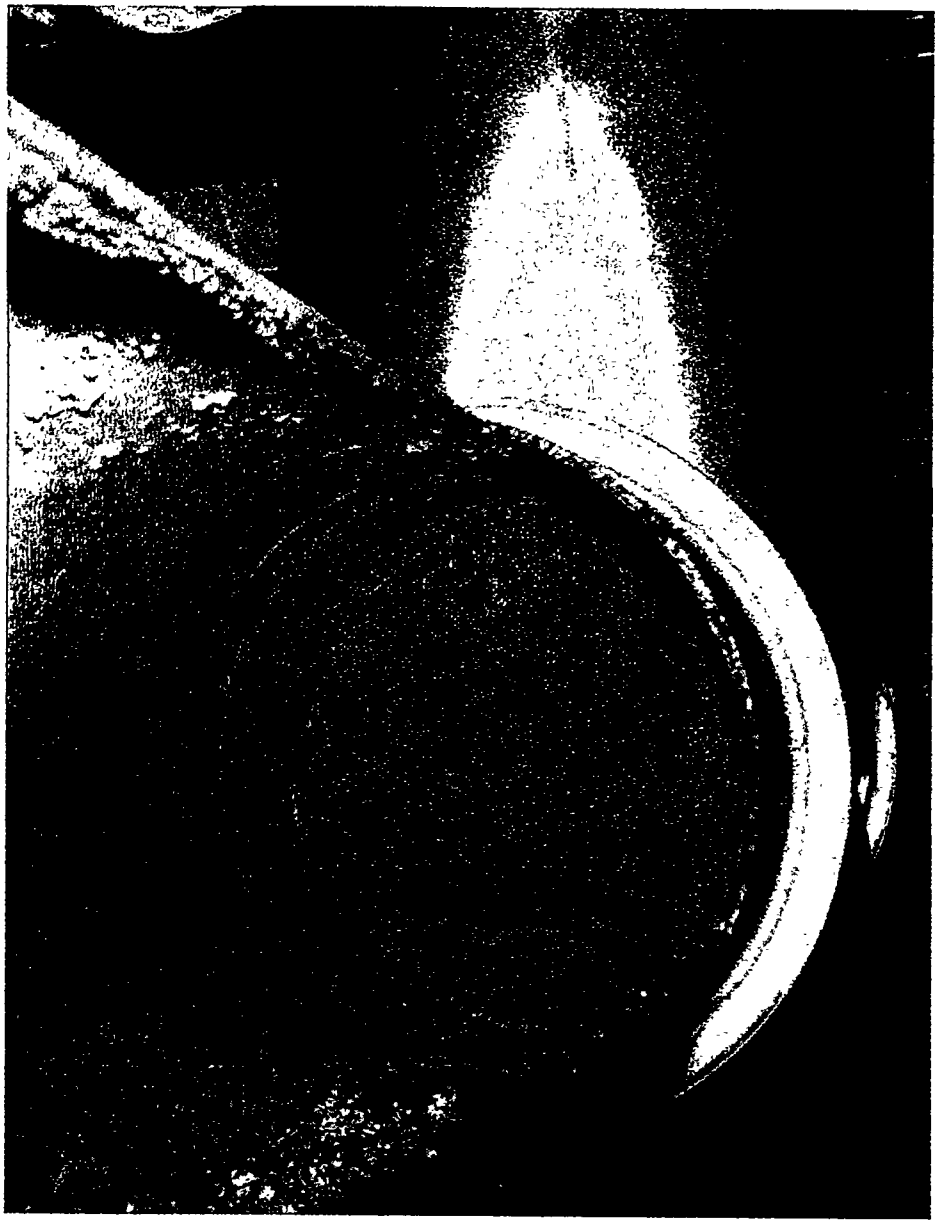

Fig. 5.13. Photograph of inside the cut Tee-Pipe showing no deposit material on the wall and very little material in the bottom of the horizontal section, which confirms the measurements.

The Hockey Stick and Tee-Pipe deposits have been packaged into cans for storage. The summary of the NDA report is given in Table 3.13 for the mass of the deposit, and additional details are given in Appendix D. The NDA measurement (which used passive neutron counting) uncertainty is estimated to be ± 50% for the masses and 20% relative to the isotopic concentration values (Appendix D). As seen from Table 3.13, the total uranium masses are 479 kg for the Hockey Stick, 14.8 kg for the block valve, and 97 kg for the Tee-Pipe. These NDA results are consistent with the deposit measurement results presented in Sect. 3.4 for the Hockey Stick and the block valve, and Sect. 4.3 for the Tee-Pipe.

6. CONCLUSION

Before the actual deposit removal activities began in the former ORGDP K-29 facility, the Deposit Removal Project team required an intrusive survey of the inside of the pipes to assess the nuclear criticality safety of the deposits. Therefore, data were needed on the spatial distribution of the deposits, the total uranium deposit mass, and the moderation level caused by hydration of the deposits, all of which affect nuclear criticality safety. To perform this task safely and effectively, the Deposit Removal Project team asked ORNL to characterize the two largest deposits (in the Hockey Stick and Tee-Pipe locations). The CFSDT measurement technique, an active neutron interrogation method developed for use at the Oak Ridge Y-12 Plant to identify nuclear weapons components in containers, was implemented for the deposit characterization measurements. These measurements used CFSDT TOF measurements of prompt neutrons and gamma rays from an externally introduced ^{252}Cf source.

Deposit characterization measurements on two deposits in K-29 were successfully performed. The CFSDT measurement results for the Hockey Stick indicated that the deposit was annular and that in part of Hockey Stick most of the deposit material was on top of the process pipe, located around an elbow in the pipe. The measured level of hydration (H/U) was 3.5 ± 0.20. The total uranium masses of 552 ± 93 and 532 ± 90 kg were obtained from the deposit distributions measured along the Hockey Stick. The Tee-Pipe deposit measurements showed a very thin deposit of material distributed on this process pipe. The total uranium mass of 93 kg was estimated for the Tee-Pipe as an upper bound from the measurements.

The Deposit Removal Project team used the measurement results to select the locations on the process pipes for the visual observations of the deposits. A fiber-optic camera was inserted through a number of holes drilled into both process pipes. At the same time, a special tool was also inserted for measuring the deposit thickness. The fiber-optic camera measurements were repeated in a number of different locations along the process pipes. In general, the intrusive camera observations at various locations were consistent with the results of the CFSDT deposit profile measurements on the Hockey Stick. Similarly, the intrusive visual observations on the Tee-Pipe were also in good agreement with the Tee-Pipe deposit measurements; that is, very thin deposits of material were distributed in the Tee-Pipe. The dominant orange and yellow-green colors observed with the fiber-optic camera indicated an H/U ~ 3–4, which was consistent with what the CFSDT measurements yielded.

The Hockey Stick and the Tee-Pipe deposits were successfully removed and the estimated total uranium were 479 kg and 98.5 kg (± 50% uncertainty), respectively, which are consistent with the CFSDT measurement findings.

The use of CFSDT technique on the K-29 deposit characterization measurements successfully demonstrated that this is a reliable active method for deposit characterization measurements. This methodology is an example of a technique developed at a DOE site for a defense program was applied in an environmental restoration project at another DOE site. The CFSDT technique was developed by ORNL (managed by Lockheed Martin Energy Research Corp.) so that uranium weapons components in storage containers could be identified at the Oak Ridge Y-12 Plant (managed by LMES). The Deposit Removal Project subsequently utilized the CFSDT technique for characterizing hydrated uranium deposits in process pipes at ETTP (formerly ORGDP), also managed by LMES. The CFSDT technique is useful for measuring deposits in process pipes at other facilities (i.e., the Paducah and Portsmouth gaseous diffusion plants) that handle UF_6 or for other analyses of process pipes and other processes with nuclear material.

ACKNOWLEDGMENTS

The authors acknowledge the continuous support of the ETTP Deposit Removal Project group, especially Connie P. Hall and Paul Larson, throughout the deposit measurements. Moreover, Ron W. Brandenburg for loaning his genie lifts and the test source, Lloyd J. Jollay for his contribution to the NCS assessments on the measurement procedure, and the help of Craig Reed with issues related to health physics are greatly acknowledged. The valuable discussions with José March-Leuba, John K. Mattingly, and Rafael Perez are greatly appreciated, and special thanks are due to Larry D. Phillips for his technical assistance during the measurements, and Sherry Abercrombie for her patience and dedication throughout the typing and preparation of this report painstakingly.

This page intentionally left blank.

APPENDIX A: HOCKEY STICK RESULTS FROM SECOND NWIS DETECTOR

The measurement results obtained from the second NWIS detector (detector #3) as indicated in Fig. 2.2, were also analyzed for the Hockey Stick deposit measurements. The cross correlation function between the source and detector #3, CCF13, was again utilized in similar fashion to the cross correlation function between detector #2 and the source data from the detector #2, obtained from the NWIS measurements. The two NWIS detectors were placed side-by-side (see Fig. 2.2) along the process pipe such that the distance between the centers of the detectors was 4.5 in. In this appendix the variations of the deposit thickness at the measurement locations of L = 44.5, 58.5, 84.5, 108.5, 137.5, and 167.5 in. obtained from the vertical and the horizontal source and detector scans (Fig. 2.13), and the source-detector rotation measurements (Fig. 2.14) performed at L = 58.5 in. and L = 108.5 in. on the Hockey Stick deposit pipe are presented. As discussed in Sect. 3.3.2, a typical uncertainty on the deposit thickness for thickness like 1.0 in. is $\Delta d/d \leq \pm$ 0.17%.

The deposit thickness was estimated from Eq. (2). The needed neutron total cross section data for E = 8.5 MeV neutrons (Fig. 2.12) was obtained by making use of the average value of H/U obtained from the iterative process performed for these measurement locations on the Hockey Stick, as discussed in detail in Sect. 3.3.

A.1. Measurement Results at L = 44.5 in.

The total deposit thickness results obtained from the vertical and horizontal scans of the source and the detector are given in Tables A.1A and A.1B, respectively. Table A.1A suggests that the deposit is asymmetric in this location, as was observed with the detector #2; more deposit material is present on the top of the pipe. Moreover, the results of both detectors are consistent with each other, except that the detector #3 results indicate slightly thicker deposit material. The results from the horizontal scan (Table A.1B) show a in-and-out symmetry with slightly more deposit material. The estimated deposit profile is given in Fig. A.1. The average H/U obtained from the iterative procedure is 2.4 and is used for determining the neutron cross section (Fig. 2.2), which is used for determining the deposit thickness.

Table A.1A. Hockey Stick iterative results of total transmission thickness from vertical source and detector #3 scan at L = 44.5 in.

Position y (in.)	$-\text{Ln}\,(I / I_0)$	Thickness (in.)
8	1.18	2.72
6	0.985	2.27
4	0.629	1.45
2	0.486	1.12
0	0.408	0.94
–2	0.291	0.67
–4	0.352	0.81
–6	0.363	0.84
–8	0.271	0.62

Table A.1B. Hockey Stick iterative results of total transmission thickness from horizontal source and detector #3 scan at L = 44.5 in.

Position x (in.)	$-\text{Ln}\,(I / I_0)$	Thickness (in.)
8	0.247	0.57
6	0.477	1.10
4	0.504	1.16
2	0.807	1.86
0	0.856	1.97
–2	0.738	1.70
–4	0.479	1.10
–6	0.395	0.91
–8	0.149	0.34

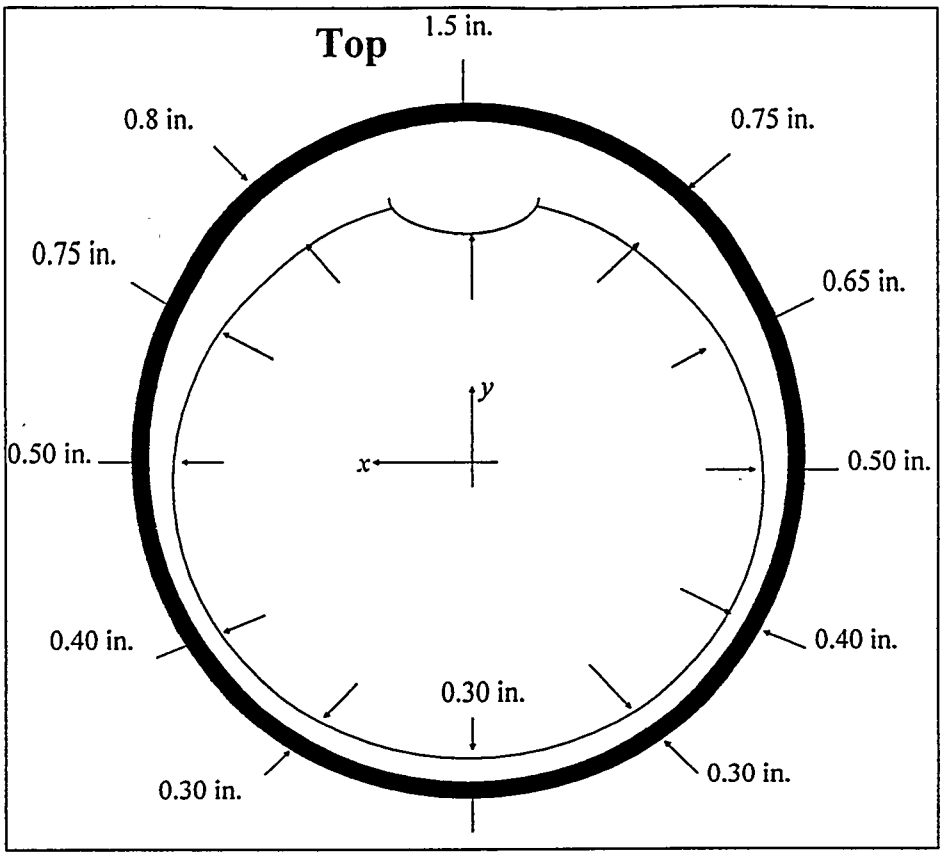

Figure A.1. Hockey Stick deposit profile at $L = 44.5$ in.

A.2. Measurement Results at $L = 58.5$ in.

The results of the total deposit thickness determined from the vertical and horizontal scans are given in Tables A.2A and A.2B, respectively, while the source-detector rotation results are presented in Table A.2C. The average value of H/U determined from the horizontal scan at this location is 4.0, obtained from the iterative procedure. The results in Table A.2A suggest that the deposit is again highly asymmetric in this location, and almost no significant deposit material is present at the bottom of the pipe, $y = -10$ in. At the midplane, $y = 0$, the total deposit is $d_x(y = 0) = 0.7 \pm 0.1$ in., which is consistent with the (0.6 ± 0.1) in. thickness given in Fig. 3.11. The results from the horizontal scan (see Table A.2B) indicate that the deposit thickness on the top is $d_y(x = 0) = 2.4 \pm 0.4$ in., and more material is present for $x > 0$, as also observed in Fig. 3.11. Thus both a top-and-bottom asymmetry and an in-and-out ($x > 0$), asymmetry are present in the deposit profile. The deposit thickness at the top, 2.5 in. as given in Fig. 3.11, is also consistent with the value obtained with this analysis.

Table A.2A. Hockey Stick iterative results of total transmission thickness from vertical source and detector #3 scan at L = 58.5 in.

Position y (in.)	$-\text{Ln}(I / I_o)$	Thickness (in.)
10	1.252	3.06
8	1.196	2.92
6	0.615	1.50
4	0.325	0.79
2	0.318	0.78
0	0.285	0.70
–2	0.2	0.49
–4	0.141	0.34
–6	0.156	0.38
–8	0.148	0.36
–10	–0.059[a]	NP[a]

[a] Note: Not physical (NP). Please see Sect. 2.2.3 for the discussions of measurements of thin deposits

Table A.2B. Hockey Stick iterative results of total transmission thickness from horizontal source and detector #3 scan at L = 58.5 in.

Position x (in)	$-\text{Ln}(I / I_o)$	Thickness (in.)
10	0.648	1.58
8	0.905	2.21
6	0.965	2.36
4	1.169	2.86
2	1.234	3.02
0	0.984	2.41
–2	1.186	2.90
–4	0.826	2.02
–6	0.686	1.68
–8	0.69	1.69
–10	0.255	0.62

Table A.2C. Hockey Stick iterative results of total radial thickness from rotation of source and detector #3 at L = 58.5 in.

Rotation α (Deg.)	$-\text{Ln}(I/I_o)$	Thickness (in.)[a]
30	0.506	1.24
60	0.352	0.86
90	0.246	0.60
120	0.356	0.87
150	0.857	2.10
180	1.057	2.58
210	0.977	2.39
240	0.456	1.12
300	0.377	0.92
330	0.672	1.64

[a] Note: Not physical (NP). Please see Sect. 2.2.3 for the discussions of measurements of thin deposits

The results of the rotation measurements (see Table A.2C) are in good agreement with the previous results (Fig. 3.11); the values for the deposit thickness at $\alpha = 90^\circ$ and 180° are the same for both detectors within the uncertainties of the measurements. Furthermore, these results also indicate that 40% more deposit material is indeed present for $x > 0$ as observed from the comparison of $\alpha = 30^\circ$ and 150° deposit thickness values. The rotation results are presented in Fig. A.2 for the two NWIS detectors. As seen from the figure, these two detector results closely follow each other. The deposit profile presented in Fig. A.3 is estimated from the results given in these tables.

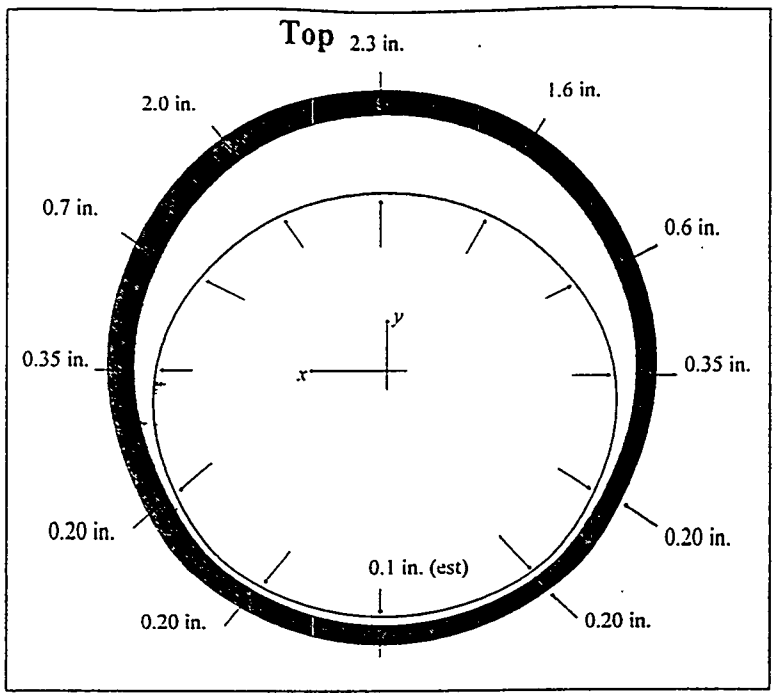

Fig. A.2. Hockey Stick deposit profile at $L = 58.5$ in.

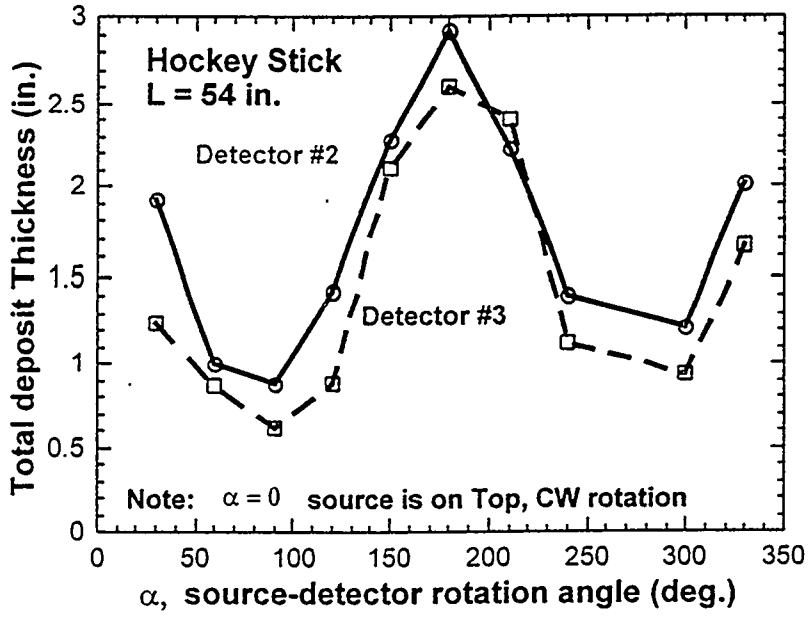

Fig. A.3. Variations of total deposit thickness obtained from source-detector #2 (and detector #3) rotation measurements at $L = 54$ in. on the Hockey Stick.

A.3. Measurement Results at $L = 84.5$ in.

This measurement location corresponds to the curved elbow section of the Hockey Stick directly below the expansion joint (see Fig. 3.5). As discussed in Sect. 3.3, only a single vertical source-detector scan was possible. The average H/U obtained from the iterative procedure is 4.3. Results from the vertical scan (Table A.3) indicate that the asymmetric deposit, primarily on the top of the process pipe, is also measured with detector #3. The deposit profile is given in Fig. A.4. By comparing results of Table 3.7 obtained from detector #2, these two results are consistent, considering the uncertainties in the measurements and the presence of some irregularities between the two locations.

Table A.3. Hockey Stick iterative results of total transmission thickness from vertical source and detector #3 scan at $L = 84.5$ in.

Position y (in.)	$-\text{Ln}\,(I / I_o)$	Thickness (in.)
10	1.49	3.74
8	1.31	3.29
6	0.755	1.89
4	0.418	1.05
2	0.441	1.11
0	0.412	1.03
–2	0.449	1.13
–4	0.411	1.03
–6	0.382	0.96
–8	0.521	1.31
–10	0.352	0.88

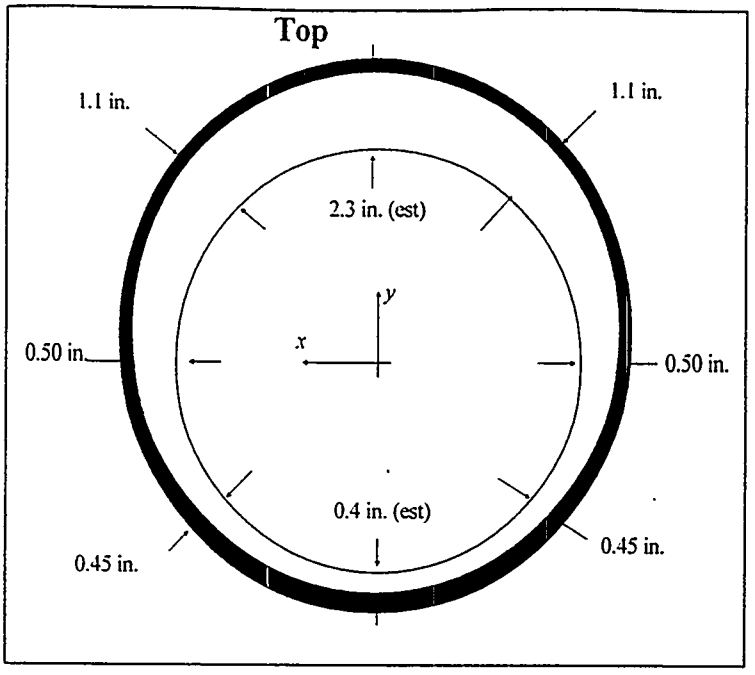

Figure A.4. Hockey Stick deposit profile at $L = 84.5$ in.

A.4. Measurement results at $L = 108.5$ in.

As shown from Tables A.4A and A.4B, obtained from the vertical and horizontal scans, the deposit is more symmetric in this location. Deposit material is in the bottom half of the process pipe, as observed before (Fig. 3.14). The total deposit at the midplane is $d_x(y = 0) =$ (1.2 ± 0.2) in., which is consistent with the (1.0 ± 0.17) in. thickness given in Fig. 3.14. Comparison of the data in Table 3.7A (obtained from the detector #2) with the data in Table A.4A indicates the existence of a structure in the deposit within 4.5 in. of the pipe between the two detector locations. Moreover, in this location it appears that the deposit is thicker and varies between 20 and 40% around the midplane and on the upper half of the pipe. The results from the horizontal scan (see Table A.2B) indicate that the total deposit thickness at $x = 0$ is $d_y(x = 0) = 1.6 \pm 0.3$ in., and about 10 to 30% more material is present for $x > 0$, which is also the case in Fig. 3.11. The average H/U value of about 3.2 is obtained from the iterative procedure.

Table A.4A. Hockey Stick iterative results of total transmission thickness from vertical source and detector #3 scan at L = 108.5 in.

Position y (in.)	$-\text{Ln}(I/I_0)$	Thickness (in.)
10	1.124	2.59
8	0.93	2.14
6	0.542	1.25
4	0.489	1.13
2	0.253	0.58
0	0.517	1.19
–2	0.486	1.12
–4	0.522	1.20
–6	0.225	0.52
–8	0.342	0.79
–10	0.286	0.66

Table A.4B. Hockey Stick iterative results of total transmission thickness from horizontal source and detector #3 scan at L = 108.5 in.

Position x (in.)	$-\text{Ln}(I/I_0)$	Thickness (in.)
10	0.755	1.74
8	0.8	1.84
6	0.63	1.45
4	0.794	1.83
2	0.589	1.36
0	0.696	1.60
–2	0.645	1.49
–4	0.311	0.72
–6	0.4	0.92
–8	0.383	0.88
–10	0.133	0.31

The source-detector rotation results given in Table A.4C suggest that a lack of material (a hole) at one angular position on the pipe (an area in which the deposit material is missing) exists along the periphery of the deposit pipe, $\alpha = 60°$, as indicated by a sudden drop in the deposit thickness at $\alpha = 60°$ and somewhat at $\alpha = 240°$. The presence of this hole is also apparent from the horizontal scan at the x = –4 in. position. In Fig. A.5, the rotation results

of the NWIS detectors are presented, and the deposit variations obtained from these two detectors are similar to each other. The deposit profile is given in Fig. A.6.

Table A.4C. Hockey Stick iterative results of total radial thickness from source and detector #3 rotation at L = 108.5 in.

Rotation α (Deg.)	$-\text{Ln}\,(I / I_o)$	Thickness (in.)
0	0.511	1.18
30	0.268	0.62
60	0.113	0.26
90	0.286	0.66
120	0.291	0.67
150	0.656	1.51
180	0.696	1.60
210	0.381	0.88
240	0.325	0.75
270	0.524	1.21
300	0.508	1.17
330	0.406	0.93

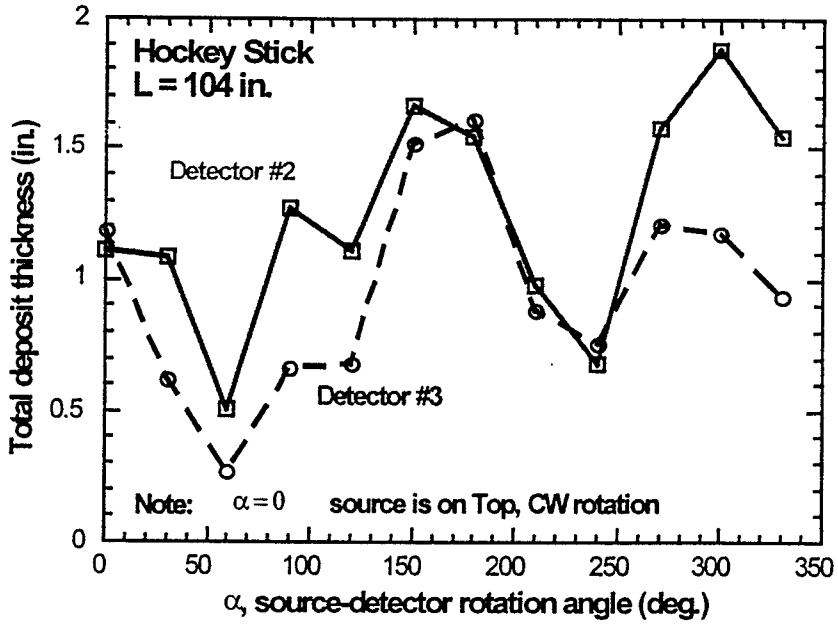

Fig. A.5. Variations of total deposit thickness obtained from source-detector #2 (and detector #3) rotation measurements at L = 104 in. on the Hockey Stick.

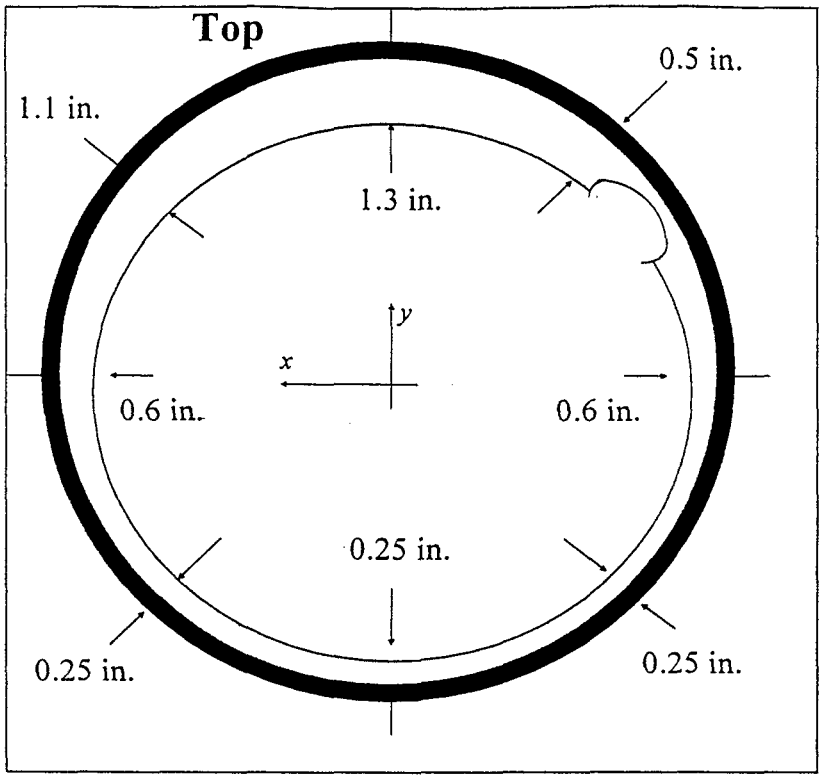

Fig. A.6. Hockey Stick deposit profile at L = 108.5 in.

A.5. Measurement Results at L = 137.5 in.

The results of the total deposit thickness determined from the vertical and horizontal scans of the source and the detector are given in Tables A.5A and A.5B, respectively. The average H/U obtained from the iterative procedure is 3.5 at this measurement location. At the midplane, $y = 0$, the total deposit is $d_x(y = 0) = 0.9 \pm 0.2$ in., which is somewhat thinner than the 1.6 ± 0.27 in. deposit thickness given in Fig. 3.15, obtained with detector #2. In general, the vertical scan data indicate an overall diminished thickness at this location compared with detector #2 results (Table 3.8A), and may be indicative of the decreasing profile moving up the pipe. This occurs because detector #3 is actually centered 4.5 in. further up the pipe, at L = 137.5 in., when detector #2 is placed at L = 133 in. The general shape of the profile is consistent with the earlier findings except that it tends to be somewhat thinner overall. The horizontal scan measurement results from detector #3 (Table A.5B) correlate well those from the detector #2 (Table 3.9B) except that detector #3 indicates somewhat less deposit material. The corresponding deposit profile is given in Fig. A.7.

Table A.5A. Hockey Stick iterative results of total transmission thickness from vertical source and detector #3 scan at L = 137.5 in.

Position y (in.)	$-\text{Ln}\,(I / I_o)$	Thickness (in.)
10	0.336	0.79
8	0.412	0.97
6	0.324	0.76
4	0.282	0.66
2	0.334	0.79
0	0.38	0.90
–2	0.43	1.01
–4	0.305	0.72
–6	0.316	0.74
–8	0.379	0.89
–10	0.397	0.94

Table A.5B. Hockey Stick iterative results of total transmission thickness from horizontal source and detector #3 scan at L = 137.5 in.

Position x (in.)	$-\text{Ln}\,(I / I_o)$	Thickness (in.)
10	0.265	0.62
8	0.559	1.32
6	0.619	1.46
4	0.708	1.67
2	0.802	1.89
0	0.637	1.50
–2	0.718	1.69
–4	0.641	1.51
–6	0.55	1.30
–8	0.716	1.69
–10	0.505	1.19

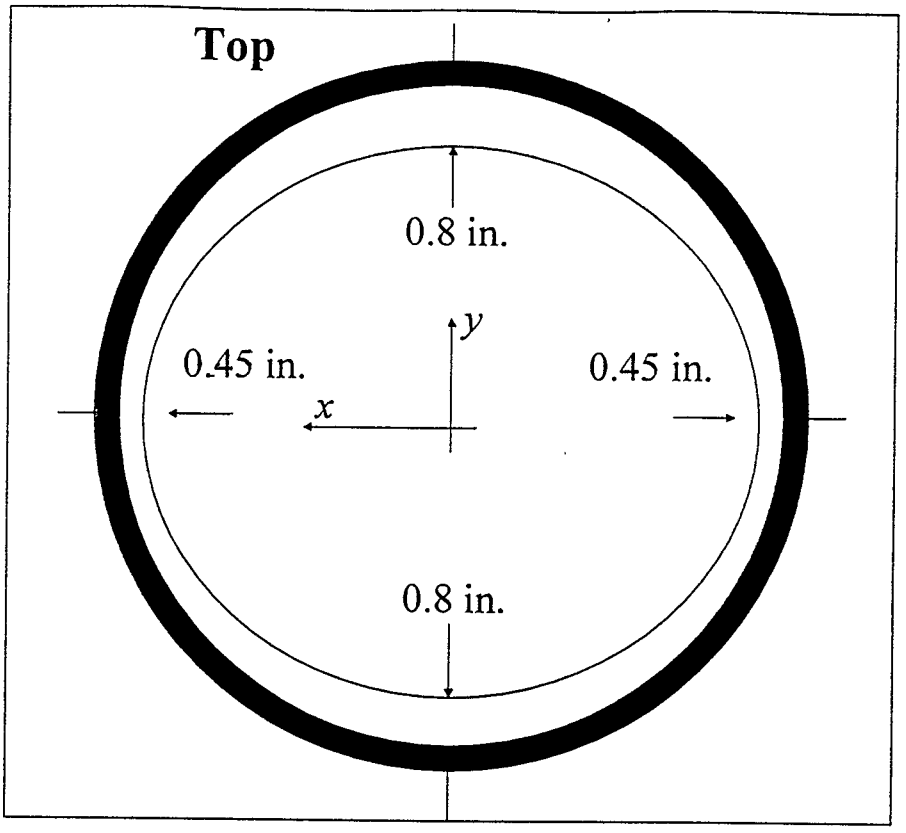

Fig. A.7. Hockey Stick deposit profile at L = 137.5 in.

A.6. Measurement Results at L = 167.5 in.

The results of the total deposit thickness determined from the vertical and horizontal scans of the source and the detector are given in Tables A.6A and A.6B. The average H/U found from the iterative procedure is 4.5. Comparison of the results from two detectors for the vertical scan exhibit the same behavior as the comparison of the vertical scan at L = 133 in. In general, the data from detector #3 indicate an overall diminished thickness at this location compared with that from the detector #2 (Fig. A.8). As previously explained, this is likely caused by the decreasing deposit thickness along the process pipe.

Table A.6A. Hockey Stick iterative results of total transmission thickness from vertical source and detector #3 scan at L = 167.5 in.

Position y (in.)	$-\text{Ln}(I / I_0)$	Thickness (in.)
10	0.178	0.45
8	0.277	0.70
6	0.334	0.85
4	0.267	0.68
2	0.404	1.03
0	0.365	0.93
−2	0.322	0.82
−4	0.328	0.83
−6	0.326	0.83
−8	0.397	1.01
−10	0.19	0.48

Table A.6B. Hockey Stick iterative results of total transmission thickness from horizontal source and detector #3 scan at L = 167.5 in.

Position x (in.)	$-\text{Ln}(I / I_0)$	Thickness (in.)
10	0.413	1.05
8	0.427	1.08
6	0.435	1.10
4	0.524	1.33
2	0.541	1.37
0	0.543	1.38
−2	0.704	1.79
−4	0.532	1.35
−6	0.452	1.15
−8	0.592	1.50
−10	0.191	0.49

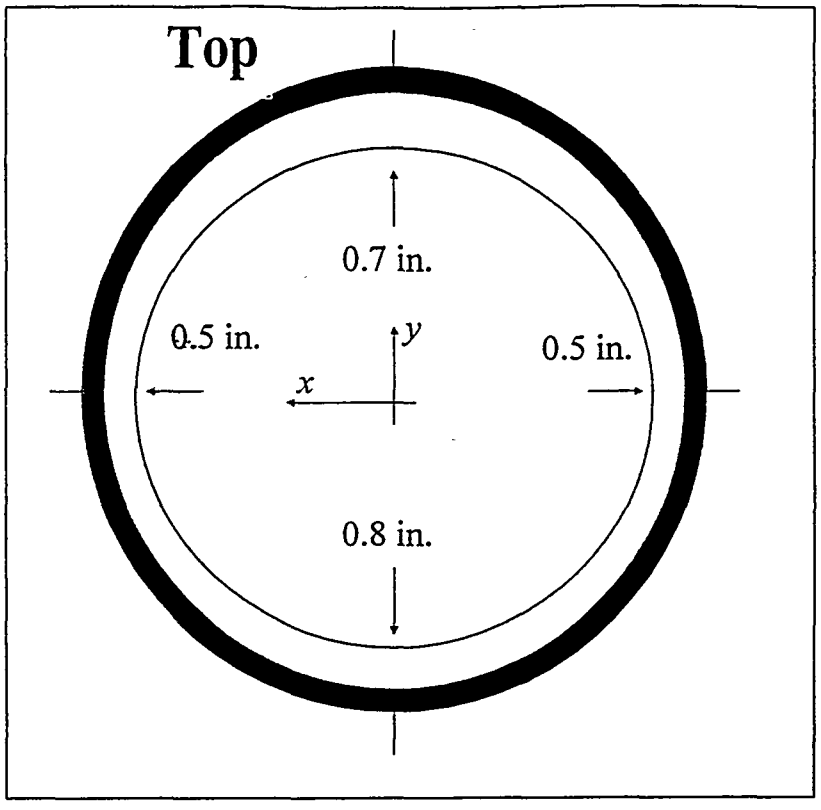

Fig. A.8. Hockey Stick deposit profile at L = 167.5 in.

The results obtained from the horizontal scans at L = 163 in. for detector #2 and detector #3 at L = 167.5 in., in general, follow each other well, with the exception of two locations at $y = -4$ in. and $y = -10$ in.; the variations of the remaining locations all agree with each other.

A.7. H/U Measurement Results

As discussed in Sect. 3.3.2, the deposit profile results together with the gamma-ray attenuation measurements obtained from the second NWIS detector (detector #3) are utilized for the data analysis of determining the values of H/U for the locations where the deposit thicknesses are more than 1 in. The results obtained from the iterative procedure are given in Table A.7, and the corresponding frequency distribution of these H/U data is presented in Fig. A.9. The H/U mean value is 3.6, which has a standard deviation of the mean of 0.24. Therefore, the Hockey Stick deposit hydration value obtained from the second detector is H/U = 3.6 ± 0.24. As discussed in Sect. 3.3.2, the H/U is H/U = 3.4 ± 0.25 obtained from detector #2, and these two results are within 5%.

Table A.7. Hockey Stick iterated values of H/U from detector #3 measurements

0.5	3	3.6	4.3	5.4
0.8	3.1	3.7	4.4	5.6
1.3	3.1	3.8	4.4	5.7
1.5	3.2	3.9	4.5	6
2.4	3.3	4	4.6	
2.7	3.4	4.2	4.7	
2.8	3.6	4.3	5.1	

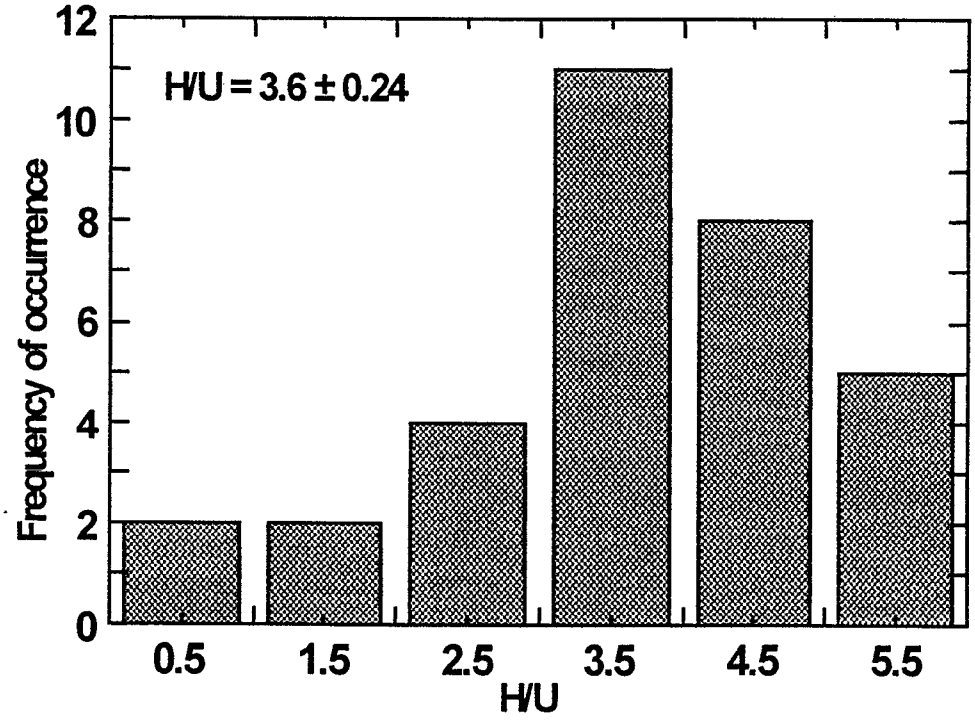

Fig. A.9. Hockey Stick frequency distribution for iterative values of H/U from detector #3 measurement data.

A.8. Total Uranium Mass

The deposit profiles obtained from the second NWIS detector, detector #3, are used to calculate the total deposit volume of the Hockey Stick in fashion similar to that discussed in Sect. 3.3.4. The findings are summarized in Table A.8. The total deposit volume of $V_d \approx 0.140$ m^3 was obtained for the Hockey Stick process pipe. The total deposit volume is the same as that estimated with detector #2 results (see Sect. 3.3.4). The density of the uranium, given by Eq. (11), is also the same value, $\rho_u \sim 3.8$ g/cc, because about the same H/U is measured with detector #3. Therefore, the total uranium mass of 531 ± 90 kg was obtained. This estimate is about the same value, within ~2%, as found with the detector #2 measurement results (see Sect. 3.3.4).

Table A.8. Hockey Stick measurement deposit segments for calculations of the deposit volume using detector #3 results

Measurement location L (in.)	Deposit profile figure	Segment location (in.)	Measurement segment length L_i (in.)[a]	Segment Average deposit thickness $\bar{d}_i$ (in.)	Segment volume V_i (in.^{3})[b]
44.5	A.1	0 – 51.5	51.5	0.60	2142[c]
58.5	A.2	51.5 – 71.5	20	0.73	1033
84.5	A.4	71.5 – 96.5	25	0.85	1495
108.5	A.5	96.5 – 123	26.5	0.60	1131
137.5	A.7	123 –152.5	29.5	0.62	1300
167.5	A.8	152.5 – 167.5	15	0.62	1436[d]

[a] Measured on the midplane of the pipe (see Fig. 3.18).
[b] Total deposit volume: $V_d = \sum_i V_i = 8537$ in^3.
[c] Includes 15-in.-long transition section with an average diameter of 22 in. (see Fig. 3.18).
[d] Includes up to the top of the Hockey Stick, assuming that the deposit thickness varies linearly to 0.1-in. thickness at the top.

This page intentionally left blank.

APPENDIX B. ADDITIONAL PHOTOGRAPHS OF THE HOCKEY STICK AND TEE-PIPE DEPOSIT MEASUREMENTS

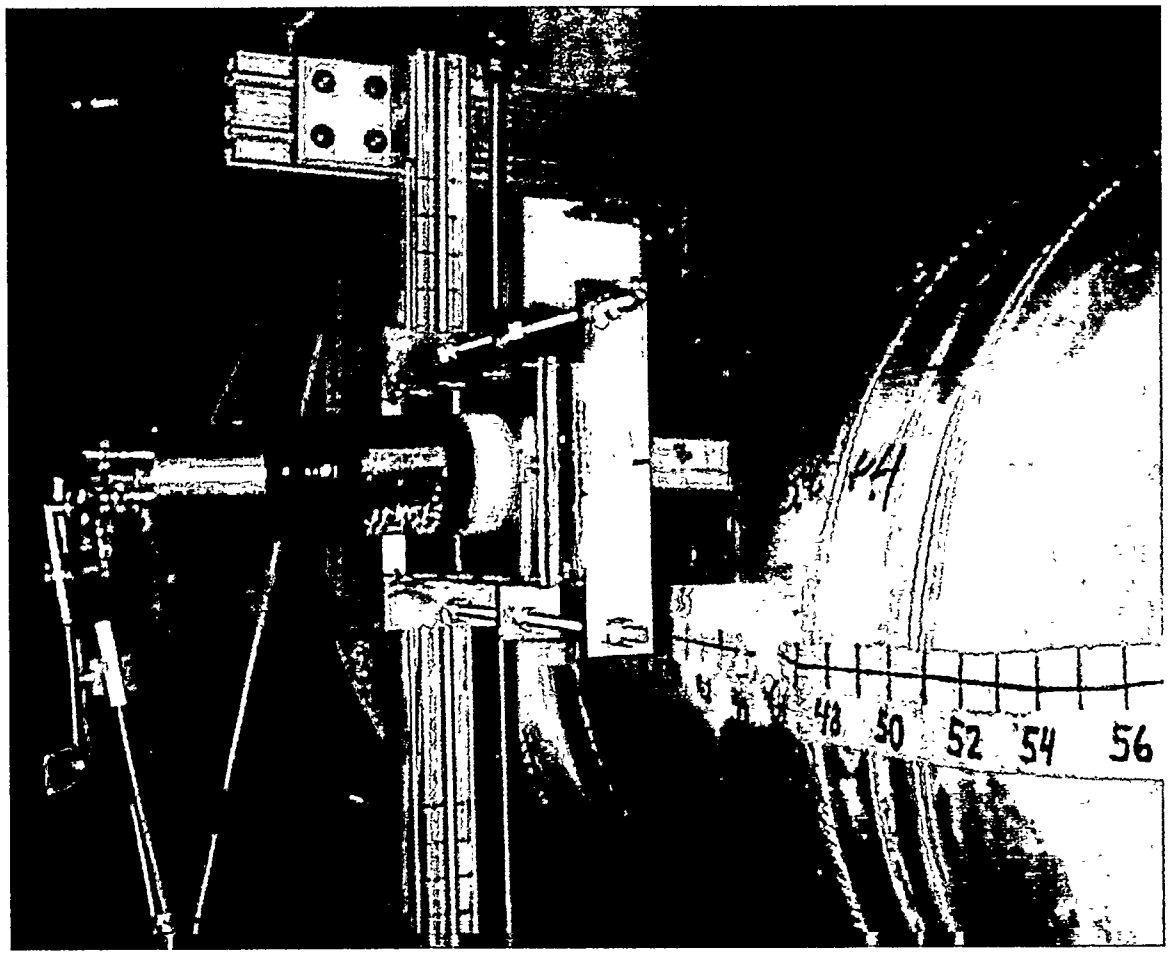

Fig. B.1. Hockey Stick source-detector vertical scan at $L = 40$ in.

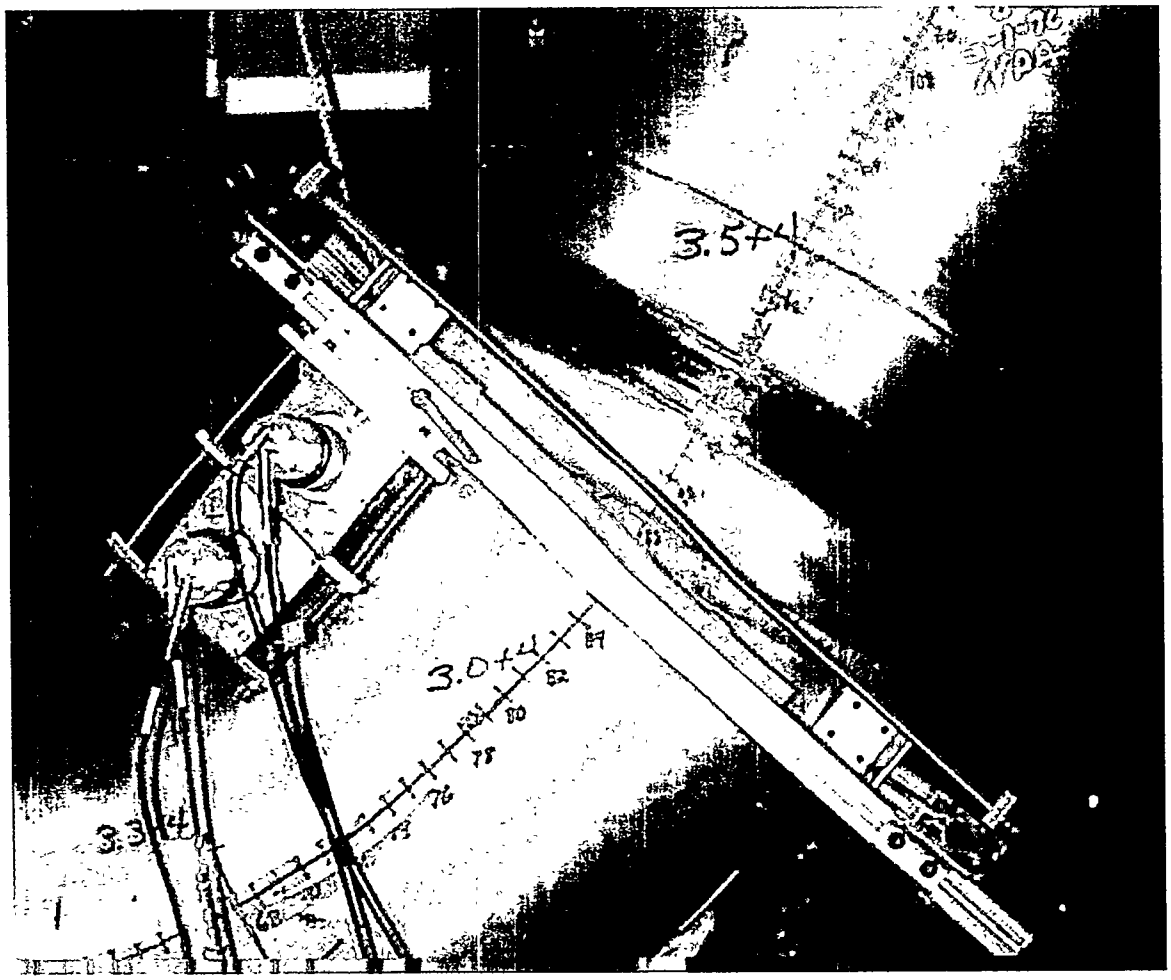

Fig. B.2. Hockey Stick source-detector vertical scan at $L = 80$ in.

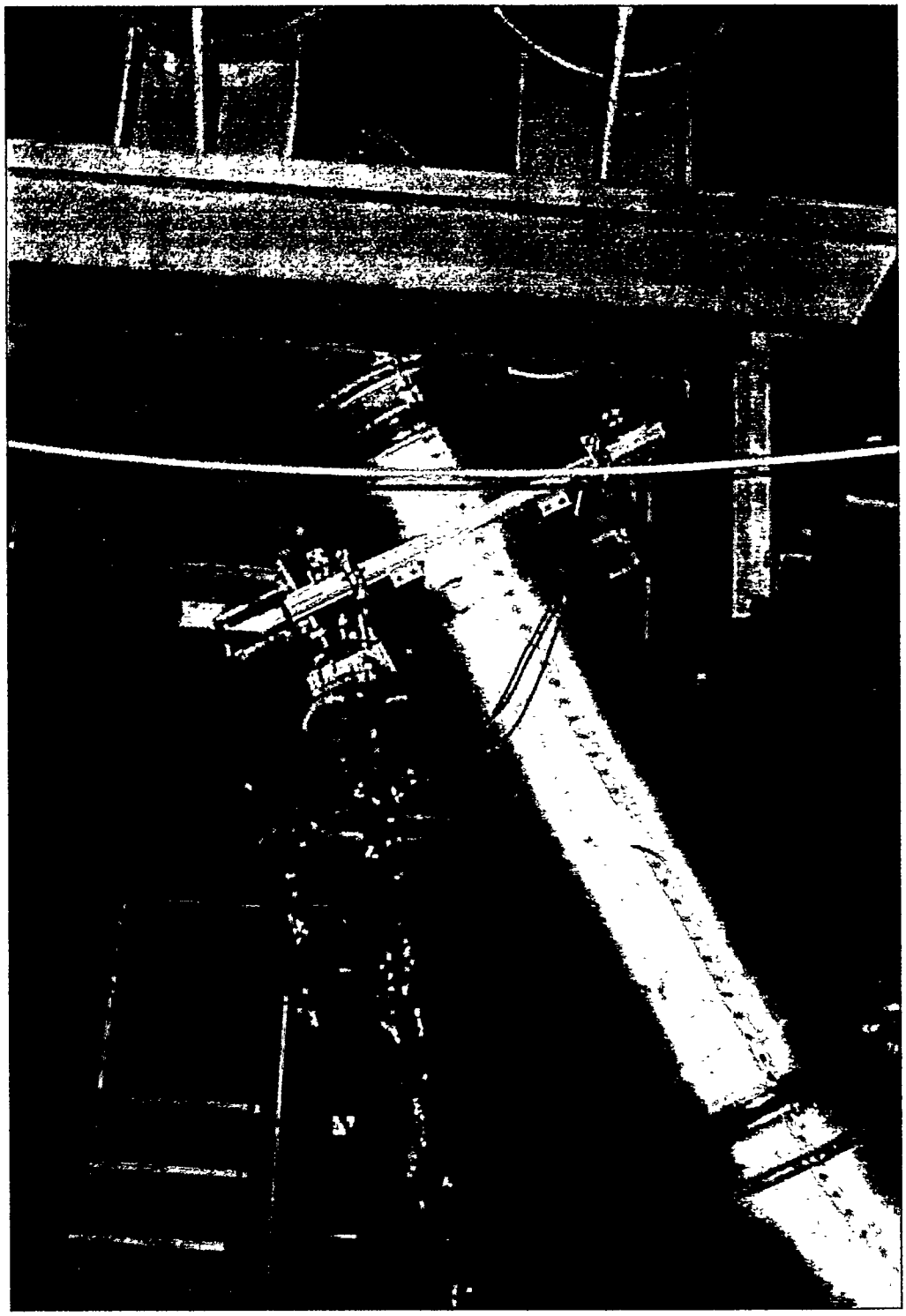

Fig. B.3. Hockey Stick source-detector vertical scan at L = 163 in.

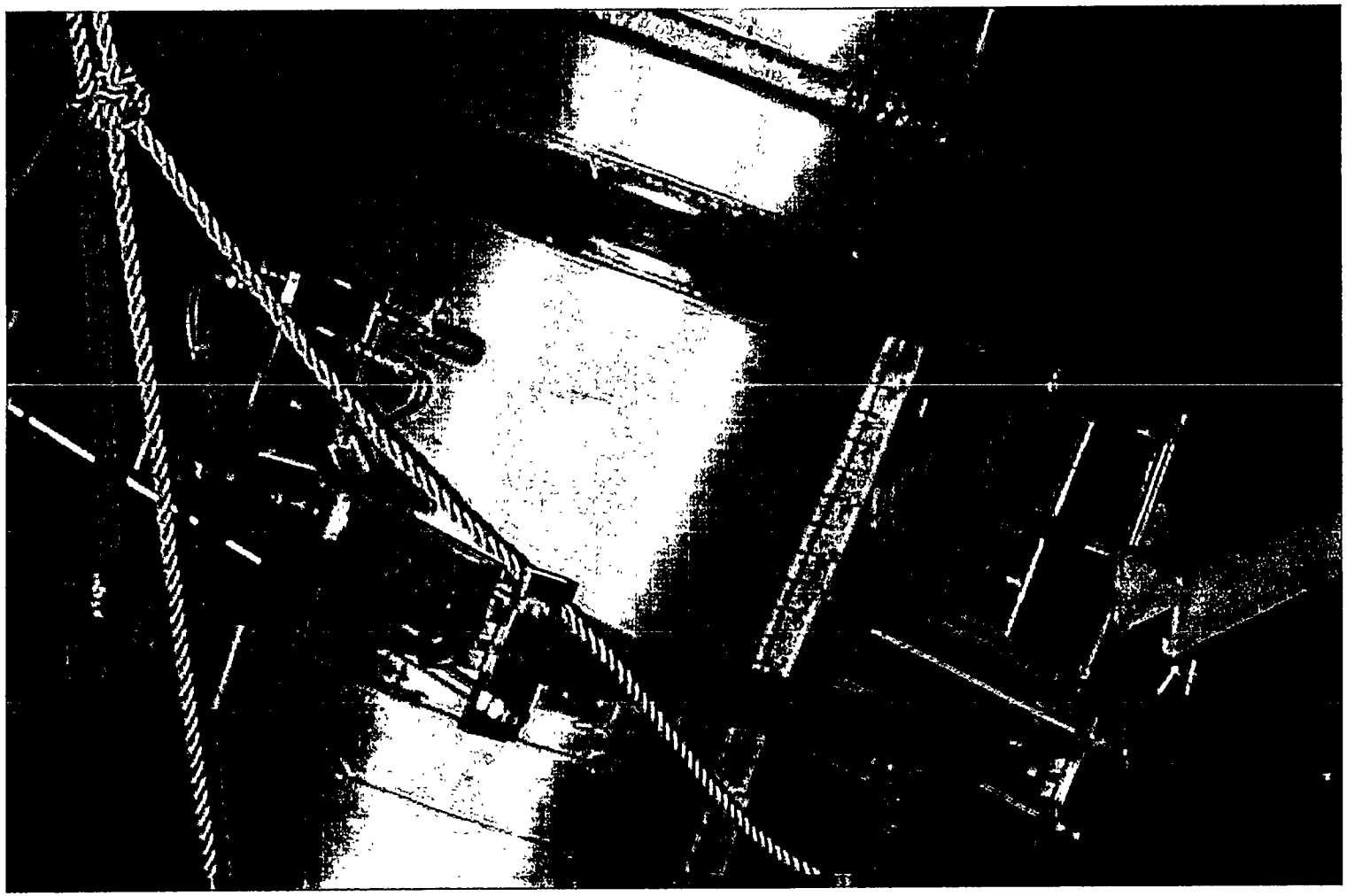

Fig. B.4. Hockey Stick source-detector vertical scan in the $y = -10$ in. position at $L = 163$ in.

Fig. B.5. Tee-Pipe deposit measurements on the horizontal section.

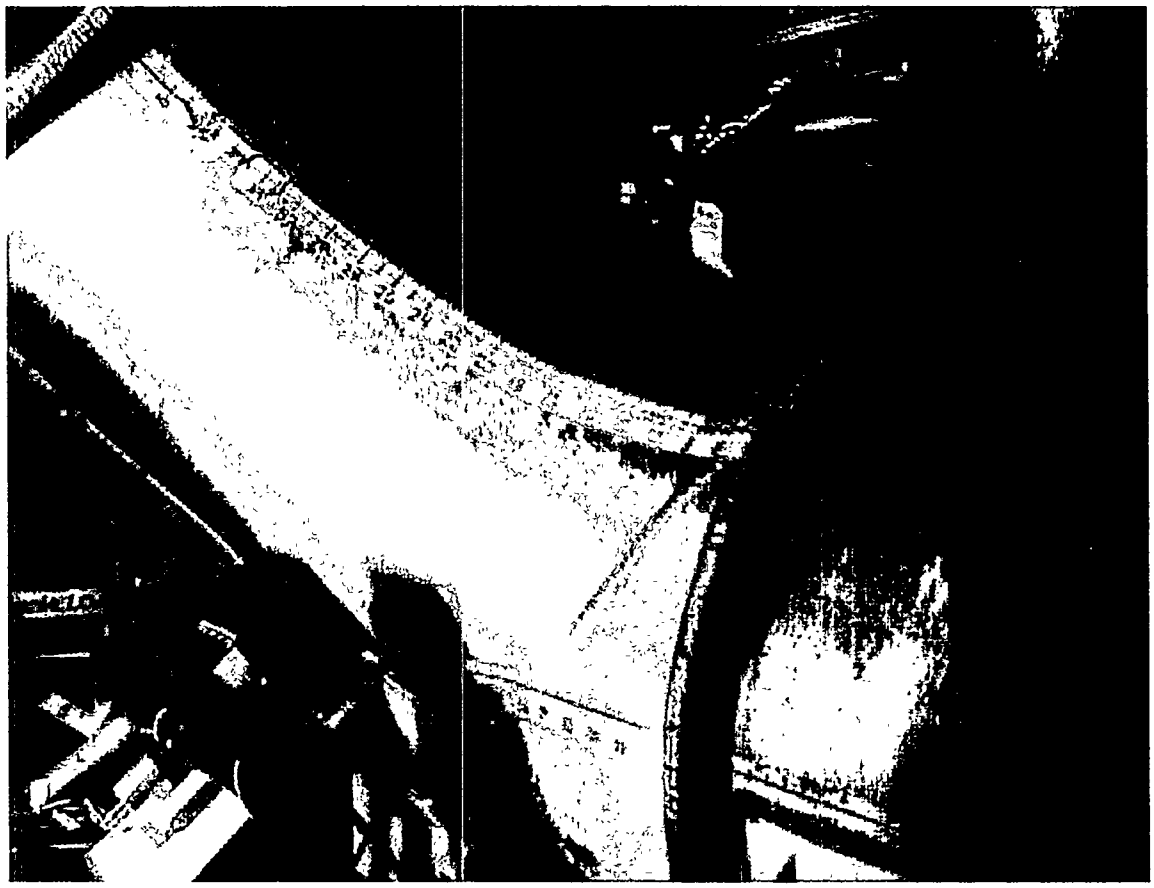

Fig. B.6. Tee-Pipe deposit measurements on the transition section.

APPENDIX C. ESTIMATION OF AN AVERAGE DEPOSIT THICKNESS

The estimation of an average deposit thickness $\bar{d}_i$ for a uniform deposit profile calculated for a measured deposit profile at the measurement location of i is obtained by making use of the total deposit surface area A_d. Figure C.1 shows a typical deposit profile in a process pipe with a diameter of D. The area of a deposit sector indicated by points A, B, C, and D in Fig. C.1 at the location of j on the deposit profile can be calculated as

$$A_j = d_j S_j (1 - d_j/D), \tag{C.1}$$

where d_j is the measured deposit thickness, S_j is the arc length between point A and B of the process pipe about j such that

$$\pi D = \sum_j S_j, \text{ with } j = 1, N_i, \tag{C.2}$$

where N_i is the total number of sectors that make up the total deposit area; that is,

$$A_d = \sum_j A_j, \text{ with } j = 1, N_i. \tag{C.3}$$

When Eq. (C.1) in Eq. (C.3) are used to express A_d for the uniform deposit profile, the average deposit thickness satisfies the following relationship:

$$A_d = \pi \bar{d}_i (D - \bar{d}_i) = \sum_j d_j S_j (1 - d_j/D), \text{ with } j = 1, N_i, \tag{C.4}$$

which is a quadratic equation in $\bar{d}_i$. This relationship can be approximated because the values for d_j and in turn $\bar{d}_i$ are much less than that of D for the deposit measurement results presented in the report. Therefore, Eq. (C.4) reduces to

$$\bar{d}_i = (1/\pi D) \sum_j d_j S_j, \text{ with } j = 1, N_i. \tag{C.5}$$

Moreover, $S_j N_i = \pi D$ in Eq. (C.5) leads to

$$\bar{d}_i = (1/N_i) \sum_j d_j, \text{ with } j = 1, N_i. \quad \text{(C.6)}$$

In terms of the subtended angle α_j of the sector (see Fig. C.1), the sector arc length becomes

$$Sj = \alpha_j D/2, \quad \text{(C.7)}$$

and using this in Eq. (C.5) gives

$$\bar{d}_i = (1/2\pi) \sum_j d_j \alpha_j, \text{ with } j = 1, N_i. \quad \text{(C.8)}$$

Depending upon the presentation of the deposit profile data, estimation of the average deposit thickness can be obtained by either using Eq. (C.6) or Eq. (C.8).

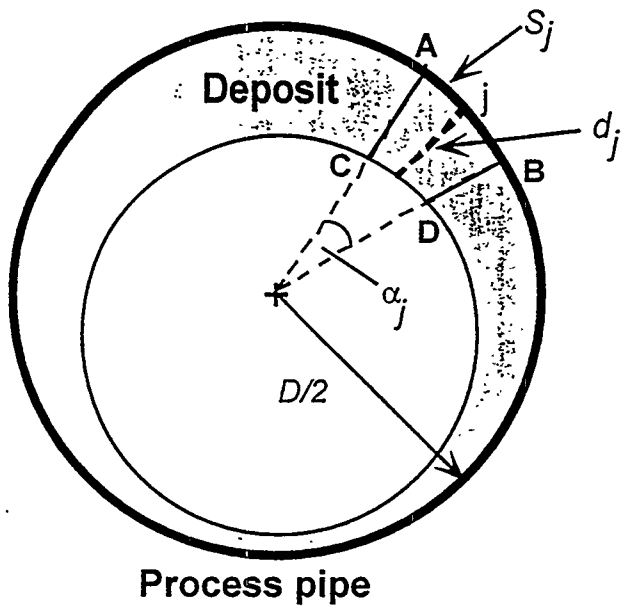

Fig. C.1. Sketch of typical deposit profile showing a deposit sector indicated with points A, B, C, and D at the location of *j* used for the estimation of an average deposit thickness as discussed in Appendix C.

APPENDIX D. INVENTORY OF REMOVED DEPOSIT MATERIAL

This appendix presents the results of the inventory of materials from the cleanup of the $UO_2F_2 \cdot H_2O$ deposits removed from the Hockey Stick and the Tee-Pipe. The weights of the cans were estimated to ± 50% with passive neutron counting; the enrichment was estimated to ± 20%. The deposit materials are now stored in cans in a managed fissile storage area after the cleanup of the deposit. The neutron counting UO_2F_2 mass for each can is given in Table D.1. The total mass of each can from weighing is also given in Table D.1, but the cans contain some other materials, such as metals from cutting the pipes. The total mass from passive neutron counting of all of the individual cans ~425 kg, which is considerably lower than the 1,300 kg (± 50% uncertainty) measured for the fully assembled Hockey Stick deposit. The actual NDA reports and correspondence on the deposit removal from the Hockey Stick and the Tee-Pipe are included after Table D.1.

Table D.1. Uranium mass from neutron counting and weighting for cans of deposit materials

Item identification	Deposit mass (kg)	
	Neutron counting	Net weight by scale
Tee-Pipe		
K2926ALAD001	18.26	23.61
K2926ALAD002	22.55	27.97
K2926ALAD003	23.96	28.65
K2926ALAD004	13.26	16.15
K2926ALAD005	4.98	6.38
Total	83.01	102.76
Hockey Stick		
K2927BLBD001	4.44	18.88
K2927BLDD001	6.02	8.88
K2927BLAD001	25.9	42.51
K2927BLAD002	12.6	24.33
K2927BLCD001	29.4	42.06
K2927BLCD002	28.7	41.15
K2927BLCD003	32.2	39.11
K2927BLCD004	26.8	35.47
K2927BLCD005	27.4	36.15
K2927BLCD006	28.1	36.15
K2927BLCD007	26.6	34.33
K2927BLCD008	5.87	8.88
K2927BLBD002	25.1	37.06
K2927BLBD003	25.3	38.88
K2927BLBD004	32.3	45.7
K2927BLBD005	26.6	35.92
K2927BLBD006	32.5	43.65
K2927BLBD007	29.2	38.65
Total	425.03	607.76

LOCKHEED MARTIN

Memorandum

Ltr.#NDA98-001

Date: January 5, 1998

To: E. P. Larson

c: J. Bailey (NDSR97-134), J. L. Frazier, T. F. Hannon, J. T. Hargrove, S. L. Henderson, R. W. Miles, T. S. Warrington, File (NoRC)

From: R. W. Brandenburg, K-1030, MS-7319 (4-9835) R W Brandenburg

Subject: Survey of Trash Bags, Pipe Sections, and 5-gal Deposit Drums in Building K-29

In support of the deposit removal activities, the Nondestructive Assay (NDA) Department surveyed 18 5-gal drums of deposit material removed from the K-502-2-7 B-line Out ("Hockey Stick"), two pipe sections, and four bags of trash in Building K-29. Table 1 lists the results of the NDA measurements of the trash bags and pipe sections; Table 2 lists the results of the NDA measurements of the drums.

A high-resolution gamma-ray detector was used to measure the ^{235}U enrichment of the uranium in the drums, and a neutron detector was used to measure the quantities in the drums and pipe sections. The quantities are based on the assumption that the deposit is pure UO_2F_2. A high-resolution gamma-ray detector was used to measure quantities for the trash bags. The average enrichment from the drum measurements was used for the trash bag and pipe section calculations. The chemical form of the material makes little difference for gamma-ray measurements. The measurement uncertainty is estimated to be ±50% for the quantitative values and ±20% relative for the isotopic concentration values.

If you have any questions or need additional information, please let me know.

Table 1. Results of NDA Measurements of Items in Building K-29

Item Identification	^{235}U (wt %)	Uranium (g)	^{235}U (g)
Trash Bag 06	3[a]	1.2	0.03
Trash Bag 07	3[a]	6.4	0.2
Trash Bag 08	3.00	2.7	0.08
Trash Bag 09	3[a]	22	0.7
Pipe Section K2927BLBH001	3[a]	9,960	299
Pipe Section K2927BLCH001	3[a]	15,150	455

[a] Estimated

Table 2. Results of NDA Measurements of 5-gal Deposit Drums in Building K-29

Identification	^{235}U (wt %)	Uranium (g)	^{235}U (g)
K2927BLAD001	2.73	25,900	776
K2927BLAD002	2.99	12,600	379
K2927BLBD001	3.09	4,440	133
K2927BLBD002	2.91	25,100	753
K2927BLBD003	3.19	25,300	759
K2927BLBD004	3.26	32,300	970
K2927BLBD005	3.21	26,600	798
K2927BLBD006	2.86	32,500	976
K2927BLBD007	2.97	29,200	876
K2927BLCD001	3.11	29,400	882
K2927BLCD002	3.41	28,700	860
K2927BLCD003	2.62	32,200	966
K2927BLCD004	3.38	26,800	804
K2927BLCD005	2.80	27,400	821
K2927BLCD006	3.32	28,100	843
K2927BLCD007	3.44	26,600	799
K2927BLCD008	3.26	5,870	176
K2927BLDD001	2.86	6,020	180
Total	3.00[a]	425,030	12,751

[a] Average

LOCKHEED MARTIN

Memorandum

Ltr.#NDA97-423

Date: December 11, 1997

To: E. P. Larson

c: J. Bailey (NDSR97-112), C. S. Fox, J. L. Frazier, T. F. Hannon, J. T. Hargrove, R. W. Miles, T. S. Warrington, File (NoRC)

From: R. W. Brandenburg, K-1030, MS-7319 (4-9835) RWBrandenburg

Subject: **Survey of the Remainder of the K-502-2-7 B-Outlet Pipe and Valve in Building K-29**

In support of the deposit removal activities, the Nondestructive Assay (NDA) Department surveyed the remaining end of the K-502-2-7 B-outlet pipe ("Hockey Stick") and valve 7BB2 in Building K-29 after initial cleaning was completed. Table 1 lists the results of the NDA measurements of these items.

A neutron detector was used to measure the uranium quantity in the pipe. The quantities are based on the assumption that the residual material is pure UO_2F_2 with an enrichment of 3.3 wt % ^{235}U from previous measurements. The measurement uncertainty is estimated to be ±50% for the quantitative values.

If you have any questions or need additional information, please let me know.

Table 1. Results of NDA Measurements of "Hockey Stick" and Valve in Building K-29

Identification	Uranium (g)	^{235}U (g)
Remaining End of Pipe	28,500	940
Valve 7BB2	14,800	490

Nuclear Materials Control and Accountability
Observation of Weighing of Accountable Nuclear Materials

Page 2 Sheet 1 of 2

Date of Observation: 12/16/97

Material Balance Area: 17

NMC&A Representative: D.L. Dunney (13970)
(Signature & Badge no.)

Item Identification	Observed Measurement	Units-(g, Kg, Lb., L)	Gross, Tare, Net	Book Value	% Diff. to Book Value	TID NUMBER
K2926ALADOO1	62.4	Lbs.	Gross	—	—	(953441)
K2926ALADOO2	72.0	Lbs.	Gross	—	—	(953442)
K2926ALA DOO3	72.5	Lbs	Gross	—	—	(953443)
K2926ALA DOO4	46.0	Lbs	Gross	—	—	(953444)
K2926 ALA DOO5	24.5	Lbs	Gross	—	—	(953454)
K2927 BLB DOO1	52.0	Lbs	Gross	—	—	(953509)
K2927 BLD DOO1	30.0	Lbs	Gross	—	—	(953510)
K2927 BLA DOO1	104.0	Lbs	Gross	—	—	(953511)
K2927 BLA DOO2	64.0	Lbs	Gross	—	—	(953512)
K2927 BLC DOO1	103.0	Lbs	Gross	—	—	(953514)
K2927 BLC DOO2	101.0	Lbs	Gross	—	—	(953515)
K2927 BLC DOO3	96.5	Lbs	Gross	—	—	(953516)
K2927 BLC DOO4	88.5	Lbs	Gross	—	—	(953517)
K2927 BLC DOO5	90.0	Lbs	Gross	—	—	(953518)
K2927 BLC DOO6	90.0	Lbs	Gross	—	—	(953519)
K2927 BLC DOO7	86.0	Lbs	Gross	—	—	(953520)
K2927 BLC DOO8	30.0	Lbs	Gross	—	—	(953521)
K2927 BLB DOO2	92.0	Lbs	Gross	—	—	(953522)
K2927 BLB DOO3	96.0	Lbs	Gross	—	—	(953523)
K2927 BLB DOO4	111.0	Lbs	Gross	—	—	(953524)
K2927 BLB DOO5	89.5	Lbs	Gross	—	—	(953525)
K2927 BLB DOO6	106.5	Lbs	Gross	—	—	(953526)
K2927 BLB DOO7	95.5	Lbs.	Gross	—	—	(953527)

TEF PIPE CANS

HOCKEY STICK CANS

HOCKEY STICK CAN

LOCKHEED MARTIN

Memorandum

Ltr.#NDA97-353

Date: October 29, 1997

To: C. P. Hall

c: J. Bailey (NDSR97-112), C. S. Fox, J. L. Frazier, T. F. Hannon, J. T. Hargrove, E. P. Larson, R. W. Miles, T. S. Warrington, File (NoRC)

From: R. W. Brandenburg, K-1030, MS-7319 (4-9835) R. W. Brandenburg

Subject: **Survey of 5-gal Deposit Buckets and Other Items in Building K-29**

In support of the deposit removal activities, the Nondestructive Assay (NDA) Department surveyed four 5-gal buckets of deposit material removed from the K-502-2-6 A-line Out ("T" pipe), four used HEPA filters, and two bags of trash in Building K-29. Tables 1 and 2 list the results of the NDA measurements of the buckets and the other items, respectively.

A high-resolution germanium detector was used to measure the ^{235}U enrichment, and a neutron detector was used to measure the quantities in the buckets. The quantities are based on the assumption that the deposit is pure UO_2F_2. Replicate measurements were made on the four buckets. A high-resolution gamma-ray detector was used to measure both the enrichment and quantities for the other items. The chemical form of the material makes little difference for gamma-ray measurements. The measurement uncertainty is estimated to be ±50% for the quantitative values and ±20% relative for the isotopic concentration values.

If you have any questions or need additional information, please let me know.

Table 1. Results of NDA Measurements of 5-gal Deposit Buckets in Building K-29

Identification	First Measurement			Replicate Measurement		
	^{235}U (wt %)	Uranium (g)	^{235}U (g)	^{235}U (wt %)	Uranium (g)	^{235}U (g)
K2926ALAD001	3.13	18,490	555	2.86	18,260	548
K2926ALAD002	3.01	22,790	684	2.99	22,550	676
K2926ALAD003	2.78	24,910	747	2.98	23,960	719
K2926ALAD004	3.01	13,560	407	2.86	13,260	398
Total	2.98[a]	79,750	2,393	2.92[a]	78,030	2,341

[a] Average

Table 2. Results of NDA Measurements of Items in Building K-29

Item Identification	^{235}U (wt %)	Uranium (g)	^{235}U (g)
Filter 1	3[a]	7	0.2
Filter 2	3.03	29.5	0.9
Filter 3	2.89	49.7	1.4
Filter 4	3[a]	16	0.5
Large Trash Bag	3[a]	19	0.6
Small Trash Bag	3[a]	10	0.3

[a] Estimated

LOCKHEED MARTIN

Memorandum

Ltr.#NDA97-373

Date: November 11, 1997

To: C. P. Hall

c: J. Bailey (NDSR97-112), C. S. Fox, J. L. Frazier, T. F. Hannon, J. T. Hargrove, E. P. Larson, R. W. Miles, T. S. Warrington, File (NoRC)

From: R. W. Brandenburg, K-1030, MS-7319 (4-9835) R W Brandenburg

Subject: **Survey of "T" Pipe in Building K-29**

In support of the deposit removal activities, the Nondestructive Assay (NDA) Department surveyed the K-502-2-6 A-line Out ("T" pipe) in Building K-29 after cleaning was completed. Table 1 lists the results of the NDA measurements of the pipe.

A high-resolution germanium detector was used to measure the ^{235}U enrichment, and a neutron detector was used to measure the uranium quantity in the pipe. The quantities are based on the assumption that the deposit is pure UO_2F_2. The measurement uncertainty is estimated to be ±50% for the quantitative values and ±20% relative for the isotopic concentration values.

If you have any questions or need additional information, please let me know.

Table 1. Results of NDA Measurements of "T" Pipe in Building K-29

		Horizontal Section		Vertical Section	
Identification	^{235}U (wt %)	Uranium (g)	^{235}U (g)	Uranium (g)	^{235}U (g)
K2926ALAH001	3.01	10,000	300	4,050	121

LOCKHEED MARTIN

Memorandum

Ltr.#NDA97-370

Date: November 7, 1997

To: C. P. Hall

c: J. Bailey (NDSR97-112), C. S. Fox, J. L. Frazier, T. F. Hannon, J. T. Hargrove, E. P. Larson, R. W. Miles, T. S. Warrington, File (NoRC)

From: R. W. Brandenburg, K-1030, MS-7319 (4-9835) R. W. Brandenburg

Subject: **Survey of a 5-gal Deposit Bucket in Building K-29**

In support of the deposit removal activities, the Nondestructive Assay (NDA) Department surveyed the fifth 5-gal bucket of deposit material removed from the K-502-2-6 A-line Out ("T" pipe) in Building K-29. Tables 1 lists the results of the NDA measurements of the bucket.

A high-resolution germanium detector was used to measure the ^{235}U enrichment, and a neutron detector was used to measure the quantities in the buckets. The quantities are based on the assumption that the deposit is pure UO_2F_2. Replicate measurements were made on the four buckets. A high-resolution gamma-ray detector was used to measure both the enrichment and quantities for the other items. The chemical form of the material makes little difference for gamma-ray measurements. The measurement uncertainty is estimated to be ±50% for the quantitative values and ±20% relative for the isotopic concentration values.

If you have any questions or need additional information, please let me know.

Table 1. Results of NDA Measurements of 5-gal Deposit Buckets in Building K-29

	First Measurement			Replicate Measurement		
Identification	^{235}U (wt %)	Uranium (g)	^{235}U (g)	^{235}U (wt %)	Uranium (g)	^{235}U (g)
K2926ALAD005	3.05	4,670	140	2.94	4,980	149

LOCKHEED MARTIN

Memorandum

Ltr.#NDA97-381

Date: November 18, 1997

To: C. P. Hall

c: J. Bailey (NDSR97-112), C. S. Fox, J. L. Frazier, T. F. Hannon, J. T. Hargrove, E. P. Larson, R. W. Miles, T. S. Warrington, File (NoRC)

From: R. W. Brandenburg, K-1030, MS-7319 (4-9835) R W Brandenburg

Subject: **Survey of a Trash Bag in Building K-29**

In support of the deposit removal activities, the Nondestructive Assay (NDA) Department surveyed a trash bag (Bag 6) in Building K-29 after cleaning of the "T" pipe was completed. Table 1 lists the results of the NDA measurements of the bag.

A high-resolution germanium detector was used to measure the ^{235}U enrichment and the uranium quantity in the pipe. The measurement uncertainty is estimated to be ±50% for the quantitative values and ±20% relative for the isotopic concentration values.

If you have any questions or need additional information, please let me know.

Table 1. Results of NDA Measurements of a Trash Bag in Building K-29

Identification	^{235}U (wt %)	Uranium (g)	^{235}U (g)
Bag 6	3.0	27	0.8

This page intentionally left blank.

REFERENCES

1. T. F. Hannon, J. R. Kirchner, and R. W. Emmett, *Preliminary Probabilistic Criticality Assessment of Selected Low-Enriched Uranium Facilities at the Oak Ridge K-25 Site*, K-25 Site Document No. K/D-6048, January 1993.

2. M. J. Haire and W. C. Jordan, *Relative Risk of Nuclear Criticality Occurring from Low-Enriched Uranium and High-Enriched Uranium Deposits at the K-25 Site, Oak Ridge, Tennessee*, Document No. K/ER-215, December 1995.

3. J. T. Mihalczo, "Use of ^{252}Cf as a Randomly Pulsed Neutron Source for Prompt Neutron Decay Measurements," *Nucl. Sci. Eng.* **41**, 296 (1970).

4. W. Mannhart, "Evaluation of the ^{252}Cf Fission Neutron Spectrum Between 0 MeV and 20 MeV," Proc. Advisory Group Mtg. Neutron Sources, Leningrad, USSR 1986 (*IAEA-TECDOC-410)*, Vienna, 1987.

5. H. Goldstein, *Fundamental Aspects of Reactor Shielding*, Addison-Wesley Publishing Company, Inc., Reading, Massachusetts, 1959.

6. J. T. Mihalczo, and V. K. Pare, "Nuclear Weapons Identification System (NWIS)," *Arms Control and Nonproliferation Technologies*, Third Quarter 1994, DOE/AN/ACNT-94C.

7. J. E. Breeding, J. A. Mullens, G. W. Turner, T. E. Valentine, J. A. McEvers, J. T. Mihalczo, and T. A. Gafford, "New NWIS Processor for Fissile System Verification," Institute of Nuclear Materials Management Meeting, Phoenix, Arizona, July 20–24, 1997.

8. J. T. Mihalczo, T. E. Valentine, J. A. Mullens, and J. K. Mattingly, *Physical and Mathematical Description of Nuclear Weapons Identification System NWIS Signatures*, Oak Ridge Y-12 Plant Report No. Y/LB-15, 946 R3, September 1997.

9. J. T. Mihalczo, T. E. Valentine, J. K. Mattingly, *NWIS Methodology*, Oak Ridge Y-12 Plant Report No. Y/LB-15, 953, October, 1997.

10. M. M. Chiles, J. T. Mihalczo, and C. E. Fowler, "Small, Annular, Double-Contained ^{252}Cf Fission Chamber for Source-Driven Subcriticality Measurements," *IEEE Trans. Nucl. Sci.* **40**, 816 (1993).

11. EG&G ORTEC, 100 Midland Road, Oak Ridge, TN 37831-0895, U.S.A.

12. BICRON Corporation, 12345 Kinsman Road, Newbury, OH 44065-9577, U.S.A.

13. S. Glastone and M. C. Edlund, *The Elements of Nuclear Reactor Theory*, D. Van Nostrand Company, Inc., 1952, p. 45.

14. The National Nuclear Data Center (NNDC) at Brookhaven National Laboratory, Upton, N.Y., http://www.nndc.bnl.gov, maintained by T. W. Burrows (nndctb@bnl.gov).

15. T. E. Valentine and J. T. Mihalczo, "MCNP-DSP: A Neutron and Gamma Ray Monte Carlo Calculation of Source-Driven Noise-Measured Parameters," *Annals of Nuclear Energy* **23,** 1271 (1996).

16. T. E. Valentine and J. T. Mihalczo, "Validation of the Monte Carlo Code MCNP-DSP," *Annals of Nuclear Energy* **24**, 79 (1997).

17. W. C. Jordan and J. C. Turner, *Estimated Critical Conditions for UO_2F_2-H_2O Systems in Fully Water-Reflected Spherical Geometry*, ORNL/TM-12292, December 1992.

18. M. G. Otey and R. A. LeDoux, "$U_3O_5F_8$-A New Compound in the U-O-F System," *J. Inorg. Nucl. Chem.* **29**, 2249 (1967).

19. E. J. Barber et al., *Investigation of Breached Depleted UF6 Cylinders at the K-25 Site*, ORNL-TM-12840, October 1994.

20. Project Completion Report for the Deposit Removal Project in the K-29 Building, East Tennessee Technology Park, Oak Ridge, Tennessee, BJC-OR-65, June 1998.

INTERNAL DISTRIBUTION

1. F. H. Akers, Jr.
2. P. L. Angelo
3. V. M. Baylor
4. R. W. Brandenburg
5. K. J. Carroll
6. R. N. Ceo
7. M. Conger
8. S. A. Cox
9. J. P. Crociata
10. J. B. Dooley
11. H. R. Dyer
12. M. H. Ehinger
13. G. D. Ellis
14. G. F. Flanagan
15. D. N. Fry
16. R. G. Gilliland
17. F. P. Gustavson
18. M. J. Haire
19. C. P. Hall
20. G. R. Handley
21-25. T. F. Hannon (5)
26. S. S. Hughes
27. J. M. Jansen
28. L. J. Jollay
29. W. C. Jordan
30. E. P. Larson
31. K. D. Lewis
32. J. A. March-Leuba
33. M. J. Maston
34. J. K. Mattingly
35. D. W. McDonald
36. J. A. McEvers
37. J. T. Mihalzco (10)
38. M. K. Morrow
39. D. L. Moses
40. J. A. Mullens
41. R. B. Perez
42. C. A. Pickett
43. D. H. Powell
44. A. W. Riedy
45. R. C. Robinson
46. L. J. Satkowiak
47. W. H. Sides
48. P. Singh
49. J. D. Stout
50. J. H. Swanks
51. R. G. Taylor
52. V. S. Tisdale
53. A. W. Trivelpiece
54. T. Uckan (10)
55. R. E. Uhrig
56. R. E. Upchurch
57. T. E. Valentine
58. R. I. Van Hook
59. P. R. Wasilko
60. J. D. White
61. R. T. Wood
62. M. C. Wright
63. Central Research Library
64-66. Laboratory Records – RC (3)
67. Y-12 Plant Records

EXTERNAL DISTRIBUTION

68. H. Beck, Environmental Measurements Laboratory, 376 Hudson Street, New York, NY 10014-3621
69. A. J. Bieniawski, Negotiations and Analysis Division, Office of Arms Control and Nonproliferation, NN-42, GA-007 (FORSTL), Washington, DC 20585
70. A. L. Boni, Savannah River Laboratory, P.O. Box A, Bldg. A-202, Room 773-A, Aiken, South Carolina 29801
71. A. J. Caffrey, Idaho National Engineering Laboratory, Lockheed Martin Idaho Technologies, P.O. Box 1625, Idaho Falls, Idaho 83415-2114
72. R. N. Cherry, U.S. DOE, International Safeguards Division, NN-44, GA-045, Forrestal Building, Washington, DC 20585
73. B. Crain, Savannah River Operations, Savannah River Site, P.O. Box A, Aiken, South Carolina 29801
74. D. W. Crawford, U.S. DOE, 1000 Independence Avenue, S.W., Germantown, NN-512 Washington, DC 20585
75. N. Diaz, Nuclear Regulatory Commission, One White Flint North, 11555 Rockville Pike, Rockville, MD 20852-2738
76. C. E. Dickerman, Argonne National Laboratory, 9700 South Case Avenue, Argonne, Illinois 60439
77. D. H. Dye, Lawrence Livermore National Laboratory, 7000 East Avenue Livermore, CA 94550
78. R. L. Ewing, Sandia National Laboratory, P.O. Box 1663, X-TM, MS-B226, Los Alamos, NM 87545
79. D. R. Finch, Savannah River Laboratory, P.O. Box A, Bldg. D-101, Room 735-A, Aiken, South Carolina 29801
80. S. Fitzgerald, DOE, Director International Policy and Analysis Division NN-42, (FORSTL), 1000 Independence Avenue, S.W., Washington, DC 20585
81. L. R. Foulke, Westinghouse Electric Corp., Bettis Atomic Power Laboratory, P. O. Box 79, West Mifflin, PA 15122-0079
82. L. Franks, Special Technologies Laboratory, 5520 Ekwill Street, Suite B, Santa Barbara, CA 93111
83. J. L. Fuller, Pacific Northwest National Laboratory, 902 Battelle Blvd., P.O. Box 999, Richland, Washington, 99352
84. D. M. Gordon, Brookhaven National Laboratory, P.O. Box 5000, Upton, NY 11973
85. T. B. Gosnell, Lawrence Livermore National Laboratory, 7000 East Avenue L-175, (366), Livermore, CA 94550
86. C. A. Goulding, Los Alamos National Laboratory, NIS-6, MS J562, TA-18, Bldg. 0147, Room 105, Los Alamos, NM 87545
87. J. D. Jackson, U.S. Department of Energy, Oak Ridge Operations Office, Acting Y-12 Site Manager, Bldg. 9704-2, MS-8009
88. M. W. Johnson, Los Alamos National Laboratory, NIS-6, MS J562, TA-18 Bldg 0129, Room 12, Los Alamos, NM 87545
89. F. A. Kloverstrom, Lawrence Livermore National Laboratory, 7000 East Avenue Livermore, CA 94550

90. J. A. Larrimore, International Atomic Energy Agency, P.O. Box 100, Vienna, A-1400 Austria
91. M. A. Livesay, U.S. Department of Energy, Oak Ridge Operations Office, 200 Administration Road, Oak Ridge, TN 37830
92. R. E. Malenfant, U.S. DOE Headquarters, NN-21, GA-293, Forrestal, 1000 Independence Avenue, S. W., Washington, DC 20585
93. E. F. Mastal, U.S. DOE Headquarters, Germantown, NE-50, 19901 Germantown Road, Germantown, MD 20874
94. G. E. Michaels, U.S. DOE Headquarters, NN-21, GA-293, Forrestal, NN20, 6F078, 1000 Independence Avenue, S. W., Washington, DC 20585
95. W. J. Mings, U.S. Department of Energy, Idaho Operations Office, 785 DOE Place, MS-1136, Room 56, Idaho Falls, ID 83401
96. J. F. Morgan, Lawrence Livermore National Laboratory, 7000 East Avenue, L-175 Livermore, CA 94550
97. M. J. Newman, U. S. Department of Energy, Headquarters, Forrestal, NN-41, 1000 Independence Avenue, S.W., Washington, D.C. 20585
98. L. Nolan, Pantex, P.O. Box 30020, Amarillo, Texas 79177
99. M. F. O'Connell, U.S. DOE. Forrestal Building, NN-20, MS-7A-049, 1000 Independence Avenue, S.W., Washington, DC 20585
100. A. J. Peurrung, Pacific Northwest National Laboratory, 902 Battelle Blvd., P.O. Box 999, Richland, Washington 99352
101. D. Pollina, Bechtel Nevada/Remote Sensing Laboratory, P.O. Box 98521, Las Vagas, NV 89193-8521
102. C. Pratt, Los Alamos National Laboratory, NIS-6, MS J562, TA-18, Bldg. 0030, Room 100, 528 35th Street, Los Alamos, NM 87545
103. D. K. Reitzel, Science Applications International Corporation (SAIC), 2109 Air Park Road S.E., Albuquerque, New Mexico 87106
104. W. L. Riffle, U.S. DOE Headquarters, Germantown, NN-521, 19901 Germantown Road, Germantown, MD 20874-1290
105. G. D. Smith, U.S. DOE Headquarters, Germantown, NN-513, 19901 Germantown Road, Germantown, MD 20874-1290
106. D. P. Spears, U. S. Department of Energy, Headquarters, Forrestal, NN-20, 1000 Independence Avenue, S.W., Washington, D.C. 20585
107. J. M. Taylor, Sandia National Laboratory, Org. 5031, P.O. Box 5800, Albuquerque, NM 87185
108. D. R. Waymire, Sandia National Laboratory, Org. 5031, P.O. Box 5800, Albuquerque, NM 87185
109. P. White, Los Alamos National Laboratory, NIS-CISA, MS K760, TA-66 Bldg 0101, Room D103, Los Alamos, NM 87545
110. T. L. Williams, Savannah River Operations, Savannah River Site, P.O. Box A, Aiken, South Carolina 29801
111. W. G. Winn, Savannah River Laboratory, P.O. Box A, Bldg. 6, Room 779-A, Aiken, South Carolina 29801
112. M. S. Wyatt University of Tennessee, Nuclear Engineering Dept., 207 Pasqua Engineering Bldg., Knoxville, TN 37996-2300